

VILNIUS GEDIMINAS TECHNICAL UNIVERSITY

Alinda DEY

CONSTITUTIVE BOND-SLIP MODELLING  
OF REINFORCED CONCRETE MEMBERS  
AT SERVICE LOAD

DOCTORAL DISSERTATION

TECHNOLOGICAL SCIENCES  
CIVIL ENGINEERING (T 002)

Vilnius, 2023

The doctoral dissertation was prepared at Vilnius Gediminas Technical University in 2019–2023.

### **Supervisor**

Prof. Dr Habil. Gintaris KAKLAUSKAS (Vilnius Gediminas Technical University, Civil Engineering – T 002).

The Dissertation Defence Council of the Scientific Field of Civil Engineering of Vilnius Gediminas Technical University:

### **Chairman**

Prof. Dr Darius BAČINSKAS (Vilnius Gediminas Technical University, Civil Engineering – T 002).

### **Members:**

Prof. Dr Raimondas BLIŪDŽIUS (Kaunas Technological University, Civil Engineering – T 002),

Prof. Dr Klaus HOLSCHMACHER (Leipzig University of Applied Sciences, Germany, Civil Engineering – T 002),

Dr Aidas JOKŪBAITIS (Vilnius Gediminas Technical University, Civil Engineering – T 002),

Prof. Dr Antanas ŠAPALAS (Vilnius Gediminas Technical University, Civil Engineering – T 002).

The dissertation will be defended at the public meeting of the Dissertation Defence Council of the Scientific Field of Civil Engineering in the Senate Hall of Vilnius Gediminas Technical University at **10 a. m. on 2 October 2023**.

Address: Saulėtekio al. 11, LT-10223 Vilnius, Lithuania.

Tel.: +370 5 274 4956; fax +370 5 270 0112; e-mail: doktor@vilniustech.lt

A notification on the intended defence of the dissertation was sent on 1 September 2023. A copy of the doctoral dissertation is available for review at the Vilnius Gediminas Technical University repository <http://dspace.vgtu.lt> and the Library of Vilnius Gediminas Technical University (Saulėtekio al. 14, LT-10223 Vilnius, Lithuania).

Vilnius Gediminas Technical University book No 2023-038-M

doi:10.20334/2023-038-M

© Vilnius Gediminas Technical University, 2023

© Alinda Dey, 2023

*alinda.dey@vilniustech.lt*

VILNIAUS GEDIMINO TECHNIKOS UNIVERSITETAS

Alinda DEY

FIZIKINIS GELŽBETONINIŲ ELEMENTŲ  
SUKIBIMO ĮTEMPIŲ IR SLINKTIES RYŠIO  
MODELIAVIMAS ESANT EKSPLOATACINEI  
APKROVAI

DAKTARO DISERTACIJA

TECHNOLOGIJOS MOKSLAI,  
STATYBOS INŽINERIJA (T 002)

Vilnius, 2023

Disertacija rengta 2019–2023 metais Vilniaus Gedimino technikos universitete.

### **Vadovas**

prof. habil. dr. Gintaris KAKLAUSKAS (Vilniaus Gedimino technikos universitetas, statybos inžinerija – T 002).

Vilniaus Gedimino technikos universiteto statybos inžinerijos mokslo krypties disertacijos gynimo taryba:

### **Pirmininkas**

prof. dr. Darius BAČINSKAS (Vilniaus Gedimino technikos universitetas, statybos inžinerija – T 002).

### **Nariai:**

prof. dr. Raimondas BLIŪDŽIUS (Kauno technologijos universitetas, statybos inžinerija – T 002),

prof. dr. Klaus HOLSCHEMACHER (Leipcigo taikomųjų mokslų universitetas, Vokietija, statybos inžinerija – T 002),

dr. Aidis JOKŪBAITIS (Vilniaus Gedimino technikos universitetas, statybos inžinerija – T 002),

prof. dr. Antanas ŠAPALAS (Vilniaus Gedimino technikos universitetas, statybos inžinerija – T 002).

Disertacija bus ginama viešame statybos inžinerijos mokslo krypties disertacijos gynimo tarybos posėdyje **2023 m. spalio 2 d. 10 val.** Vilniaus Gedimino technikos universiteto senato posėdžių salėje.

Adresas: Saulėtekio al. 11, LT-10223 Vilnius, Lietuva.

Tel.: (8 5) 274 4956; faksas (8 5) 270 0112; el. paštas doktor@vilniustech.lt

Pranešimai apie numatomą ginti disertaciją išsiųsti 2023 m. rugsėjo 1 d.

Disertaciją galima peržiūrėti Vilniaus Gedimino technikos universiteto talpykloje <http://dspace.vgtu.lt> ir Vilniaus Gedimino technikos universiteto bibliotekoje (Saulėtekio al. 14, LT-10223 Vilnius, Lietuva).

# Abstract

The current dissertation aims to introduce a new interaction model between concrete and reinforcement to effectively address the inner mechanism of Reinforced Concrete (RC) structures.

For investigating the concrete-reinforcement interaction, traditional methods have typically dealt with a constant bonding relationship or a perfect interaction between two materials. This can further lead to numerous models that lack consistency and compatibility with one another. However, current research advocates for implementing the stress transfer methodology, which suggests the presence of force exchange between the reinforcement bars and the surrounding concrete, in other words, the bond stress. The present study develops a new model that establishes the ascending part of a bond-slip model. It is an essential step towards a constitutive bond-slip model in future, which will be able to accurately predict the serviceability performance of RC members, such as deflection, crack spacing/width etc.

The first chapter reviews the mechanism of the reinforcement-concrete interface under the tensile load. Multiple approaches have been discussed to investigate the serviceability performance of RC structures. A major part of this chapter is dedicated to reviewing the existing bond stress and bond-slip models with their respective backgrounds. The last part of the chapter reviews various strain monitoring tools and techniques to extract strains from the core of the reinforcement bars encased within the concrete.

The second chapter represents three experimental campaigns which consist of double pull-out tests of 14 short RC ties equipped with three distinct bar diameters (16.20 and 25 mm). The results of the mentioned tests, in terms of reinforcement strain distribution along the specimen lengths, have been displayed. A mathematical algorithm programmed in MatLab has been introduced, capable of deriving bond-slip relationships from the experimental strain output. Lastly, the obtained bond-slip relationships of all 14 specimens have been portrayed at multiple load levels.

The third chapter demonstrates the formation of a novel bond-slip model based on the experimental dataset. In the latter part, the newly proposed model has been validated with the experimental results of 14 (in-sample) specimens and eight independent (out-of-sample) specimens. Furthermore, a novel validation tool has been demonstrated, which is capable of predicting reinforcement strains from a given bond-slip model. Based on the tool, another layer of validation has been performed with independent data through reinforcement strain distribution. The chapter ends with a thorough statistical analysis for assessing the existing bond-slip models in terms of their strain prediction capability.

# Reziუმэ

Šioje disertacijoje pristatomas naujas betono ir armatūros sąveikos modelis, leidžiantis tiksliai ir efektyviai modeliuoti gelžbetoninių (toliau – GB) konstrukcijų armatūros ir betono sukibimo elgseną.

Tyrinėjant betono ir armatūros sąveiką tradiciniais metodais, dažnai daromos itin supaprastintos prielaidos, kurios dažnai neatspindi realios konstrukcijų elgsenos – laikoma, kad tarp armatūros ir betono egzistuoja ideali sąveika, arba daroma prielaida, jog sukibimo įtempiai tarp betono ir armatūros per visą nagrinėjamojo elemento ilgį yra pastovūs. Dėl šių supaprastinimų yra sukurta daugybė prieštaringų teorinių modelių, kurių rezultatai dažnai neatitinka realios GB elementų sukibimo elgsenos. Šioje disertacijoje, remiantis įtempių perdavimo gelžbetoninėse konstrukcijose metodika, kuri pagrįsta armatūros strypų ir juos supančio betono jėgų sąveikos prielaida, kitaip tariant, sukibimo įtempių perdavimu, siūloma sukibimo įtempių ir slinkties modelio nauja kylančioji dalis. Pirmajame skyriuje apžvelgiamas armatūros ir betono sąveikos mechanizmas veikiant eksploatacinei apkrovai. Taip pat aptariami keli literatūroje plačiai žinomi metodai, taikomi GB konstrukcijų tinkamumui eksploatuoti užtikrinti. Didžioji šio skyriaus dalis skirta esamų sukibimo įtempių ir slinkties modelių apžvalgai. Paskutinėje šio skyriaus dalyje apžvelgiami įvairios deformacijų stebėsenos prietaisai ir metodai, skirti armatūros deformacijoms betone nustatyti.

Antrajame skyriuje pristatomos trys eksperimentinės programos, kurias vykdant buvo atlikta 14 trumpų GB tempiamų elementų dvipusio ištraukimo bandymai naudojant tris skirtingo skersmens strypus (16, 20 ir 25 mm). Šiame skyriuje taip pat pateikiami minėtųjų bandymų rezultatai, susiję su armatūros deformacijų pasiskirstymu išilgai nagrinėjamų bandinių. Pristatomas matematinis algoritmas, suprogramuotas naudojant MATLAB programinį paketą, kuriuo, remiantis eksperimentiniais armatūros deformacijų rezultatais, galima nesunkiai nustatyti sukibimo ir slinkties ryšį. Skyriaus pabaigoje pateikiamos visų 14 bandinių sukibimo įtempių priklausomybės nuo slinkties kreivės.

Trečiajame skyriuje aprašoma, kaip, remiantis surinkta eksperimentinių duomenų imtimi, sukuriamas naujas sukibimo ir slinkties modelis. Modelis tikrinamas remiantis 14 bandinių iš autoriaus eksperimentinės programos ir 8 nepriklausomų bandinių iš įvairių literatūros šaltinių eksperimentiniais rezultatais. Be to, pristatyta nauja programa, leidžianti prognozuoti armatūros deformacijas pagal atitinkamą sukibimo ir slinkties modelį. Taikant šią programą ir pasitelkiant nepriklausomus duomenis, surinktus iš įvairių šalių literatūros šaltinių, buvo atlikta armatūros deformacijų patikra. Skyriaus pabaigoje pateikiama išsami statistinė analizė, skirta esamiems sukibimo ir slinkties modeliams įvertinti, atsižvelgiant į jų gebėjimą prognozuoti armatūros deformacijas.

---

# Notations

## Symbols

- $\varepsilon$  or  $\varepsilon_s$  – strain in reinforcement steel;  
 $\varepsilon_{exp}$  – experimentally obtained strain in reinforcement bar;  
 $\varepsilon_{model}$  – model predicted strain in reinforcement bar;  
 $\bar{\varepsilon}$  – strain ratio;  
 $\bar{\varepsilon}_m$  – mean strain ratio;  
 $\varepsilon_c$  – strain in concrete;  
 $\emptyset$  - reinforcement bar diameter;  
 $\Delta s$  – change in slip;  
 $\tau$  – bond stress;  
 $A_c$  – cross-section area of concrete;  
 $A_{groove}$  – cross-section area of a groove;  
 $A_{s,mod}$  – a modified area of a reinforcement bar;  
 $A_s$  – cross-section area of reinforcement bar, net;  
 $c$  – concrete cover;  
 $E_c$  – elastic modulus of concrete;  
 $E_s$  – elastic modulus of a reinforcement steel;  
 $f_c$  – compressive strength of concrete;  
 $f_{ct}$  – tensile strength of concrete;  
 $f_{ft}$  – flexural strength of concrete;

$f_R$  – relative rib area;  
 $f_y$  – yield strength of reinforcement bar;  
 $i$  – number of iterations;  
 $l$  or  $L$  – embedded length;  
 $l_R$  – clear spacing between two ribs;  
 $l_t$  – transfer length;  
 $L_d$  – de-bonding length;  
 $n$  – number of segments;  
 $N_c$  – force driven by concrete;  
 $N_s$  – force driven by reinforcement steel;  
 $pt\%$  - reinforcement ratio;  
 $P$  – subjected tensile load;  
 $s$  – slip;  
 $S_{rm}$  – mean crack spacing.

## **Abbreviations**

3D – three-dimensional;  
COV – coefficient of variation;  
RC – reinforced concrete;  
DOE – design of experiments;  
DOFS – distributed optical fibre sensor;  
FBG – fibre Bragg grating;  
MLR – multiple linear regression;  
OPC – ordinary Portland cement;  
Std.Dev. – standard deviation;  
UTM – universal testing machine.

---

# Contents

INTRODUCTION .....	1
Problem Formulation.....	1
Relevance of the Dissertation.....	2
The Object of the Research .....	2
Aim of the Dissertation .....	2
Tasks of the Dissertation .....	3
The Research Methodology.....	3
The Scientific Novelty of the Dissertation .....	3
Practical Value of the Research Findings.....	4
Defended Statements.....	4
Approval of the Research Findings .....	5
The Structure of the Dissertation.....	5
Acknowledgement.....	5
1. REVIEW OF CONCRETE–REINFORCEMENT INTERACTION AND BOND STRENGTH INVESTIGATION TECHNIQUES .....	7
1.1. Serviceability of Reinforced Concrete Structures .....	7
1.1.1. Concrete–Reinforcement Interaction.....	9
1.1.2. Cracking and Failure of Reinforced Concrete Tension Members .....	10
1.2. Bond–Slip Models.....	13
1.2.1. Test Methods .....	14
1.2.2. Bond–Slip Laws .....	15
1.2.3. Parameters Influencing Bond–Slip Relationships .....	25

1.3. Strain Monitoring Techniques from Embedded Bar .....	28
1.3.1. Electrical Strain Gauge Sensors .....	28
1.3.2. Fibre Bragg Grating.....	29
1.3.3. Distributed Optical Fibre Sensor .....	30
1.4. Conclusions of the First Chapter and Formulation of the Dissertation Tasks ....	32
2. EXPERIMENTAL CAMPAIGNS FOR STEEL STRAIN MONITORING IN REINFORCED CONCRETE MEMBERS .....	35
2.1. Experimental Campaigns .....	36
2.1.1. Specimens' Geometry .....	36
2.1.2. Material Properties .....	40
2.1.3. Strain Gauge Installation .....	42
2.1.4. Double Pull-out Test.....	43
2.2. Strain Distribution Results .....	45
2.3. Derivation of Bond–Slip Relationship .....	48
2.3.1. Theoretical Approach .....	49
2.3.2. Bond–Slip Relationship Results .....	52
2.4. Conclusions of the Second Chapter.....	57
3. NOVEL BOND–SLIP MODEL: FORMATION AND VALIDATION .....	59
3.1. Bond–Slip Model: Theory and Formation.....	60
3.1.1. Data Collection and Normalisation .....	60
3.1.2. Multiple Linear Regression .....	62
3.1.3. Model Selection.....	65
3.2. Model Validation.....	65
3.2.1. In-sample Validation .....	66
3.2.2. Out-of-sample Validation.....	68
3.3. Reinforcement Strains from Bond–Slip Models: Application and Validation ...	71
3.3.1. Validation Tool: Theoretical Background .....	72
3.3.2. Validation Tool: Application.....	75
3.3.3. Statistical Analysis .....	83
3.4. Conclusions of the Third Chapter.....	87
GENERAL CONCLUSIONS .....	89
REFERENCES .....	91
LIST OF SCIENTIFIC PUBLICATIONS BY THE AUTHOR ON THE TOPIC OF THE DISSERTATION .....	99
SUMMARY IN LITHUANIAN .....	101

---

# Introduction

## Problem Formulation

Serviceability is one of the most essential qualities of a Reinforced Concrete (RC) structure. It can be assessed in several categories. Nonetheless, performance-based design can be managed by deflection and cracking. Even today, the mean strain approach (based on constant bond relationship or perfect interaction between concrete and reinforcement) is commonly used for performance-based serviceability analysis, which over-simplifies the behaviour of RC structures and may not accurately represent their internal mechanisms, resulting in models' performance disparities. To tackle these challenges effectively, this dissertation aimed to develop a new model that defines the correlation between bond stress and slip in RC structures through the modern and realistic stress transfer approach based on accurate and precise data from the concrete–reinforcement inner-working, using potential strain monitoring tools. As an integral component of a broader investigation, the current model exclusively encompasses the ascending branch of a constitutive bond–slip model. The descending branch that involves such phenomena as damage, de-bonding, internal cracking, tension softening etc., requires a significant amount of experimental data and remains the object for future investigations. This aspect can potentially enable the prediction of serviceability analysis (cracking and deformation) for RC structures, thus offering valuable utility

in practical applications. Additionally, it was found that no efficient tool is available that can smoothly corroborate and quickly calibrate the existing/newly created models. The present study is also focused on resolving the issue by developing a validation tool which will be well capable of predicting strain distributions from a given bond–slip model.

## **Relevance of the Dissertation**

The stress transfer approach is a contemporary theory based on force transfer, which suggests the interplay of concrete and reinforcement. The correlation among these materials, commonly referred to as bonds, exerts a significant impact on the structural dynamics. Bond is typically characterised by the governing principles of shear stresses (occurring within the interface region) and slip (the relative displacement between these materials). Bond stress and slip are two interconnected fundamental elements of force transmission. It is established that the stress-transfer approach reveals the actual inner workings at the concrete–reinforcement interface. However, the existing bond–slip models cannot accurately predict the serviceability limit state behaviour of RC structures. Hence, it is imperative to create a novel bond–slip model founded on the stress transfer approach that can provide precise predictions of reinforcement strains, hence the serviceability behaviour of RC structures. Furthermore, it is crucial to create a new validation tool that can help bridge the gap between the development of a model and its validation, particularly regarding the serviceability behaviour of RC structures. Also, it creates the scope for “assessing” the existing and new models with respect to their experimental counterparts.

## **The Object of the Research**

The object of the present study is to investigate the correlation between bond stress and slip at the interface of concrete and reinforcement in RC structures, specifically between two adjacent cracks under the range of service loads.

## **Aim of the Dissertation**

Developing a new bond model of reinforcement bar and concrete for reinforced concrete tensile members at service load.

## Tasks of the Dissertation

The subsequent steps were taken to achieve the aim:

1. To conduct a comprehensive literature review on the existing bond models and critically analyse their performance.
2. To assess the impact of different factors on the bond stress–slip relationship of RC structures.
3. To design and execute double pull-out experiments for extracting strains from the central part of the reinforcement bars encased within the concrete using strain monitoring devices.
4. To create a physical bond–slip model between reinforcement and concrete under the service load.
5. To establish an efficient tool (computational algorithm) for predicting strain distribution from a given bond–slip model for corroboration and validation of new or existing models.
6. To perform statistical analysis on models' strain prediction assessment.

## The Research Methodology

The methodology employed in this dissertation incorporates a new approach to investigate the underlying mechanism at the interface between concrete and reinforcement by examining their bond–slip relationship. This was achieved by conducting double pull-out tests equipped with strain gauge sensors, which effectively captured the behaviour of the concrete–reinforcement interaction under service load conditions. Through mathematical and parametric analyses, a new formulation of bond–slip modelling for RC structures was proposed. A computational algorithm implemented in MatLab was utilised to determine the distribution of reinforcement strain based on the proposed model, which was subsequently validated against both in-sample and independent experimental results. Finally, a statistical analysis was conducted to evaluate the reliability and validity of the proposed model compared to existing ones.

## The Scientific Novelty of the Dissertation

The scientific innovations resulting from the theoretical and experimental investigation are outlined as follows:

1. The double pull-out test method effectively addresses the limitations encountered in standard pull-out tests, including issues related to average bond stress, ideal material interaction, concrete compression etc. By incorporating strain gauge sensors, a set of novel data from the current experimental campaigns covering a diverse range of parameters overcome the scarcity of experimental data in this domain.
2. Established on the stress transfer approach and double pull-out tests, a new formulation of bond–slip modelling has been proposed to anticipate the rising part of bond–slip relationship in RC structures.
3. The proposed validation tool can fast-track the strenuous and lengthy mathematical and experimental corroboration and comparison process between similar existing models. Besides, this tool opens a prospect for investigations on stress transfer analysis, bond–slip modelling, and, eventually, the serviceability of RC structures.

## **Practical Value of the Research Findings**

1. The suggested model can be utilised in analytical and numerical research to perceive the actual behaviour of RC structures, leading to a more consistent and economical structural design.
2. The reinforcement strain predictions from the application of the validation tool create the path for model assessment/comparison/validation and can be used in novel future investigations related to stress transfer analysis, bond–slip modelling, and, eventually, the serviceability of RC structures.

## **Defended Statements**

The following statements can be defended based on the results of the current investigation and the defendant's experience:

1. Within the service load range, the proposed bond model is capable of accurately predicting the bond stress and slip correlation between the cracks of an RC tensile element.
2. The proposed model indicates that concrete strength and slip/diameter ratio have a notable influence on the bond–slip relationship of RC structures.
3. The ability of reinforcement strain predictions by various models can be checked/validated/compared by the proposed validation tool.

4. The proposed bond model is capable of offering a sufficient level of accuracy in predicting the reinforcement strain in an RC structure within the service load range, as compared to the existing models.

## Approval of the Research Findings

During the course of the PhD studies (2019–2023), the author has published the dissertation results in three international journals indexed in Web of Science (Dey et al., 2021a; Dey et al., 2021b; Dey et al. 2022) and two in international scientific conferences:

1. Dey, A., Bado, M. F., Sokolov, A., and Kaklauskas, G. (2020), “Distributed sensing, fibre Bragg gratings and strain gauges for strain monitoring of RC tensile elements”, Proceeding of the fib Symposium 2020, Concrete Structures for Resilient Society, 22–24 November, Shanghai, China.
2. Dey, A., Valiukas, D., Sokolov, A., Jakubovskis, R., and Kaklauskas, G. (2021), “Experimental and Numerical investigation of the bond performance of RC tension members”, fib Symposium 2021, 14–16 June, Lisbon, Portugal.

## The Structure of the Dissertation

The dissertation contains an introduction, three chapters, a general conclusion, a reference list of 83 cited sources, a list of the author’s publications on the dissertation’s research topic with five articles and a summary in Lithuanian. The dissertation volume is 112 pages with 41 figures and 12 tables.

## Acknowledgement

The author would like to express the deepest appreciation and gratitude to his parents, Mrs Asima Dey and Mr Swapan Kumar Dey, his sister Subarna and his constant companion in life, Sarmistha, for their unwavering love, support, encouragement and motivation throughout the years.

The author is also sincerely grateful to his supervisor of doctoral studies, Prof. Dr Habil. Gintaris Kaklauskas, the Department of Reinforced Concrete Structures and Geotechnics, for his invaluable guidance, expertise, patience and trust. The author thanks his entire working team, particularly Dr Mattia Francesco

Bado, Dr Aleksandr Sokolov and Mr Domas Valiukas, for their various support throughout the course of this research. Furthermore, the author would like to extend his gratitude to Prof. Dr Darius Bačinskas, Dr Aidas Jokūbaitis, Dr Vladimir Popov and Dr Raimondas Bliūdžius for their advice and comments on the improvement of the dissertation, and Prof. Dr Juozas Valivonis and Assoc. Prof. Dr Ronaldas Jakubovskis, Dr Skirmantė Mozūriūnaitė, Ms Vaiva Miškinytė, Ms Daiva Jurėnienė and Ms Dovilė Jodenytė, for their friendly and supportive motivation. Additional thanks go to Mr Amarjeet, Mr Kunal, Ms Simran and Mr Karolis for always being supportive. Finally, the author is grateful to the Doctoral School of Vilnius Tech and Research Council of Lithuania for providing financial support during his doctoral studies and the University of Trento (UniTN) for offering the opportunity to gain rewarding experience during his internship.

# 1

---

## **Review of Concrete–Reinforcement Interaction and Bond Strength Investigation Techniques**

This chapter aims to provide a multifaceted background literature review on the mechanism at the reinforcement–concrete interface under tensile load. Also, multiple existing bond–slip models have been discussed with their respective backgrounds. Moreover, various methods and tools used to determine the mechanism at the concrete–reinforcement interface have been reviewed. Additional focus was given to the methods of strain monitoring from an embedded reinforcement in RC tensile elements. Multiple modern tools recently implemented in civil engineering, including distributed optical fibres, have been discussed as well. This chapter ends with composing the primary objective and methodology of the current study. The research findings are published in the author’s publications (Dey et al., 2020; Dey et al., 2021a).

### **1.1. Serviceability of Reinforced Concrete Structures**

Structural design has two essential criteria, safety and serviceability. The former defines a facility that must withstand the design loads throughout its design life.

In comparison, the serviceability part of a structure limits the deflection and cracking of a structure under any circumstances. It refers to the overall performance, working conditions and usefulness through its service life. The allowable limit of both requirements (safety and serviceability) is known as the “limit state” (IS 456, 2000). The objective of the limit state design is to ensure a structure is fit-for-use for which it is intended. In other words, the “serviceability limit state” is associated with the regular and comfortable performance or service of a structure. As an example, the serviceability limit state does not allow large deflections/deformations, long or wide cracks, vibrations or damage to appear on a structure which creates discomfort to the users and risks their lives, ultimately failing to continue serving its original intention (fib Model Code, 2013).

Previously, serviceability was not an issue in the case of allowable or working stress methods of structural designing, as serviceability problems are not prominent at low-stress levels. In contradiction, serviceability becomes requisite for the limited state of design, which is fundamentally based on probability (Serviceability research, 1986). The service life of a structure can be assumed, which must comply with various codes and standards worldwide. Through their distinctive life span, an optimum performance by the structure is also expected. Eventually, the structural system fails to meet expectations, accompanied by deterioration. This performance explicitly relates to the material properties, environmental circumstances, and repair and maintenance implementations. Serviceability endeavours to enhance the member’s performance by reducing the degradation of its structural integrity. Although, a structurally strong or safe facility can be un-serviceable in nature. This is because it is unable to reach the required reliability. RC slabs having exposed reinforcements at their soffit and posing no danger of collapsing are a perfect example of such cases.

The designing formulation and analysis criteria for the RC structure’s serviceability are complex. The main reason behind this issue is concrete and its inherent non-linearity in the stress–strain relationship. Concrete develops elastoplastic behaviour in compression. On the contrary, it develops crack formations while in tension, leading to a radical twist in the behaviour of RC structures. Over and above, the reinforcement (steel) also shows elastoplastic behaviour, followed by strain hardening under cyclic loading (Gilbert, 2001). Combining concrete and reinforcement steel (RC), a composite material inherently exhibits non-linear behaviour and sometimes unpredictable performances. Furthermore, the interaction between the two materials in the RC structure fluctuates with time and with the time-dependent factors acting on it. Most importantly, concrete shrinkage (contraction mainly due to the loss of moisture) and concrete creep (increase in strain under a constant load) alone or together can lead to the malfunction of an RC structure. If not addressed or prevented, it can result in serious serviceability issues, such as the collapse of plaster or concrete chunks, large deflection in beams,

water seepage etc. Considering the entire non-linearity of RC, in general, the probabilistic calculations for the serviceability design of RC structures are indeed complex and strenuous in nature (Stewart, 1996).

### 1.1.1. Concrete–Reinforcement Interaction

Reinforced concrete has emerged to be the most compatible and hence most demanding construction material since its appearance. As a composite material, RC also deals with the most complex issue of the interaction between concrete and reinforcement (two constitutive materials). Although, it is the dominating factor that controls the performance related to the serviceability of RC structures. Concerning the importance, the concrete–reinforcement interaction is still one of the hot topics of investigation, currently running throughout the globe. According to available studies, the theoretical models of the concrete–reinforcement interaction are divided into two categories:

- *Smearred Approach*
  - Represents the average value of cracking and deformation.
  - Based on numerical methods, contains semi-empirical and analytical models.
  - Simplicity and effective methodology are the advantages.
  - Lack of versatility – unable to produce explicit crack patterns (crack spacing and width).
- *Discrete Approach*
  - Extracts deformation output, and analyse the crack formation.
  - Based on the stress transfer mechanism.
  - Simple and realistic.
  - Lack of adequate laws governing the analysis.
  - The present investigation directly works on the drawback towards developing a new model (law).

Previously, a common practice was to assume a constant relationship throughout the concrete–reinforcement interface with no relative displacement. However, this approach became unrealistic as far as the serviceability behaviour of RC structures is concerned (Kaklauskas et al., 2012). As an alternative to this classical approach, the stress transfer approach has become more popular in modern research (Kaklauskas, Sokolov et al., 2019). This approach recommends the concrete–reinforcement interaction in terms of a force transfer along the interface, which can be introduced as the bond. In another way, bond or bond stress (defined as  $\tau$ ) is constitutionally the shear stress, which evolves at the outer face of the steel reinforcement bar. It prevents the displacement of the reinforcement bar in relation to the surrounding concrete (slip). On an important note, bond stress is crucial

when the development of structural performance is concerned. The primary reason is the entire process by which forces are transmitted between the reinforcement bar and the surrounding concrete by means of the existing bond at their interface (Jakubovskis and Kaklauskas, 2021). Also, the event of a slip may result in some local damage in RC, in terms of cracking, which further leads to a major serviceability concern. It is also observed that these cracked sections in the interface reduce the existing bond action remarkably (Ruiz et al., 2007).

There are three basic elements on which the concrete-reinforcement bond is based upon:

- chemical adhesion,
- frictional resistance, and
- mechanical interlock.

First, the hydration process evolves the adhesion properties in cementitious materials, which initiate the chemical adhesion (Lundgren, 2005). Second, frictional resistance is the combined outcome of the strain (induced by shrinkage in concrete) and the presence of roughness on the steel reinforcement surface (Magnusson, 2000). Lastly, the mechanical interlock is completely fortified by the ribs or the projection on the surface of the reinforcement (Siempu and Pancharathi, 2018). The latter does not take place in the case of plain bars due to the nonexistence of the ribs. In the case of ribbed bars, adhesion and friction have a negligible influence. The adhesion effects between the bars and surrounding concrete diminished rapidly, resulting in the tension load being transmitted through the ribs or interlocking of the bars (Sulaiman et al., 2017). The transfer of tensile force from a ribbed bar to the surrounding concrete induces the formation of bearing stresses, which can be categorised into longitudinal and radial components. The longitudinal component, also known as bond stress, acts along the contact surface between the bar and the surrounding concrete.

### **1.1.2. Cracking and Failure of Reinforced Concrete Tension Members**

Concrete holds up the strength and rigidity of the structure, which also produces resilience against structural deformation. It manifests the brittleness property present in the concrete material. Also, its limited tensile strength capacity is a pivotal aspect in cracking on its surface. Cracking occurs once the tensile stresses affecting the structural member surpass the maximum tensile capacity of the concrete material (Leonhardt, 1988). The issue is even more complex for RC structures due to multiple additional factors. A crack in the concrete having a direct effect on structural stability can surely be a serviceability concern. Various standards and design codes provide serviceability limit state analyses that are complicated and

inconsistent (Kaklauskas, Ramanauskas et al., 2019). However, many studies are in the process of deepening the understanding of the crack mechanism's complexity in RC structures in terms of serviceability.

As previously discussed, the serviceability performance (deflection and cracks) of an RC structure is linked with the bonding between concrete and reinforcement. Such integrity of the concrete–reinforcement bonding can be interrupted after the formation of cracks followed by an inherent behavioural change in RC structures. It is seen that the type of embedded reinforcement steel (plain and deformed) has a notable influence on the formation of cracking (Bischoff, 2001; Gribniak, 2009). The appearance pattern of lateral cracks (primary) is similar in both cases of plain and deformed reinforcements. Moreover, for plain bars, relatively bigger primary crack spacing and wider cracks can be found than the deformed ones. On the other hand, at higher stress levels, additional transverse cracks (smaller in size) were noticed around the deformed bar in distinctly different inclinations than the primary ones (Goto, 1971). These minuscule internal cracks can be indicated as secondary cracks or “Goto cracks”, unfolding the new dimension of the crack mechanism. In general, secondary cracks are compacted and rooted around the projected ribs of the bar; they do not appear on the surface of the concrete (Fig. 1.1). It is reported that this internal cracking can degrade the bond acting between the concrete and reinforcement surface, hence threatening the stability of the structure. It may cause severe deformation in the close vicinity of the deformed bar, potentially causing damage to the section (Gribniak, Rimkus et al., 2018). With disparity, plain bars do not manifest such a complex mechanism of cracking, as the bonding without ribs relies on adhesion and friction only (Tepfers, 1979).

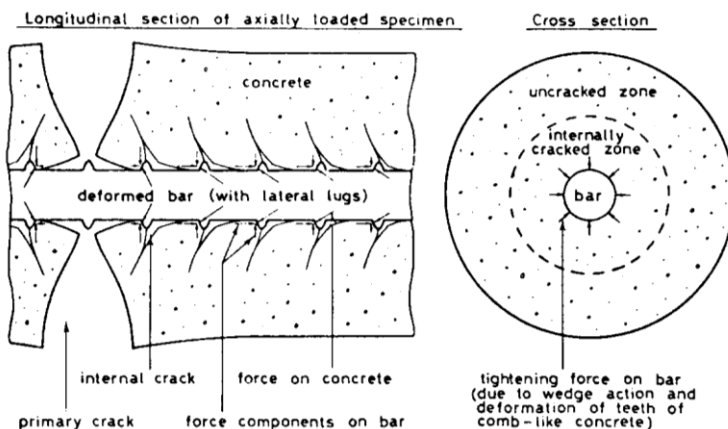


**Fig. 1.1.** Deformation and crack formation in concrete around steel reinforcement (Goto, 1971)

According to the stress transfer approach, the serviceability performance (cracking) of an RC structure can be divided into three sequences, illustrated in Fig. 1.2:

- *Elastic stage*, no permanent deformation takes place at this stage. Linear elastic response (with bond–slip) occurs at the element terminals.
- *Crack formation stage*, the transferred stress to concrete exceeds its tensile strength ( $f_{ct}$ ), which initiates the crack formation at the weakest section. After that, strain compatibility acting between concrete and reinforcement bar is demolished. At the cracked section, concrete stress drops to nil, and steel strain reaches a sudden peak, as the latter holds all the stresses alone. With the distance from the cracked section, concrete tensile stress grows. At a distinct gap, concrete–reinforcement strain compatibility is restored, referred to as transfer length ( $l_t$ ).
- *Stabilised cracking stage* appears at the time when the load level becomes 1.3 times higher than the cracking load (fib Model Code, 2013). The member splits into multiple segments, demarcated by the cracks. No fresh crack can form as the segment lengths are inadequate to let the concrete stress meet its tensile strength capacity. The mean crack spacing ( $s_{rm}$ ) is reported to be in the range between (1.3–1.5) times  $l_t$  (Borosnyoi and Balazs, 2005).

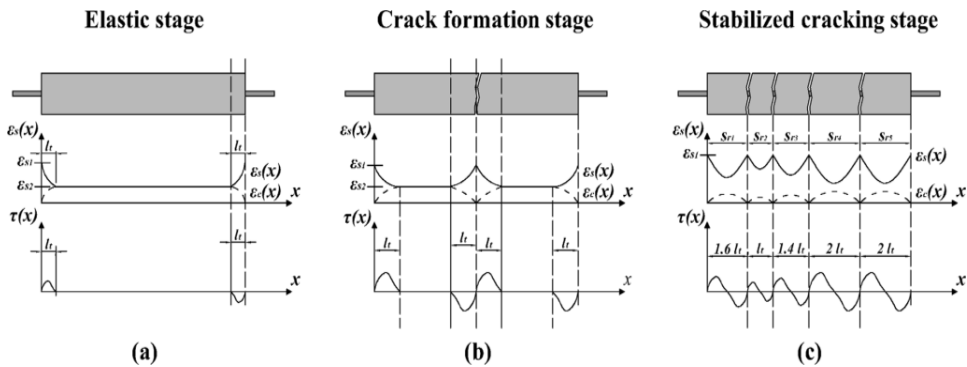


**Fig. 1.2.** Three stages of crack formation in reinforced concrete members: (a) elastic stage, (b) crack-formation stage and (c) stabilised cracking stage (Bado et al., 2021)

Various types of cracks can be observed in RC structures. Although, it depends upon the type of failure of a particular structure. In the present study, the experimental focus is given to pull-out tests. In such tests, the failure of RC tensile members can be categorised into four following modes:

- *Splitting failure* is one of the dominant failures in such types of testing. This happens mainly on the surrounding concrete around the steel reinforcement. In this event, the stresses acting on concrete exceed the design capacity, and splitting occurs. Due to its brittle property, the concrete close to the ribs fails to carry further stresses, and the failure starts. Both longitudinal and lateral cracks appear in such type of failure. Cracks can be observed on the top loading face of the RC specimen only.
- *Pull-out failure* is one of the rare cases when sufficient confinement is provided by large concrete covers. Naturally, the concrete exhibits a large stress-carrying capacity, which controls the bond strength at the concrete–reinforcement interface. It eventually prevents the splitting failure.
- *Tension failure* is observed for an RC specimen with large reinforcement bar diameters or large reinforcement ratios. In this case, steel offers a large yielding capacity, whereas concrete reaches its maximum tensile limit at an application of a certain tensile load. Around the mid-section of the RC specimen, one can observe the presence of lateral cracks.
- *Steel rupture failure* happens when steel reaches its maximum tensile load-carrying capacity. Eventually, the load interrupts the concrete–reinforcement bond, and the failure occurs.

Eventually, all serviceability performances of RC structures are concealed in the concrete–reinforcement interplay. An ample amount of research was done using various investigating techniques to explore the concrete–reinforcement internal mechanism. They demonstrate that bond stress and slip relationship (hereinafter – bond–slip) is one of the finest ways to portray the concrete–reinforcement interaction in an RC structure. The next sub-chapter will discuss a few existing bond–slip models with their establishment background.

## 1.2. Bond–Slip Models

The existing concrete–reinforcement bond can be classified into two distinct categories: flexural and development bond. In more detail, the flexural bond comes into the picture during the alterations in the bending moment throughout the member’s length. A full-scale beam test can be appropriate to investigate the evolution pattern of the flexural bond. On the flip side, the development bond, also known as the anchorage bond, is certainly active only through the development length of RC members. As demonstrated, this type of bond ensures reliable force transmission from the reinforcement to concrete through the development length. A direct pull-out test is an effective method for thoroughly examining the anchorage bond (Sulaiman et al., 2017). Various test methods and extracted bond–slip laws are discussed below.

### 1.2.1. Test Methods

To investigate the concrete–reinforcement bond, the most popular technique is to pull the bar from the concrete through tensile forces. This methodology is rooted in the concept of the force–displacement relationship (Windisch, 1985). Using the same theory, several researchers have performed pull-out tests (Chapman and Shah, 1987), push-in tests, full beam tests (Kemp, 1986) or beam-end tests (Esfahani and Rangan, 1998). However, such tests yield information about the distribution of average bond stress through the anchorage length as a function of slip (Siempu and Pancharathi, 2017a). A few drawbacks of this method cannot be ignored, such as the formation of compressive stresses near the support, non-uniform bond stress distribution, specimen deformation at high stresses and dissimilar slip at both ends (free and loaded) of the specimen (fib Model Code, 2013). These may lead to an inaccurate output of the local bond–slip relationship (Kaklauskas, Sokolov et al., 2019). Some illustrations of different test methods are presented in Fig. 1.3.

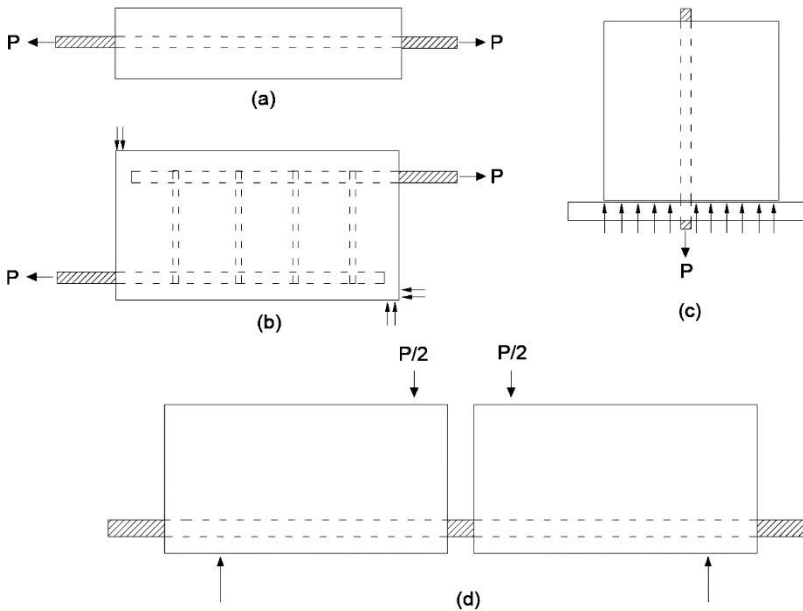


**Fig. 1.3.** Various test setups for evaluating bond strength:

(a) tensile test, (b) cantilever beam test, (c) pull-out test and (d) modified beam test  
(elaborated by the author)

Alternatively, modern researchers brought the idea of direct strain measurement from the embedded reinforcement bar, from which the slip and bond stress

can be derived. In this case, a double pull-out test is performed with an RC tensile member, where the tensile forces are applied from both specimen ends (Dey, Valiukas et al., 2022). It is found to be a more accurate and realistic approach to investigating the concrete–reinforcement interaction (Kaklauskas, Sokolov et al., 2019; Scott and Gill, 1987). According to this theory, strain profiles at various load levels are obtained first. Then, bond stress can be calculated from the reinforcement strain gradient, as they are proportional to each other. Besides, slip (relative displacement) can be determined from the integration of reinforcement strain curves (Mattia Francesco Bado, Casas and Kaklauskas, 2021; Shima et al., 1987). Overall, a double pull-out test can be assessed as a simple and realistic technique to investigate the local bond–slip relationship of an RC tensile member, hence the concrete–reinforcement interaction in its tensile zone (Mattia Francesco Bado, Casas, Dey et al., 2021).

### 1.2.2. Bond–Slip Laws

At the beginning of the twentieth century, a relationship between force and deformation was observed at the concrete–reinforcement contact zone (Abrams, 1925). Since then, one of the most significant experimental campaigns was carried out by Rehm, who performed several experiments related to the extraction of reinforcement bars from concrete at extreme conditions (Rehm, 1961). Established on the experimental result, he proposed a new bond–slip law for concrete–reinforcement interaction (Table 1.1). It was probably the first bond–slip law reported, followed by multiple non-linear bond–slip laws proposed by various scientists (Martin, 1973; Mirza and Houde, 1978; Nilson, 1971). Mathematical expressions to evaluate the bond stress ( $\tau$ ) based on the slip ( $s$ ) are presented in Table 1.1.

**Table 1.1.** Bond–slip models

References	Bond–slip model	Notes/Description
Rehm (1961)	$\tau = f_c (\varphi s^\alpha \pm \psi s)$	$f_c$ is the concrete strength; $\varphi, \alpha, \psi$ are the empirical coefficients
Nilson (1968)	$\tau = 3.606 \times 10^6 s - 5.356 \times 10^9 s^2 + 1.986 \times 10^{12} s^3$	$\tau$ in psi and $s$ in inches
Martin (1973)	$\tau = \tau_0 + cs^b$	$\tau_0$ is bond constant; $c, b$ are the empirical coefficients
Mirza and Houde (1979)	$\tau = 1.95 \times 10^6 s - 2.35 \times 10^9 s^2 + 1.3 \times 10^{12} s^3 - 0.33 \times 10^{15} s^4$	$\tau$ in psi and $s$ in inches

A few more popular bond–slip laws have been established in the last few decades. They are discussed in detail below.

### **Model of Eligehausen et al., 1982**

The primary objective of this study was to examine the impact of large plastic deformation on the functioning of RC structures. In that regard, 120 specimens (prisms) were prepared to perform a pull-out test with three different bar diameters (19, 25 and 32 mm). Established on the test results, an analytical expression was proposed to determine bond stress ( $\tau$ ) in terms of slip ( $s$ ) presented in Eq. 1.1 below.

$$\tau = \tau_1 (s/s_1)^\alpha, \quad (1.1)$$

where,  $\tau_1$  is the maximum bond stress, which is proportional to the root of the compressive strength of concrete;  $s_1$  is the slip corresponding to maximum bond stress;  $\alpha$  is a factor that depends upon reinforcement type and bond conditions.

The experimental results led to certain conclusions:

- Bond–slip relationship for different diameters of reinforcement is extremely close or identical.
- The maximum peak slip value is the main factor influencing the degradation of bond strength.
- The performance of the bond is not influenced by such factors as bar diameter, embedment length and concrete cover.
- Bond stress increases slightly when the distance between two bars increases.

The proposed model by (Eligehausen et al., 1982) was convenient due to its simple numerical approach, later adopted by the global design recommendation CEB-FIP (1990), which is reflected in the modern version of Model Code 2010 (fib Model Code, 2013).

### **Model of Shima et al., 1987**

Shima et al. performed an extensive series of experiments to establish a universal bond–slip law, which can be applied to a large range of specimens. So, the chosen test specimens were of highly unequal properties and divided into five groups. Two-fold experiments were conducted, the first one was a direct pull-out test, and another one was an axial tension test, where 40 times the nominal bar diameter was the length of specimens. Along with the varied steel diameter, aluminium reinforcement (lower ductility) was also used in the experimental campaign (Shima et al., 1987).

According to the authors, the bond stress ( $\tau$ ) is a function of slip ( $s$ ) and strain ( $\varepsilon$ ). The mathematical expression derived for the bond–slip–strain relationship for any boundary condition is represented in Eq. 1.2. For long enough embedment, the bond–slip relationship can be expressed as Eq. 1.3.

$$\tau = \frac{0.73 f_c [\ln(1+5s)]^3}{1+\varepsilon \times 10^5}; \quad (1.2)$$

$$\tau = 0.9 f_c^{2/3} (1 - e^{-40s^{0.6}}), \quad (1.3)$$

where,  $f_c$  is concrete strength;  $S = 1000 s/\phi$  for Eq. 1.2 and  $S = s/\phi$  for Eq. 1.3;  $s$  is the slip and  $\phi$  is the bar diameter;

The authors have drawn the following conclusions:

- Bond–slip are formulated in a simple form by considering the influence of concrete strength and bar diameter.
- In case the strain is nil, the bond stress can be described as a function of slip only.
- Bond–slip relationships depend on the spot located along the bar, the distance from a point where strain is nil.

The authors have extended their investigation to the post-yield range of steel reinforcement, even under the application of cyclic loading.

### **Model of Kankam, 1997**

The author has reported some fundamental observations in his study, such as:

- The concrete segment between two consecutive cracks has a remarkable effect on the tensile resistance of RC members.
- In that segment of concrete, the strain in embedded reinforcement reduces depending upon two factors: crack spacing as well as concrete–reinforcement bond characteristics.
- Also, the distribution of stress in tensile reinforcement at the cracked section is entirely dependent upon concrete–reinforcement bond characteristics.
- The stress in tensile reinforcement reaches its peak at the cracked section and drops to the minimum value gradually at about the midway of two consecutive cracks.
- Bond stress is dependent on the stress in reinforcement and the slip between two materials.

The primary objective of this experiment was to extract the reinforcement strain distribution along the embedded bar. The author has carried out a double

pull-out test on the prismatic specimen of dimension 150x150x200 mm, embedded with 25 mm diameter steel reinforcement. Three different types of steel reinforcements, one mild steel and the other two types of ribbed bars (hot rolled and cold worked), were used in these experimental campaigns. A sufficient number of strain gauges were installed at the core central axis of the embedded bar to extract the reinforcement strain precisely. Such kind of test setup was used for the first time, which opened a new dimension in the field of strain monitoring techniques.

In the double pull-out test, the applied tensile load ranged from 0 to 60 kN for mild steel reinforcement and up to 98 kN for ribbed ones. Maximum bond stress was observed at about 1 MPa for mild steel RC specimens and 6 MPa for the ribbed steel RC specimens. For plain bars, the bond stress developed because of the roughness present on the surface of steel reinforcement. However, it starts falling at a certain amount of slip, which is because of the radial contraction of the bar and also due to the drop in pressure by the surrounded concrete. The empirical expression of bond stress ( $\tau$ ) and slip ( $s$ ) relationship for the plain bar is shown in Eq. 1.4, where  $\sigma_s$  is the stress in steel reinforcement.

$$\tau = (41.7 - 0.2\sigma_s)s^{0.5}; \quad (1.4)$$

$$\tau = (55 - 0.5x)s^{0.5}; \quad (1.5)$$

$$\tau = (35 - 0.3x)s^{0.5}. \quad (1.6)$$

For ribbed bars, it is observed that for a constant slip, bond stress increases as the distance from the point of loading ( $x$ ) increases. Hence, the author has proposed the local bond stress–slip relationships separately, one for cold-worked ribbed bars shown in Eq. 1.5 and another for hot-rolled ribbed bars presented in Eq. 1.6 (Kankam, 1997).

### Model of Marti et al., 1998

So far, in most of the models, bond stress depends on slip and sometimes on such additional parameters as concrete strength. But in this case, the derivation of bond stress is simplified by making it constant, independent of slip. The proposed bond stress law can be represented by Eq. 1.7. Moreover, according to the authors, once the reinforcement reaches its yield point, the bond stress drops down to half of its value, as in Eq. 1.8.

$$\tau = 2f_{ct}; \quad (1.7)$$

$$\tau = f_{ct}, \quad (1.8)$$

where,  $f_{ct}$  is the tensile strength of concrete.

The authors (Marti et al., 1998) have applied the proposed simplified model to the analysis of plastic hinges to solve deformation calculations. It was demonstrated that this simplified model can obtain approximate quantitative results in certain cases only. However, for precise crack and deformation (serviceability) analysis, the current model is not suitable for its oversimplified constant characterisation.

### Model of Model Code, 2010

The proposed bond–slip model by the current version of Model Code 2010 (will be referred to as MC2010) (fib Model Code, 2013) is capable of effectively predicting the average or maximum bond stress acting in an RC member. Categorised by two types of failures (pull-out and splitting), the relationship between bond stress and slip can be expressed and calculated through Eq. 1.9 to 1.12, which are shown in Table 1.2 and the parametric inputs are represented in Table 1.3.

**Table 1.2.** Bond stress–slip prediction (Model Code 2010, 2013)

$\tau = \tau_{max} \left(\frac{s}{s_1}\right)^\alpha$	$0 \leq s \leq s_1$	(1.9)
$\tau = \tau_{max}$	$s_1 < s \leq s_2$	(1.10)
$\tau = \tau_{max} - (\tau_{max} - \tau_f) \left(\frac{s-s_2}{s_3-s_2}\right)$	$s_2 < s \leq s_3$	(1.11)
$\tau = \tau_f$	$s > s_3$	(1.12)

**Table 1.3.** Parameters defining bond stress–slip relationship (Model Code 2010, 2013)

	Pull Out		Splitting			
	Good bond condition	Other bond condition	Good bond conditions		All other bond cond.	
			unconfined	stirrups	unconfined	stirrups
$\tau_{max}$	$2.5\sqrt{f_{ck}}$	$1.25\sqrt{f_{ck}}$	$7.0 \left(\frac{f_{ck}}{20}\right)^{0.25}$	$8.0 \left(\frac{f_{ck}}{20}\right)^{0.25}$	$5.0 \left(\frac{f_{ck}}{20}\right)^{0.25}$	$5.5 \left(\frac{f_{ck}}{20}\right)^{0.25}$
s1	1.0mm	1.8mm	s( $\tau_{max}$ )	s( $\tau_{max}$ )	s( $\tau_{max}$ )	s( $\tau_{max}$ )
s2	2.0mm	3.6mm	s1	s1	s1	s1
s3	$l_R$	$l_R$	1.2 s1	0.5 $l_R$	1.2 s1	0.5 $l_R$
$\alpha$	0.4	0.4	0.4	0.4	0.4	0.4
$\tau_f$	0.4 $\tau_{max}$	0.4 $\tau_{max}$	0	0.4 $\tau_{max}$	0	0.4 $\tau_{max}$

where,  $l_R$  is the clear spacing between two ribs.

The bond–slip model curve is illustrated in Fig. 1.4, which applies to a wide range of cases with confined and unconfined concrete. This explains:

- The rising part of the curve signifies the penetration of ribs inside the mortar identified by micro cracking and local crushing.
- For confined concrete only, the flat stage occurs, where bond stress remains constant with the increase in slip. Concrete goes through crushing and shearing off at this stage, at the proximity of the ribs.
- In the presence of a high reinforcement ratio and large concrete cover, the integrity of bond stress remains intact at this flat stage of the curve.
- The downward branch of the curve signifies the drop in bond stress, as the concrete between the ribs was already crushed at this stage.
- For the splitting failure of the unconfined concrete, a sharp decrease in bond stress can be seen (Fig. 1.4).

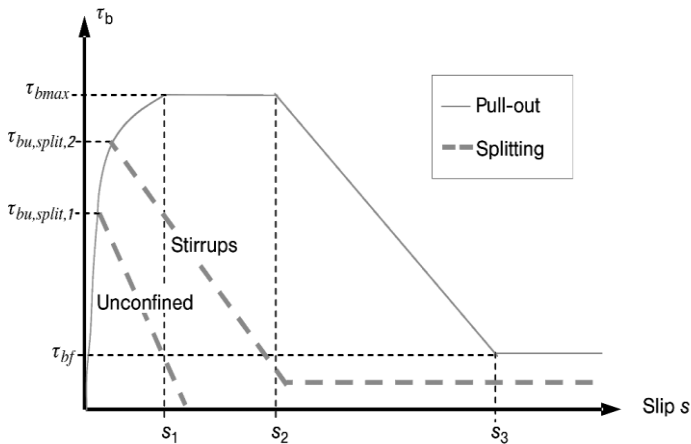


**Fig. 1.4.** Analytical bond–slip relationship under monotonic load (Model code 2010, 2013)

### Model of Hong and Park, 2012

The authors have acknowledged the crucial contribution of concrete–reinforcement interaction in the bond mechanism of RC structure. According to them, the axial tension test is more realistic than direct pull-out or double pull-out tests. In this case, the external tensile force is increased monotonically. Several specimens of rectangular and circular cross-sections were prepared with both vertically and horizontally casted bars of multiple diameters as reinforcement. Various concrete grades were provided, ranging from 30 to 50 MPa, casting lengths ranging from

764 to 964 mm and 40 mm clear cover for all the specimens. As a result, stress developed at the tensile zone for both concrete and reinforcement, as illustrated in Fig. 1.5.

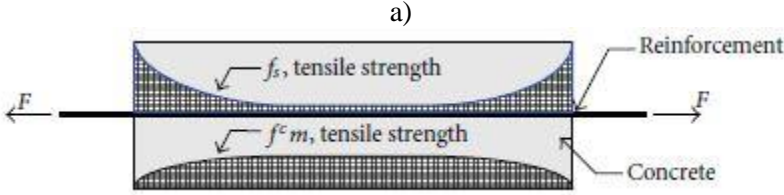


**Fig. 1.5.** Stress development under axial tension (Hong and Park, 2012)

The stress increases with the increase in applied external load until the interface reaches its transmission capacity. Beyond that, the integrity of the interface is disturbed, the bar-surrounding concrete loses its grip and unavoidable slip takes place.

The authors finally proposed a bond–slip law that works successfully under axial boundary conditions. The mathematical expression of the proposed law is shown in Eq. 1.13.

$$\tau = k f_c^{2/3} \left[ 1 - \exp \left\{ -4500 \left( \frac{s}{\phi} \right)^{1.45} \right\} \right]^{0.5} \exp \left\{ -5 \left( \frac{s}{\phi} \right) + 5.5 f_R^{0.9} \right\}; \quad (1.13)$$

$$f_R = \frac{A_R}{\pi \phi l_R}. \quad (1.14)$$

This can be noticed that the proposed bond–slip law includes concrete strength ( $f_c$ ), bar diameter ( $\phi$ ), relative rib area ( $f_R$ ) and slip ( $s$ ) as dependent parameters for determining bond stress ( $\tau$ ). Relative rib area has a notable effect on the bond–slip relationship of RC structure, which can be derived from Eq. 1.14, where  $A_R$  is the projected rib (single) area of a deformed bar and  $l_R$  is the clear spacing between two ribs. In addition, the coefficient ( $k$ ) in Eq. 1.13 depends upon the bar positioning and presence of stirrups in RC members. For example, in the case of a vertically casted bar without and with stirrup, Eqs. 1.15 and 1.16 can be followed, respectively. For horizontally casted bar without and with stirrup, Eqs. 1.17 and 1.18, respectively, provide the value of the coefficient  $k$ .

$$k = 0.2 \cdot \exp \left[ \left\{ -0.45 + 55(3.06 f_R - 0.24) \right\} \frac{100}{A_c} \right]; \quad (1.15)$$

$$k = 0.2 \cdot \exp \left[ \left\{ -0.45 + 55(3.06 f_R - 0.24) \right\} \frac{100}{A_c} \right]; \quad (1.16)$$

$$k = 0.2 \cdot \exp \left[ \left\{ -0.45 + 55 f_R \right\} \frac{100}{A_c} \right]; \quad (1.17)$$

$$k = 0.2 \cdot 0.85 \cdot \exp \left[ \left\{ -0.45 + 55 f_R \right\} \frac{100}{A_c} \right]. \quad (1.18)$$

The authors concluded that the position of the reinforcement bar has no remarkable influence on bond–slip relationships (Hong and Park, 2012). Although, the proposed bond–slip model was also validated with a bunch of experimental data, which shows a good agreement. Furthermore, the model is competent to determine accurate maximum bond stresses at the corresponding slip, which is essential for crack spacing assessment.

### Model of Barbosa and Filho, 2016

The authors have conducted multiple direct pull-out tests with various concrete strengths (20–100 MPa) and different diameters of steel reinforcement bars (16 and 20 mm). The study shows that the slipping of steel bars seriously interrupts the behaviour of the components in an RC structure. The authors also considered the effect of the phenomenon of tension stiffening and crack formation on the bond–slip relationship of RC structure. Finally, two empirical models of bond–slip relationship were proposed, which can be considered reliable as they exhibit a fair agreement with multiple experimentally obtained results. Categorised by concrete strength, Eqs. 1.19 and 1.20 represent the proposed bond–slip laws (Barbosa and Filho, 2016).

$$\tau = 19.36 s^{0.51} \text{ for } f_c < 50 \text{ MPa} \quad (1.19)$$

$$\tau = 32.58 s^{0.48} \text{ for } f_c > 50 \text{ MPa} \quad (1.20)$$

### Slip-independent bond models

In addition to the above-mentioned bond–slip laws, different bond models independent of the “slip” parameter are available in the literature. Instead, they are dependent on multiple other characteristics, like the concrete cover, concrete strength, reinforcement bar type, bar diameter, bar spacing, reinforcement ratio and embedment length (Moallemi Pour and Alam, 2016; Rao et al., 2007). The bond models of such kind are represented in the following Table 1.4 with their respective test specimen types.

Orangun et al. (1977) performed multiple beam splice tests and reported the results. The main objective of the study was to design the “development length” of an RC member through bond stress calculation. Also, investigating the influence of transverse reinforcements in initiating the specimen’s failure was the other objective of their study. Finally, the proposed bond stress model by the authors involves concrete strength, cover, bar diameter and development length (Eq. 1.21). It is also stated that the splice length and the development length are identical.

**Table 1.4.** Various bond stress models

References	Bond stress models	Equation no.	Test methods
Orangun et al., 1977	$\tau = \left[ 1.22 + 3.23 \left( \frac{c}{\phi} \right) + 53 \left( \frac{\phi}{l} \right) \right] \sqrt{f_c}$	(1.21)	Beam splice
Kemp, 1986	$\tau = 232.2 + 2.716 \left( \frac{c}{\phi} \right) \sqrt{f_c}$	(1.22)	Cantilever beams
Chapman and Shah, 1987	$\tau = \left[ 3.5 + 3.4 \left( \frac{c}{\phi} \right) + 57 \left( \frac{\phi}{l} \right) \right] \sqrt{f_c}$	(1.23)	Direct Pull-out
Darwin et al., 1992	$\tau = \left[ \left\{ 1.06 + 2.12 \left( \frac{c_{min}}{\phi} \right) \right\} \{ 0.92 + 0.08 \left( \frac{c_{max}}{c_{min}} \right) \} + 75 \left( \frac{\phi}{l} \right) \right] \sqrt{f_c}$	(1.24)	Beam splice
Al-Jahdali et al., 1994	$\tau = \left[ -0.879 + 0.324 \left( \frac{c}{\phi} \right) + 5.79 \left( \frac{\phi}{l} \right) \right] \sqrt{f_c}$	(1.25)	Direct Pull-out
Esfahani and Rangan, 1998	$\tau = 4.9 \left( \frac{c/\phi + 0.5}{c/\phi + 3.6} \right) f_{ct} \quad \text{for } f_c < 50 \text{ MPa}$	(1.26)	Beam end
	$\tau = 8.6 \left( \frac{c/\phi + 0.5}{c/\phi + 5.5} \right) \quad \text{for } f_c > 50 \text{ MPa}$ where, $f_{ct} = 0.55 f_c$	(1.27)	
Harajli, 2004	$\tau = 0.75 \sqrt{f_c} \left[ \left( \frac{c}{\phi} \right)^{2/3} \right] \quad \text{for } f_c < 48 \text{ MPa}$	(1.28)	Beam splice
	$\tau = 0.95 \sqrt{f_c} \left[ \left( \frac{c}{\phi} \right)^{2/3} \right] \quad \text{for } f_c > 48 \text{ MPa}$	(1.29)	
Desnerck et al., 2010	$\tau = \left[ 1.87 + 0.35 \left( \frac{c}{\phi} \right) \right] \sqrt{f_c}$	(1.30)	Beam splice
Siempu and Pancharthi, 2018	$\tau = \left[ 0.21 + 0.26 \left( \frac{c}{\phi} \right) + 6.32 \left( \frac{\phi}{l} \right) \right] \sqrt{f_c}$	(1.31)	Direct pull-out

Kemp (1986) carried out an extensive experimental campaign with 157 numbers cantilever beams. The specimens were categorised based on the presence and positions of stirrups. It was discerned that crack patterns at the failure of the beams vary based on the concrete cover. Eventually, the author proposed Eq. 1.22, where the bond stress depends on the concrete cover, strength and bar diameter only.

Chapman and Shah (1987) performed their experiments on 56 numbers pull-out specimens. Among these, 46 RC specimens were reinforced with deformed bars and the rest with plain bars. Various bar diameters and embedment lengths were used in this experimental campaign. According to the authors, the concentric pull-out test is the most realistic exhibition of the internal mechanism of an RC beam. They concluded that the embedment length and concrete strength control the mode of failure of the member for a deformed bar. Also, concrete strength has a notable impact on the bond strength in the case of members with long embedment. Based on these observations, the authors proposed a bond stress model (Eq. 1.23) where the dependent parameters are concrete strength, cover, bar diameter and development length.

Darwin et al. (1992) developed a bond stress model that accurately captures the influence of bar spacing, bar diameter, concrete cover and steel stress. The authors indicated that the force in steel reinforcement increases linearly with concrete cover and bar spacing but the same in a nonlinear manner in the case of development length as well as cross-section area of the reinforcement bar. Based on these, the authors modified the previous expression by Orangun et al. (1977) and the newly proposed Eq. (1.24).

Al-Jahdali et al. (1994) relied on a direct pull-out test for investigating the bond strength of RC structures. They carried out pull-out tests on 36 short RC specimens with various bar diameters (ranging from 14–20 mm), embedment lengths and concrete strengths (ranging from 42–78 MPa). The authors found a linear relationship between the tensile load and slip until yielding. Although, large embedment length produces excessive slip at the post-yielding stage. The mathematical equation of the proposed bond model is presented in Eq. (1.25).

Esfahani and Rangan (1998) performed the beam-end tests with 45 RC specimens. They are reinforced with two various types of steel bars based on their rib face angles and a large range of concrete compressive strength. The embedment length of the specimens was kept fairly long for investigating the bond stress variation throughout the member length. Interestingly, the crushing of concrete was noticed at the proximity of the ribs for a major group of the specimens. It is probably because of lower concrete strength (compressive). Finally, the proposed bond model can be used for normal-strength concrete (Eq. 1.26) and also high-strength concrete (Eq. 1.27) by changing the coefficient.

Harajli (Harajli, 2004) investigated the average bond strength at the reinforcement bar failure, which is embedded in both normal and high-strength concrete specimens. Established on the extensive beam-splice experiments, the authors proposed two different bond models for normal (Eq. 1.28) and high-strength concrete (Eq. 1.29) separately. It was reported that the distribution of average bond stress is highly non-uniform. It is much more pronounced for high-strength concrete compared to normal one.

Desnerck et al. (2010) studied the local bond–slip relationship for self-compacting concrete instead of conventional concrete. The authors preferred to perform beam tests to evaluate a realistic bond stress distribution. The specimens were prepared of different bar diameters and embedment lengths. The obtained test results exhibit higher bond strength for self-compacting concrete as compared to the normal one. The analytical model for the bond strength is based on bar diameter, concrete strength and cover, presented in Eq. 1.30.

Siempu and Pancharthi (2017) introduced an analytical model of the bond strength of concrete which was prepared with recycled aggregate obtained from demolition wastes. A handful of pull-out specimens were tested with various bar diameters, embedment lengths and water-cement ratios. From the obtained result, the authors proposed a mathematical model (Eq. 1.31) to obtain average bond stress in terms of concrete strength, cover, bar diameter and embedment length. Based on this literature review, a detailed parametric analysis of bond stress and slip was done and will be discussed in the next section.

### 1.2.3. Parameters Influencing Bond–Slip Relationships

Multiple factors influence the concrete–reinforcement bond, which can be categorised as concrete properties (strength, cover), reinforcement properties (type, diameter) and structural characteristics (bar spacing, transverse bar, and embedment length) etc. (ACI Committee 408, 2003; Hadi, 2008; Moallemi Pour and Alam, 2016; Rao et al., 2007). Such parameters and their influences on the bond–slip relationship of RC structure are discussed in detail:

- *Concrete strength* is one of the predominant influencers of concrete–reinforcement interaction, hence the correlation of bond stress and slip in an RC structure. It is reported that the rise in concrete strength increases the bond stress throughout specimen length (Al-Jahdali et al., 1994). In the higher grade of concrete, the strength of the binding paste is higher. It results in stronger bonding between concrete and reinforcement, and hence larger load is required to break the bond between the two materials. When the compressive strength of concrete escalated from 26.1 to 48.5 MPa and from 48.5 MPa to 68.7 MPa, an 8–13% increase in bond stress was observed (Siempu and Pancharthi, 2018).

- *Bar diameter* plays a significant role in concrete–reinforcement bond–slip relationships. Eventually, the bond stress decreases with a rise in bar diameter. Reinforcement bars with higher diameters offer a larger contact area between the concrete and the reinforcement surface. It enhances the area of non-uniform stress transfer from the surface of the reinforcement bar to the surrounding concrete, resulting in a drop in the bond stress between the two materials. A notable fall in bond stress (18–19%) was reported with the increment in bar diameter from 12 to 16 mm (Siempu and Pancharathi, 2018). For the same reason, the slip value (which corresponds to the maximum bond stress) also escalates with the increment in bar diameter (Desnerck et al., 2010). However, the Model Code 2010 (fib Model Code, 2013) does not include the influence of reinforcement bar diameter in the calculation of the bond–slip relationship.
- *Concrete cover* and its influence on bond–slip relationship between concrete–reinforcement is significant for normal-strength concrete only. Concrete–reinforcement interactions are often studied in confined RC specimens with large concrete (clear) covers. Such cases usually prevent the splitting phenomenon in RC structures (Al-Jahdali et al., 1994). Commonly lower concrete covers are in general practice, which may produce splitting cracks on the concrete surface. However, splitting cracks have serious unfavourable impacts on the bond mechanism (Kanazawa et al., 2017). It was noticed that the bond stress drops with an increase in concrete cover. The primary cause of this can be the radial crack formation around the ribs due to the stress transfer mechanism between reinforcement and concrete. A 3–9% fall in bond stress was reported for the rise in concrete cover from 16 to 40 mm (Siempu and Pancharathi, 2018). However, this drop in bond stress can be minimised by providing transverse reinforcements in the RC structure. On the other hand, the concrete cover has no remarkable impact on the bond–slip relationship for high-strength concrete.
- *Development length* is also termed embedment length in different literature. Few studies were found investigating the influence of embedment length on the bond–slip mechanism of an RC structure. Al-Jahdali et al. (1994) and Siempu and Pancharathi (2017) reported a decrease in bond stress due to the increase in embedment length. Also, a similar pattern was observed by Chapman and Shah (1987). The latter also stated that the impact of the embedment length on the bond strength could be minimised by lowering the compressive strength of concrete. The longer the development length, the larger the slip at failure, as the energy required to pull the bar from the RC specimen increases (Siempu and Pancharathi, 2017).

The comprehensive review of the existing bond models indicates the disparity among them. It is seen that the majority of the models have been derived based on the data primarily obtained from pull-out tests, followed by full-beam tests and beam-end tests etc. The practical limitations associated with these tests are outlined at the beginning of Section 1.2.1. Besides the employment of unrealistic testing methods, a significant proportion of the models present an average bond stress distribution that does not accurately depict the intricate behaviour at the interface between concrete and reinforcement. A critical model comparison (Siempu and Pancharathi, 2017a) has shown that the model by Chapman and Shah (1987) underestimates the bond stress for specimens with lower embedment lengths (2.5 to 5 times diameter). The models proposed by Orangun et al. (1977), Harajli (2004) and Darwin et al. (1992) are sourced from beam splice tests but under-estimates the bond stress from pull-out specimens. The model by Al-Jahdali et al. (1994) was sourced from a pull-out test but under-estimates bond stress in the case of specimens with lower diameters. Another notable concern about the models' contradiction pertains to the inconsistency in defining the influencing parameters of bond stress. In this regard, significant diversification can be observed across the existing models. For example, the models by Marti et al. (1998), Model Code 2010 (2013), Barbosa and Filho (2016), Shima (1987) etc., do not consider bar diameter in their respective models. This implies that the bar diameter has zero impact on the bond stress, which contradicts the models proposed by Kemp (1986), Hong and Park (2012), Desnerck (2010) etc. Similarly, the models by Siempu and Pancharathi (2018), Darwin et al. (1992), Al-Jahdali et al. (1994) etc., indicate the influence of embedment length on the bond stress, whereas the models by Eligehausen et al. (1982), Kemp (1986), Harajli (2004) etc. completely deny it. Notably, some researchers consider “slip” as a significant factor influencing bond stress (Kankam, 1997; Mirza and Houde, 1978; Nilson, 1971). Considering that the prediction of reinforcement strain is a crucial aspect in the serviceability analysis of RC structures, a comparative study of existing bond–slip models has been conducted based on this criterion (Dey, Bado, and Kaklauskas, 2022). Referring to the experimental results of the reinforcement strain distribution in an RC tie, the model by Shima et al. (1987) exhibits the prediction with an average relative error of 6.4%, which is the closest. It is followed by the increasing relative error, which is 10.4% found by Barbosa and Filho model, 16.4% – by Kankam (1997) model, 19% – by Model Code 2010 (2013), 95% – by Nilson (1971) model, and 128% – by Mirza and Houde model (1978).

Considering the significant diversification and contradiction observed among the existing bond–slip models, it becomes apparent that there is a need for a novel model that employs an effective methodology with a realistic approach to accurately depict the true behaviour at the interface between concrete and reinforcement. The next sub-chapter discusses the different strain monitoring tools and their performances.

### 1.3. Strain Monitoring Techniques from Embedded Bar

Apart from the test methods of obtaining bond–slip relationship, another key task is to calculate the local slip data throughout the reinforcement bar. For this purpose, accurate and precise strain data extraction from reinforcement is essential. This sub-chapter discusses the different strain monitoring tool and their performance in terms of extracting local strains from reinforcement bars embedded into the concrete.

As previously discussed, the double pull-out test is one of the modern and realistic experimental methods to investigate the concrete–reinforcement interaction. It provides a lucid and pragmatic view of real-life RC tensile members in design practice. The fundamental approach of this experimental method is based on strain recording data of the reinforcement bar embedded inside the concrete. In such experiments, strain distribution data are analysed to obtain the bond–slip relationship of an RC specimen. The result also exhibits the force-transfer operation at the interface, bond mechanics and also invention of novel bond–slip models (Scott and Gill, 1987). Therefore, it is essential to extract precise and accurate bar strain data from the experimental setups. For that purpose, some potential strain monitoring tools are discussed in the following sections.

#### 1.3.1. Electrical Strain Gauge Sensors

Electrical strain gauge sensors emerged as a strain monitoring tool in the last few decades of the twentieth century. Aimed at extracting the strain distribution data from the core of the embedded reinforcement, these strain sensors needed to be deployed inside the bar. Initially, a steel reinforcement bar is prepared by dividing it into longitudinal half sections, followed by a groove (2 mm × 10 mm) on the internal surface. Then, the sensors were fixed with glue inside the groove, wired and soldered (Fig. 1.6). Now, after joining the two halves, a full bar section was prepared for further casting and testing. This technique was initially applied on short (200 mm) RC tensile specimens (Houde, 1974; Kankam, 1997). Afterwards, the extensive use of electrical strain gauges in the field of strain monitoring has been noticed in the current century. This technique was successfully used in the investigations on bond stress and local bond–slip models (Jakubovskis and Kaklauskas, 2019; Kaklauskas, Sokolov et al., 2019) and also in some studies on parametric analysis (Lee et al., 2016; Wenkenbach, 2011). Moreover, the benefits of this tool were used in the topics of bond deterioration (Jakubovskis and Kaklauskas, 2021) and the effect of corrosion on it (Masukawa, 2012). However, the installation part of this tool is delicate, time-consuming and laborious

(Kaklauskas, Sokolov et al., 2019). Although these electrical sensors offer extremely accurate and precise strain data, it fails to monitor at small distant points with low spatial resolution.

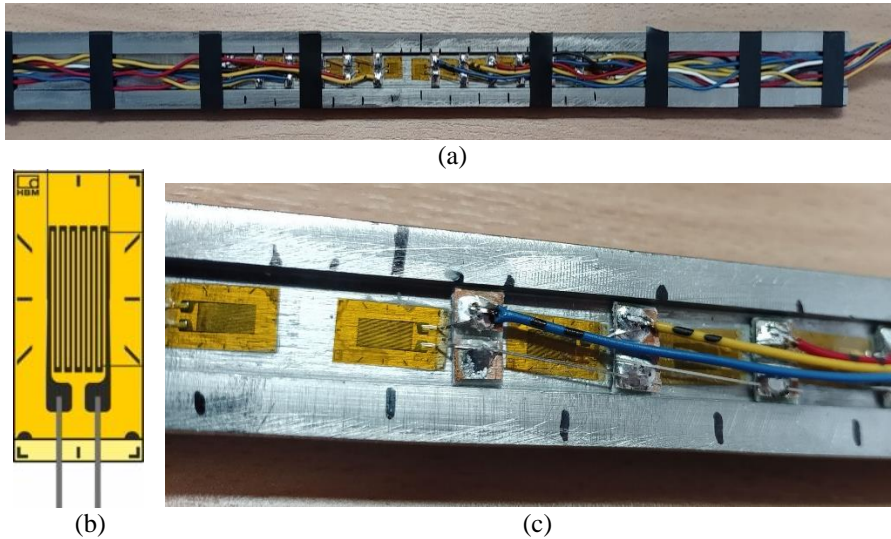


**Fig. 1.6.** Strain gauge sensors as a strain monitoring tool: (a) sensors fixed into the groove of reinforcement bar, (b) graphical illustration of the sensor device and (c) enlarged view of the sensor installation bar with required soldering and wiring (Kaklauskas et al., 2019)

### 1.3.2. Fibre Bragg Grating

As a simpler but highly expensive alternative, Fibre Bragg Grating (FBG) came up as single-wire optical fibre (Fig. 1.7). It consists of up to 286 FBGs in a single wire, which can be pasted inside a small groove (1 mm × 1 mm) on the surface of the reinforcement bar (Kenel et al., 2005). From the beginning of this century, FBG optical fibre was extensively used as a multifaceted health monitoring tool in the marine industry (Friebele, 1998), aviation industry (Di Sante, 2015) and infrastructure industry (Capoluongo et al., 2005; Kerrouche et al., 2009). Using its advantage of multipoint measurement, FBG was successfully used in measuring early shrinkage strain in a mortar (Slowik et al., 2004), creep and shrinkage strain (Yazdizadeh et al., 2017) in concrete and real-time strain (Lau et al., 2001; Leng et al., 2006) from the core of composite structures. Kaklauskas et al. (2019) effectively used this tool in the investigation of bond stress and slip in short RC tensile members.

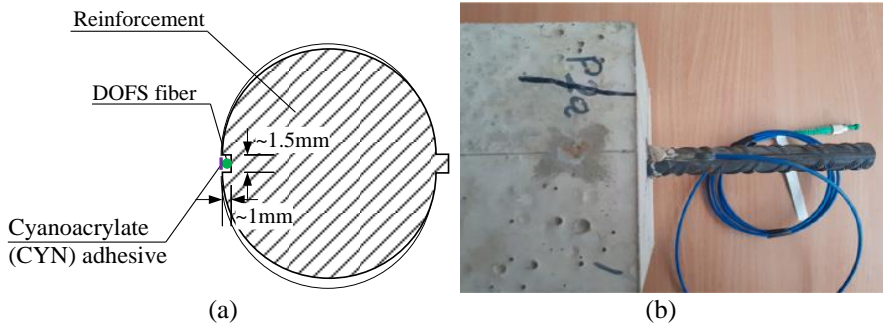


**Fig. 1.7.** FBG optical fibre as strain monitoring tool:  
 (a) graphical illustration of bar cross-section and  
 (b) enlarged view of test specimen (Kaklauskas et al., 2019)

### 1.3.3. Distributed Optical Fibre Sensor

Distributed optical fibre sensor (DOFS) is the most modern and sensitive tool that emerged recently in the field of health monitoring. A human hair-like ( $125\ \mu\text{m}$ ) thick, glass-made fibre can be glued easily on the surface of the reinforcing bar (Fig. 1.8).

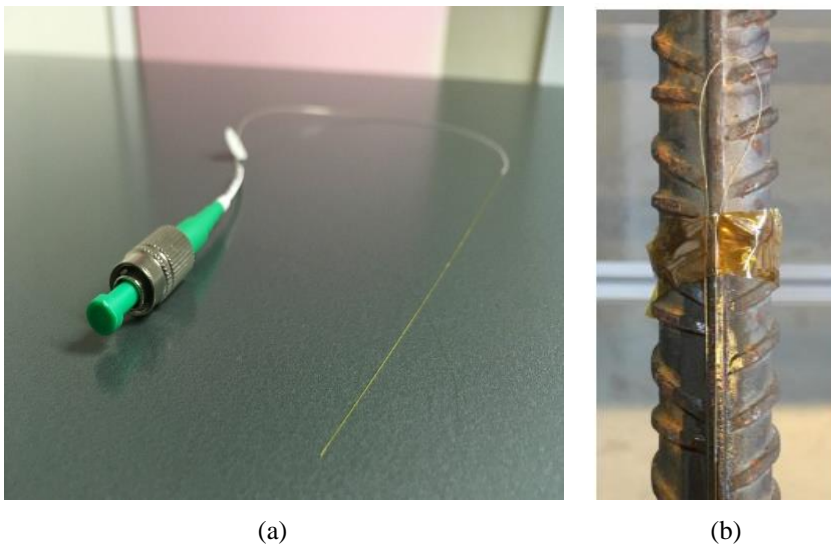


**Fig. 1.8.** DOFS as strain monitoring tool: (a) hair-like thick optical fibre and  
 (b) enlarged view of the DOFS attached bar (Bado et al., 2021)

In fact, no groove is required to accommodate the fibre on the bar surface. A DOFS fundamentally functions based on light propagation (back-scattered) through the glass medium. Based on the working principle, DOFS can be categorised into three sections. First, Raman scattering is inelastic in nature and used in the detection of physical and chemical features of materials and variation temperature (Cantarero, 2015). Second, Brillouin scattering is sensitive to strain and temperature. This kind of DOFS has an extended functioning range of several kilometres. This feature enables it to be capable of executing large-scale practical investigations in the geotechnical field (Zeni et al., 2015) and the infrastructure industry (Hong et al., 2017). Later, this tool was successfully used in various crack monitoring projects of RC structural members (Deif et al., 2010) and also for strain monitoring in steel bridge girders (Yoon et al., 2011). Lastly, Rayleigh scattering is the most suitable for investigations in a laboratory environment. It is especially capable of fault detection and strain extraction with high-resolution output (Bado et al., 2020). This tool was widely used in the research field for strain extraction from embedded reinforcement bars (Bado et al., 2020; Davis et al., 2016) as well as from the surface of RC structural members (Henault et al., 2012; Villalba and Casas, 2013).

An experimental comparative study was performed by Dey et al. (2020) with above mentioned three strain monitoring tools to check their performance capabilities and to determine their pros and cons. It is reported that electrical strain gauges provided the most accurate and consistent strain distribution data, but it is limited in terms of multipoint monitoring. Furthermore, the installation process, specifically the tasks of wiring and soldering, entails a high level of delicacy and demands a significant amount of time (Kaklauskas, Sokolov et al., 2019). Some inconsistency was found in the output data by FBG optical fibre, though it was easier in terms of setup and installation. In addition, it is important to note that the preparation of FBG-equipped wire requires access to a specialised factory facility with advanced capabilities. Furthermore, it is a costly endeavour (Capoluongo et al., 2005; Friebele, 1998). Finally, the DOFS technique was found to be the quickest and simplest process among all others. Also, it provided almost consistent strain distribution data with extremely high resolution. This technique demonstrates the intelligent approach to early detection of malfunctions, specifically deformation and cracking in the RC members (Henault et al., 2012; Hong et al., 2017). However, certain anomalies were also noted in the strain profiles observed through DOFS arrangements, probably due to its over-sensitive nature (Deif et al., 2010). To prevent unnecessary noise in the output, it is highly recommended to handle the fibre with great care and ensure the application of a protective coating (Mattia Francesco Bado, Casas and Kaklauskas 2021).

Despite its delicate and time-consuming nature, the strain gauge sensor has been identified as the most consistent and accurate option among the available alternatives. Considering the aforementioned observations from the literature, the author has opted for the strain gauge sensor as the strain monitoring tool in the ongoing experimental campaigns.

## **1.4. Conclusions of the First Chapter and Formulation of the Dissertation Tasks**

The extensive literature review provides some revelations that are essential for understanding the concrete–reinforcement interaction by means of the serviceability performance of RC structures:

1. The standard pull-out test used for assessing bond behaviour in reinforced concrete structures is associated with several limitations. Additionally, the bond models derived from these tests provide averaged bond stress values rather than local bond stress values. A review of existing models reveals their inadequacy in accurately predicting the bond behaviour of reinforced concrete structures under diverse conditions. Conversely, the double pull-out test, which involves recording reinforcement strains along the bonded length, overcomes these limitations and offers a more reliable approach for evaluating bond behaviour.
2. Several studies have identified numerous factors that can impact bond–slip, and these factors are often inconsistent. This inconsistency can confuse readers when trying to determine the true parameters that influence bond stress.
3. Among the existing strain monitoring tools, the strain gauge sensors are the most consistent and accurate in performance. Some inconsistency and over-sensitivity were noticed in the case of FBG and DOFS, respectively.
4. The literature review indicated a need for a new model that employs an effective methodology with a realistic approach to accurately depict the true behaviour at the interface between concrete and reinforcement.

Therefore, the present study is dedicated to creating a precise bond–slip model between concrete and reinforcement concerning the serviceability of RC structures, along with an effective and reliable strain-derivation tool for model validation purposes. Established from this background, the author has set the following objectives and the associated tasks to fulfil the current study:

- A handful number of double pull-out tests in the laboratory by varying parameters, such as bar diameter, concrete strength, cover, etc.

- 
- Establish a MatLab program for the mathematical calculations to derive the bond–slip relationships from a test extracted reinforcement strain distribution rooted in the stress transfer approach.
  - Establish a reverse MatLab program to determine the strain distribution from a given bond–slip law. This automated program can be used as an effective validation tool to check the reliability and credibility of an existing bond–slip model.
  - Finally, to develop an analytical bond–slip model for RC structures in relation to significantly influencing parameters. This model can be effectively used for the serviceability analysis of RC structures.



# 2

---

## **Experimental Campaigns for Steel Strain Monitoring in Reinforced Concrete Members**

This chapter manifests the author's experimental endeavour towards the formation of bond–slip relationships between concrete and reinforcement in RC structural members. The first segment of the chapter explains the entire experimental procedure starting from the installation process of electrical strain gauge sensors (used for strain extraction from the reinforcement embedded inside concrete) to the double pull-out tests in the laboratory. It also includes the geometrical properties of test specimens and material characteristics for three experimental campaigns. The second part manifests the strain distribution result as the output of the experimental campaigns. The final part demonstrates the derivation of the bond–slip relationship from the experimentally extracted strain distribution profile. A systematic algorithm, along with its background and applications, are presented in detail. The research findings are published in the author's publications Dey et al. (2021b) and Dey et al. (2021c).

## 2.1. Experimental Campaigns

This sub-chapter presents all the experiments performed during this study in detail. The experiments are mainly divided into three different campaigns, which are executed at different times. All three experimental campaigns were conducted in the laboratory of the Civil Engineering Faculty of Vilnius Gediminas Technical University. This part aims to narrate the experimental campaigns through the potential performance of strain gauge sensors. Geometrical details of specimens, material properties, sensor installation mechanism and double pull-out test setup are elaborated on in the subsequent sections.

### 2.1.1. Specimens' Geometry

RC tensile members (or RC prisms) are often used in laboratory investigations due to their ease of use and capability to represent the mechanics at the concrete–reinforcement interface. It provides a fairly good and realistic reflection of strain distribution in the tensile zone and internal force distribution at the concrete–reinforcement interface of an RC structure (Ruiz et al., 2007). Such specimens were also used to depict the deformation, cracking and bond behaviour of RC structures (Bado, Casas, Dey et al., 2021; Jakubovskis and Kaklauskas, 2021).

The dimensions of RC specimens (hereinafter – RC ties) were chosen based on two essential circumstances. Usually, the formation of a new crack (primary) can interrupt the bond–slip investigation, as it significantly alters the mechanism at the concrete–reinforcement interface (Gribniak, Jakubovskis et al., 2018). To prevent the risk factor of crack formation, the lengths of the specimens were kept shorter than its mean crack spacing (Fig. 2.1). The latter can be computed by considering the bar diameter and reinforcement ratio (Kaklauskas et al., 2017; Kaklauskas, Ramanauskas et al., 2019). In terms of output, these short-length RC ties are capable of bypassing any major distortions in their strain profile due to transversal cracks. Furthermore, the bond–slip behaviour of an RC structure is influenced by many factors, such as bar diameter, rib pattern, concrete strength, cover etc. (Dey, Valiukas et al., 2022). Also, the cover/diameter ratio directly classifies the confinement status of concrete. Model code 2010 (fib Model Code, 2013) stated the cover/diameter ratio must be greater than 5 for a well-confined concrete. Some studies also suggested the cover/diameter ratio should be higher than 2.5 to avoid splitting failures (Cairns and Jones, 1995; García-Taengua et al., 2014). Despite being short, the embedment lengths of the specimens were intentionally varied to examine their impact on the internal behaviour of RC prisms. Based on a diverse range of influencing parameters, the geometrical characteristics of experimental RC ties were designed.

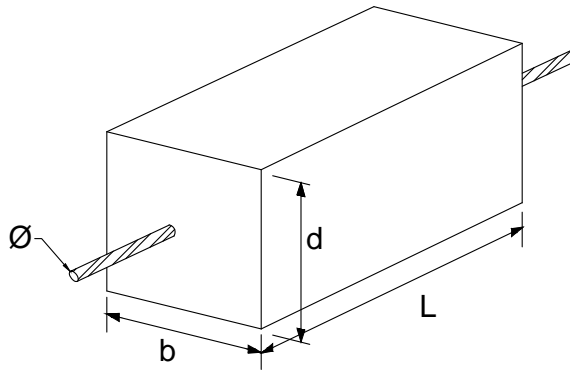


**Fig. 2.1.** Standard geometry of an RC tie

The author carried out three experimental campaigns, all of which contained short RC ties of different geometrical specifications. The primary objective was to obtain strain distribution from the steel reinforcement bar, utilising electrical strain gauge sensors. Through this experimental endeavour, the author was able to:

- understand the force transfer mechanism at the concrete–reinforcement interface at different stress levels;
- assess the stability and consistency in the performance of electrical sensors and also conduct its comparative study with alternative strain monitoring tools such as FBG and DOFS;
- learn the distribution pattern of concrete strain, bond stress and slip;
- obtain a bond–slip relationship between reinforcement and concrete; and
- finally, to establish a bond–slip model concerning the serviceability of an RC structure.

The three experimental campaigns consist of a total of 14 RC ties reinforced with three different bar diameters ( $\emptyset$ ). Among these, 20 mm  $\emptyset$  bar in five specimens, 16 mm  $\emptyset$  bar in six specimens and 25 mm  $\emptyset$  bar in three specimens were provided. The geometrical characteristics of all the specimens are mentioned in Table 2.1 and illustrated in Fig. 2.2.

As shown in Fig. 2.2a, campaign 1 consists of five RC ties, all of which are reinforced with  $\emptyset 20$  reinforcement bars. In this campaign, the first two specimens, 150×150×210\_D20 and 150×150×240\_D20, were cast in the first batch of concrete, and the other three were cast in the second batch of concrete. Campaign 2 was prepared with only one batch of concrete. In this group, all four RC ties were equipped with  $\emptyset 16$  reinforcement bars but of different dimensions (Fig. 2.2b).

Campaign 3 was the combination of 5 RC ties, among which two were prepared with  $\emptyset 16$  and 3 with  $\emptyset 25$  reinforcement bars (Fig. 2.2c). This campaign was also cast in two separate batches of concrete, as mentioned in Table 2.1.

**Table 2.1.** Geometry of RC ties

Campaign	Batch	Specimen	b or d (mm)	L (mm)	$\emptyset$ (mm)
1	I	150×150×210_D20	150	210	20
		150×150×240_D20	150	240	20
	II	200×200×270_D20	200	270	20
		200×200×330_D20	200	330	20
		200×200×390_D20	200	390	20
2	I	120×120×210_D16_I	120	210	16
		120×120×210_D16_II	120	210	16
		150×150×270_D16	150	270	16
		200×200×330_D16_I	200	330	16
3	I	200×200×330_D16_II	200	330	16
		100×100×150_D16	100	150	16
	II	150×150×150_D25	150	150	25
		200×200×270_D25	200	270	25
		200×200×330_D25	200	330	25

Each mentioned RC tie is referred further through a code, in which the first pair of numerical values indicate the cross-section in mm, followed by the specimen length in mm and the numeric value after “D” signifies the diameter of the embedded reinforcement bar inside the concrete in mm. For example, the code 150×150×210\_D20 refers to the RC tie of cross-section 150×150 (mm), length 210 mm and reinforced with a 20 mm bar. The properties of the materials used in these campaigns are discussed in the next section.

The primary reasons for not casting control twin specimens are the involvement of a high level of expertise, diligent effort, substantial time commitment, and significant economic investment. Undoubtedly, the production of such specimens in large numbers posed a considerable challenge for the author. Furthermore, prior experience working with three identical short RC specimens (Jakubovskis and Kaklauskas, 2019) has consistently demonstrated remarkably similar output, with the results nearly coinciding.

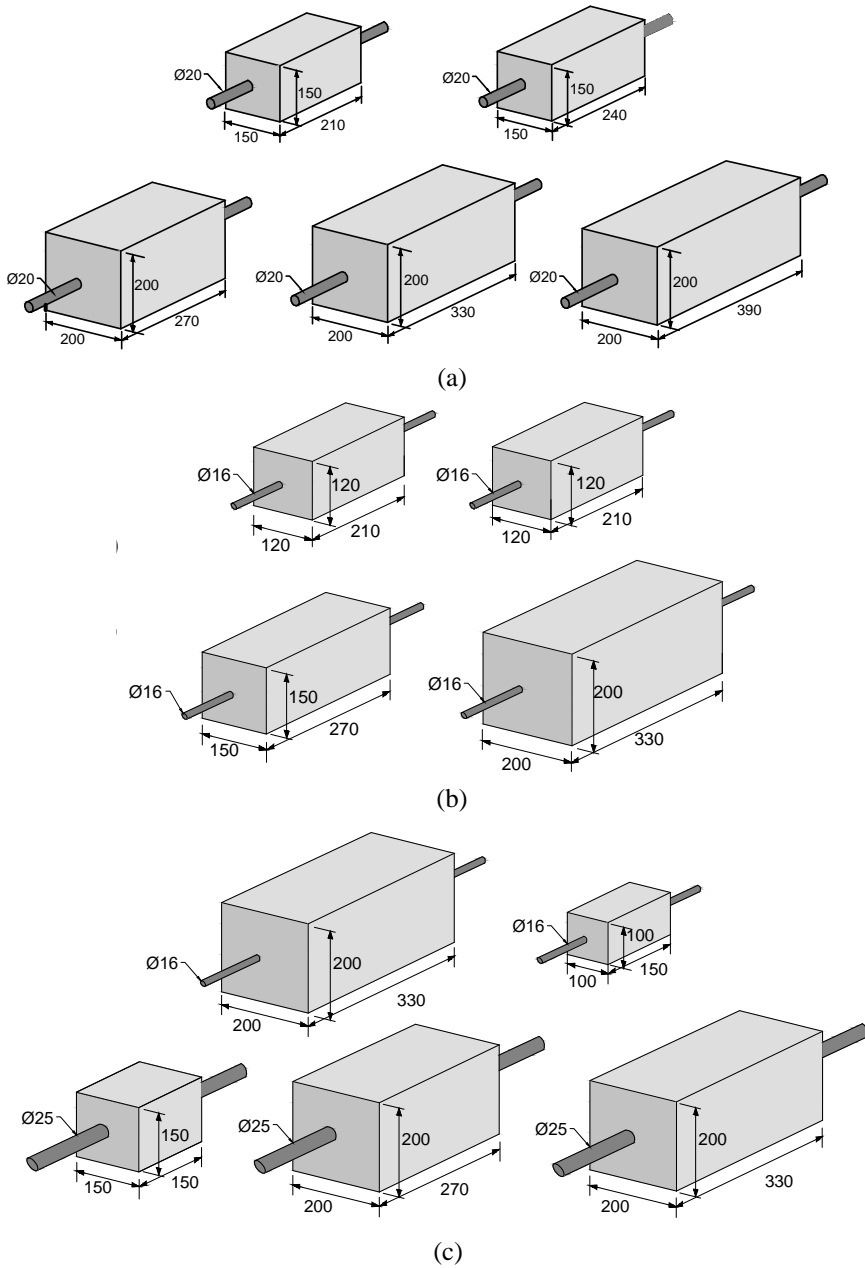


**Fig. 2.2.** Geometrical illustrations of experimental RC ties for: (a) campaign 1, (b) campaign 2, and (c) campaign 3

In addition, it is worth mentioning that the present investigation represents an initial component of a larger study that encompasses numerous similar experimental campaigns and numerical simulations. Given the complexities involved in conducting such tests, expanding the parametric ranges posed a challenge for the author. However, it is important to note that this study is still in progress, and in the future, additional tests that cover a wide range of parameters will be conducted.

### 2.1.2. Material Properties

The required concrete for the casting in all experimental campaigns was prepared in the laboratory by machine mixing. The raw materials used in this concrete preparation are grade 42.5R Ordinary Portland Cement (OPC), natural fine aggregate (sand) and coarse aggregates (sourced from crushed granite) of grade 0/4 mm and 5/8 mm, respectively. Additionally, polycarboxylic ether polymer was added as a super-plasticiser to reach the aspired workability of concrete. It is worth mentioning that multiple batches of concrete were produced in some experimental campaigns. The common chemical composition of all concrete batches in different campaigns is mentioned in Table 2.2.

**Table 2.2.** Chemical compositions of concrete

Chemical Compositions	Quantity in (kg/ m <sup>3</sup> )
Ordinary Portland Cement (42.5R)	425
Fine aggregate (0/4 mm)	1165
Coarse aggregate crushed (5/8 mm)	715
Water-cement ratio (0.35–0.45 by mass)	150–190
Concrete plasticiser (1.0–1.5% of cement mass)	4.25–6.4

It is worth mentioning that at the post-de-moulding stage, the entire concrete surface of RC ties was properly covered with wet clothes for curing. Additional concrete members (cubes, cylinders and prisms) were also kept in curing for 28 days to extract mechanical properties. Subsequently, concrete cubes of dimensions 150×150×150 mm were used to evaluate split tensile strength, concrete cylinders of 150 mm in diameter × 300 mm in height were used for compressive strength and concrete prisms of dimensions 100×100×400 mm were used for flexural strength of concrete. The modulus of elasticity of concrete was calculated following Eurocode 2 (Standard, 2004). Besides, steel reinforcements of Ø16, 20 and 25 mm and grade S500 were tested to obtain their yield strength and modulus

of elasticity. The properties associated with the mechanical behaviour of concrete and steel reinforcement are shown in Table 2.3 and Table 2.4, respectively.

It can be noticed that despite similar chemical compositions, the achieved mechanical properties of concrete vary for different batches. This is because of the varying water–cement ratio and volume of plasticisers added to the mixture. Diversified mechanical properties of concrete were certainly desired for the parametric analysis of a wide range of concrete strengths.

**Table 2.3.** Mechanical properties of concrete

Concrete casting		$f_c$ (MPa)	$f_t$ (MPa)	$f_{fl}$ (MPa)	$E_c$ (GPa)
Campaign 1	Batch I	44.8	3.1	6.5	33.8
	Batch II	71.3	4.5	6.6	41.5
Campaign 2	Batch I	65.0	3.8	6.4	35.5
Campaign 3	Batch I	63.3	4.6	6.9	37.2
	Batch II	67.5	4.6	7.9	35.2

where  $f_c$  is compressive strength,  $f_t$  is split tensile strength and  $f_{fl}$  is the flexural strength of concrete.  $E_c$  represents the elastic modulus of concrete.

**Table 2.4.** Mechanical properties of reinforcement steel

Bar properties	Ø20	Ø16	Ø25
$f_y$ (MPa)	486	405	353
$A_s$ (mm <sup>2</sup> )	315	201	491
$A_{groove}$ (mm <sup>2</sup> )	40	40	40
$A_{s,mod}$ (mm <sup>2</sup> )	275	161	451
$E_s$ (GPa)	201.7	194.5	189.5

where  $f_y$  is yield strength,  $A_s$  is cross-section area and  $E_s$  is the modulus of elasticity of steel reinforcement.

As mentioned earlier, the loss of area in the steel bar was considered during the post-processing of data. A new modified reinforcement area ( $A_{s,mod}$ ) was calculated by deducting the area of a groove ( $A_{groove}$ ) from the actual cross-section area of the bar ( $A_s$ ). The testing method is discussed in the next section.

As previously stated, the current campaigns serve as the preliminary phase of a broader study; the scope of this dissertation was limited to a specific range of concrete strength. However, it is important to emphasise that the future phase of the study will undoubtedly address the full spectrum of concrete strength parameters, including both normal and low strength.

### 2.1.3. Strain Gauge Installation

The most delicate and laborious part of the specimen preparation phase is undoubtedly the installation of strain gauge sensors inside the core of the reinforcement. However, the optimistic side is the uninterrupted and consistent performance of the strain gauge sensors, as they are strain-sensitive and fixed inside the core of the embedded reinforcement bars (Dey, Valiukas et al., 2022).

First, a steel reinforcement bar was longitudinally cut in half, followed by the milling of a groove at its internal surface (Fig. 2.1.a). The groove dimension was kept 2 mm deep and 10 mm wide to accommodate the devices along with their wirings. The particular type of strain gauge sensor used in these experimental campaigns, named LY11-6/350, is manufactured by HBM, Germany (Fig. 1.7b). Each strain gauge sensor has physical dimensions of about 6 mm x 10 mm. These devices contain one measuring grid and are characterised as linear type. Also, it holds the capacity of normal resistance of 350  $\Omega$ . The author has tried to place the sensors as close as possible inside the groove to achieve the maximum number of strain monitoring points. However, for accommodating wires associated with each sensor, it was not possible to provide a centre-to-centre gap lesser than 20 mm between two consecutive devices (Fig. 2.3).



(a)



(b)

**Fig. 2.3.** Installation of strain gauge sensors: (a) glued inside the bar groove, (b) with wiring and soldering

As shown in Fig. 2.3 a, the sensors were extremely carefully fixed inside the longitudinal bar groove with the help of cyanoacrylate glue. It is worth mentioning that the arrangement of strain gauge sensors inside the reinforcement groove was in perfect symmetry to track and compare the output data from two sides with respect to the centre of the longitudinal section of the bar. After fixing the sensors, soldering of each with required wirings were executed consciously (Fig. 2.3b). Finally, the sensor-equipped half part of the steel bar was adhered with its counterpart by means of two-component epoxy glue. The modified bar was then clamped and kept at rest for a few hours before the next process.

This is worth bearing in mind that the loss of sectional area in the reinforcement bar due to the milling of the groove is considered in the computation of the cross-sectional area and elastic modulus of the reinforcement steel. It is explained in the materials properties section in detail.

#### 2.1.4. Double Pull-out Test

Relying on the simplicity and pragmatic approach, a double pull-out test was chosen over other alternatives for all the RC ties by using a Universal Testing Machine (UTM), as shown in Fig. 2.4.

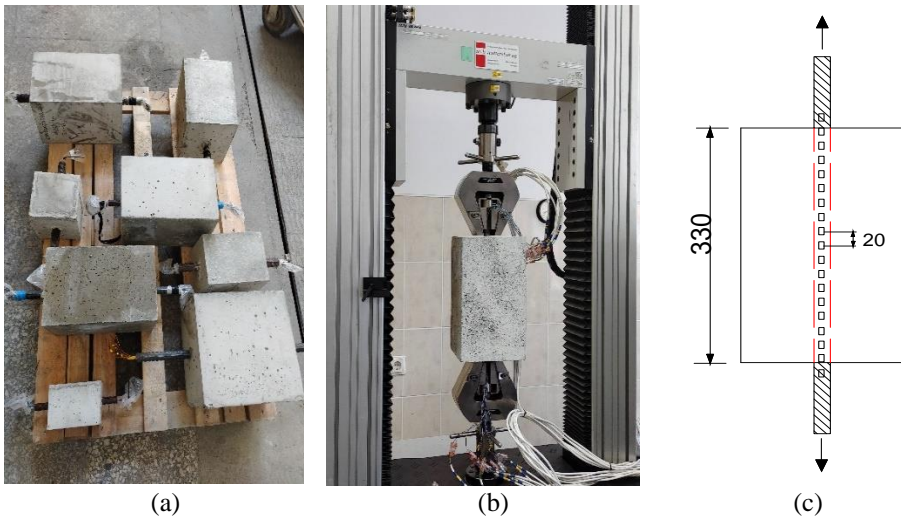


**Fig. 2.4.** Few RC ties in the laboratory: (a) before testing, (b) during a double pull-out test, (c) a graphical illustration of a sample specimen of 330 mm in length

The double pull-out test is designed to apply tensile force to both sides of the RC specimen, graphically illustrated in Fig. 2.4c. In this test, the reinforcement

bar is securely held by machine grips on both sides (Fig. 2.4b), enabling the transmission of the applied force. It is important to highlight that the machine grips do not come into direct contact with the concrete surface; their role is solely to transmit the tensile force to the reinforcement bar, which subsequently transfers the force to the concrete. For example (Fig. 2.4c), a 330 mm long RC specimen consists of 19 strain gauge sensors, each spaced 20 mm apart. Notably, the terminal sensors are positioned beyond the edges of the concrete, strategically placed to measure the strains exclusively produced in the reinforcing bar without interference from the concrete. The grips were also carefully positioned to minimise their impact on the terminal sensor and the vertical joint where two halves of the reinforcement bar meet.

The tensile load was monotonic and employed in a displacement-controlled manner. The testing machine was well equipped with a digitally controlled load application and data procuring system. The loading rate was restricted to 0.4 mm per minute till the reinforcement bar reached its yielding limit. The grip between the reinforcement bar terminals and the machine was carefully handled to avoid any interruption by wires, which may result in distortion in the data output. In the end, the experimental data output was collected by the device ALMEMO 5690-2 (Fig. 2.5a), assisted by the data acquisition software AMR WinControl for the first experimental campaign. For campaigns 2 and 3, the author has used the data recorder device QUANTUM<sup>X</sup> CX22B-W (Fig. 2.5b) along with HBM-CATMAN as data acquisition software.



(a)

(b)

**Fig. 2.5.** Strain sensor data recording devices: (a) ALMEMO 5690-2 for campaign 1, (b) QUANTUM<sup>X</sup> CX22B-W for campaigns 2 and 3

## 2.2. Strain Distribution Results

The author has demonstrated the double pull-out experiments executed in the laboratory in the previous sub-chapter. This sub-chapter aims to represent the output result of all the experiments.

Monitoring the strain data at different locations of the embedded reinforcement was the principal function of the strain gauge sensors. From the double pull-out tests, the steel strain values were extracted at multiple load levels through the data acquisition systems. The obtained strain data offers a graphical representation, including spatial changes in distribution throughout the reinforcement length (Fig. 2.6). It is worth mentioning that the design of RC ties and the placement of strain gauge sensors were done in such a way that the symmetry in output to the mid-section of the reinforcement bar could be considered. For this reason, the strain distribution at the left and right portions of the bar was averaged and then mirrored to obtain a full strain distribution profile. For demonstration purposes, a random RC tie ( $200 \times 200 \times 390\_D20$ ) was chosen as a case study specimen from experimental campaign 1. Its strain distribution output is illustrated, as shown in Fig. 2.6.

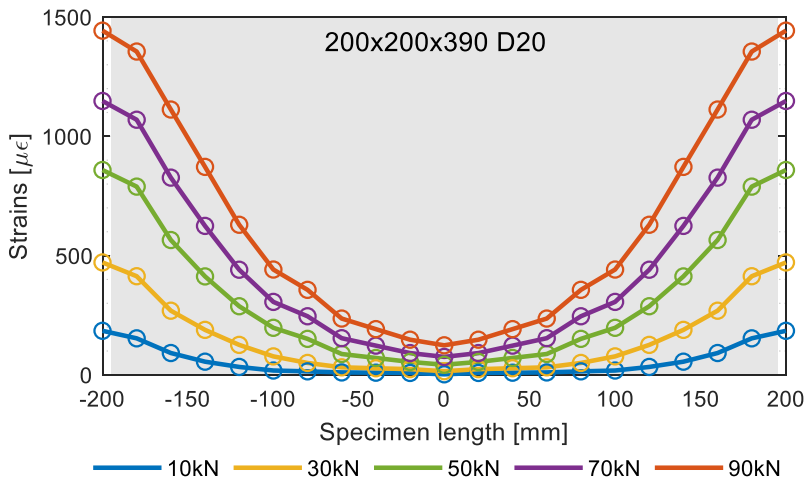


**Fig. 2.6.** Strain distribution profile of the case study specimen  $200 \times 200 \times 390\_D20$  at multiple load levels

Here, the obtained strain profiles at five different load levels (from 10 kN to 90 kN) are displayed sequentially. It is seen that, at lower load levels, such as 10 kN, the strain distribution varies from almost 0 to 150  $\mu\epsilon$  whereas, at 90 kN load, the same varies from 150 to 1440  $\mu\epsilon$ . It can be anticipated that with the increase in load level, the slopes of the strain profiles become steeper (Fig. 2.6).

This outcome has a direct influence on the bond characteristics. An increase in the slope of the strain profile signifies an increase in bond stress. The small circles on the strain profiles indicate the position of strain monitoring points where the sensors were placed (20 mm apart). In this particular RC tie, a total of 21 numbers of strain gauge sensors were installed; hence 21 strain monitoring points are indicated with small circles. The solid grey background of the plot signifies the concrete block, which is 390 mm long for the current specimen. It can be observed that the terminal sensors (both sides) were positioned outside of the concrete block. This was intentionally designed to detect the strains at the bare bar.

Similarly, the strain distribution profiles for the other 13 members are displayed in Fig. 2.7.

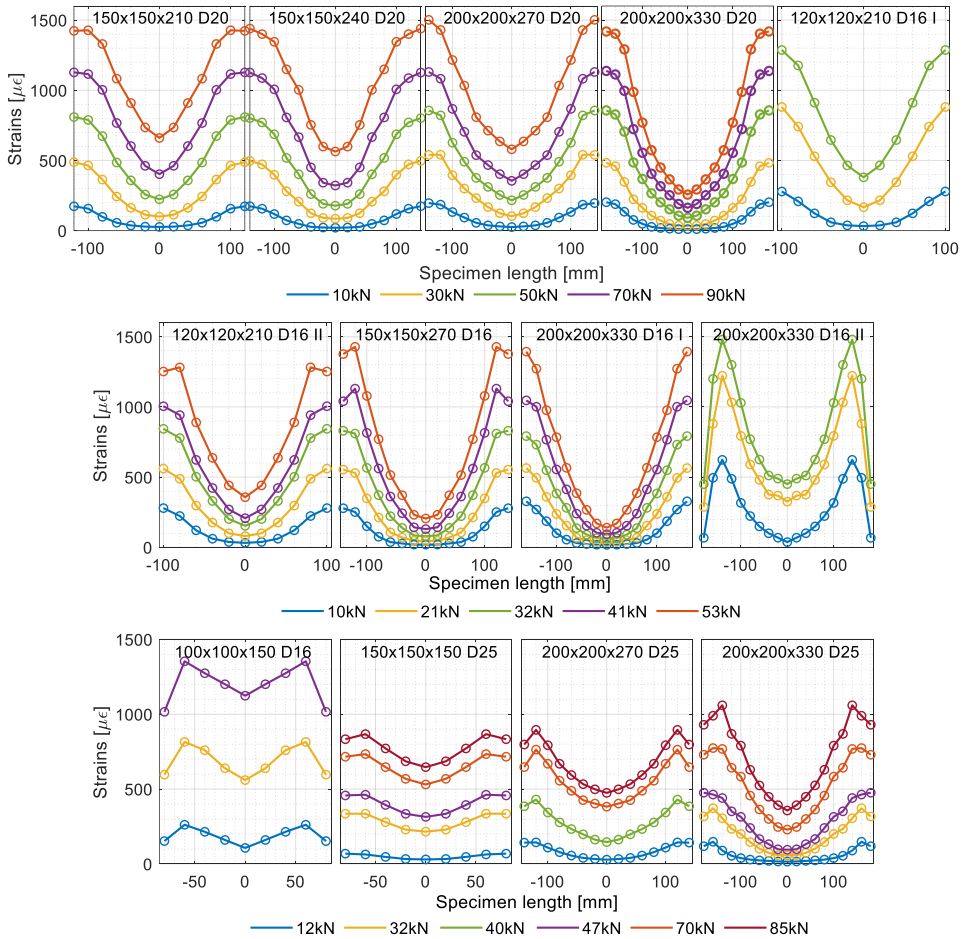


**Fig. 2.7.** Strain distribution profiles of 13 RC ties at multiple load levels

In most cases, the strain distribution curves are observed to flatten out towards the specimen edges (conceptually considered as cracks). It happens due to the damage in the bond at the proximity of the cracks (Kaklauskas, 2017). This particular area of bond deterioration can be referred to as a de-bonding zone; extremely limited study has been done on this part (Jakubovskis and Kaklauskas, 2021).

An almost similar pattern of strain distribution can be seen for all RC ties of diverse characteristics (Fig. 2.7). Only the magnitude of strain value differs based on the load levels and specimen features. During the experiments, the tensile load was applied approximately to the maximum yielding capacity of respective reinforcement bars. That is why the non-uniform variation in legends (load levels) of Fig. 2.7 can be noticed. For example, the maximum load level for specimen 200×200×270\_D20 is 90 kN, but for 200×200×330\_D16\_I maximum load was provided as 53 kN. Moving to the variation in strain magnitude, the maximum strain attended by a  $\varnothing 20$  specimen (200×200×270\_D20) is 1500  $\mu\epsilon$  at load 90 kN and by a  $\varnothing 25$  specimen (200×200×330\_D25) is 1060  $\mu\epsilon$ , at almost similar load level (85 kN). In comparison, a  $\varnothing 16$  specimen (200×200×330\_D16\_II) projects a maximum of 1490  $\mu\epsilon$  at only 32 kN load level. This disparity in strain magnitude can be seen probably because of elongation in reinforcement bars. Lowering the bar  $\varnothing$  means a lower cross-section area and provides lower resistance to tensile load which results in higher elongation and hence higher strains in reinforcement bars. For all  $\varnothing 25$  specimens and a few  $\varnothing 16$  specimens (100×100×150\_D16 and 200×200×330\_D16\_II), noticeable decreases in strains are observed at both ends of the strain distribution curves. This phenomenon is likely attributed to the influence of gripping or clamping forces applied in close proximity to the terminal sensor. Specifically, in these cases, the machine clamping was positioned very near the lateral surface of the concrete. However, it is worth noting that this observation presents an intriguing area for future research.

Due to the low spatial resolution, the experimentally extracted strain distribution curves are not smooth and unfit to use directly as an input in further complex mathematical calculations. Therefore, to make the curves smoother, the author has increased the spatial resolution by performing a polynomial fitting operation of a specific degree. Fig. 2.8 displays the polynomial approximations of strain distribution curves for the case study specimen 200×200×390\_D20 at (a) 4<sup>th</sup> degree, (b) 6<sup>th</sup> degree and (c) 8<sup>th</sup> degree. The resulting strain distributions exhibit dissimilarities due to differences in the degree of polynomial approximation. An inappropriate degree can notably alter the pattern of strain distribution; hence a correct choice of degree is pivotal in terms of performance analysis (Bado, Casas and Kaklauskas 2021).

The higher degree polynomial approximations substantially capture the loss of concrete-steel compatibility near the edge of the specimens, which can be noticed in the extra-flattened end part of the strain profiles (Fig. 2.8c).

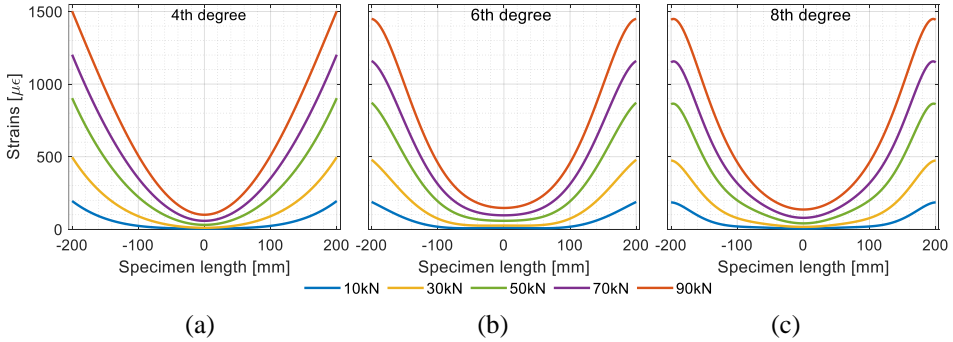


**Fig. 2.8.** Different polynomial approximations of strain profiles for the specimen  $200 \times 200 \times 390\_D20$  at multiple load levels: (a) 4<sup>th</sup> degree (b) 6<sup>th</sup> degree and (c) 8<sup>th</sup> degree

Sometimes, it amplifies the flattened part, which imparts an immense effect on the bond stress and slip distributions in that area (Bado, Casas and Kaklauskas 2021). Additionally, in the case of relatively rough strain profiles (often obtained due to largely spaced sensor arrangements or the presence of flawed sensors), higher-degree polynomial approximations can produce a curvy and twisted output, which would not be well represented. Concerning such possibilities, a lower degree (4<sup>th</sup>/5<sup>th</sup>) of polynomial approximation is advantageous, which is followed in the upcoming calculations.

In this way, a polynomial approximation of strain distribution curves was performed for all the specimens at various load levels. The next sub-chapter will demonstrate the derivation of bond–slip relationships from strain profiles along with its mathematical background.

### 2.3. Derivation of Bond–Slip Relationship

The primary objective of the ongoing experimental campaigns is to determine the local bond–slip relationship between concrete and reinforcement. However, the experimental double pull-out test only provides local strain measurements from the core of the reinforcement bar embedded in the concrete at specific load levels. To derive the local bond stress and slip, further calculations are required. In this regard, the current research relies on a realistic and widely accepted stress transfer approach. This approach is fundamentally based on the mechanism of force transfer from the

reinforcement bar to the surrounding concrete. The following subsections present a detailed calculation methodology and its application for deriving the bond stress and slip, along with their respective influences at the concrete–reinforcement interface, using the extracted strain profiles obtained from the experimental campaigns.

### 2.3.1. Theoretical Approach

The stress transfer approach was followed for further calculations to determine bond stress and slip from the strain distribution data. According to this theory, bond stress is directly governed by the strain in reinforcement. It was noticed in Fig. 2.6 that the gradient in the strain profile is becoming steeper with the increase in loads. It can rightly direct to the bond stress as a function of strain gradient (Ruiz et al., 2007) shown in Eq. 2.1.

$$\tau(x) = \frac{\emptyset E_s}{4} \frac{d\varepsilon_s(x)}{dx}, \quad (2.1)$$

where  $\tau$  represents the bond stress,  $E_s$  is the modulus of elasticity,  $\varepsilon_s$  represents the local strain in the reinforcement bar and  $\emptyset$  is the bar diameter. Here,  $x$  specifies the considered co-ordinate of the section. Based on Eq. 2.1, local bond stress was determined from the reinforcement strains for further calculations.

The stress transfer theory also considers the concrete–reinforcement interface directly influences the strains in both materials through the slip (fib Model Code, 2013). The latter can be defined as the relative displacement between concrete and reinforcement bars. This concept puts this approach in an advantageous position in terms of obtaining the bond–slip mechanism in RC structures. Furthermore, the slip was obtained by calculating the area between the concrete and reinforcement strain curves. However, this is a complex mathematical calculation for which the author has developed a program in MatLab. It determines bond stress and slip relationship from a given strain distribution profile. The mathematical steps of this algorithm are explained below.

Consider the total transmitted tensile load is  $P$ , which is resisted by a concrete-driven force ( $N_c$ ) and a reinforcement-driven force ( $N_s$ ). From the concept of equilibrium of forces, the transaction can be shown in Eq. 2.2. Also, the resisting forces by the materials can be expressed in terms of strains acting on it, represented as Eq. 2.3, where  $\varepsilon$ ,  $E$  and  $A$  are the local strains, elastic modulus and cross-section area, respectively. The underscores  $c$  and  $s$  denote concrete and steel reinforcement, respectively.

$$P = N_c + N_s; \quad (2.2)$$

$$P = \varepsilon_{c,i} E_c A_c + \varepsilon_{s,i} E_s A_s \mid i = 1, 2, \dots, n. \quad (2.3)$$

At the initial stage, the program demands some input data, such as the specimen's geometric characteristics and the experimentally obtained strain distribution data with its' corresponding (monitoring) location throughout the specimen length. Assuming symmetry at both sides with respect to the mid-section, the program takes the average strain value and considers half of the block for further calculations. As the strain gauge sensors were placed at a 20 mm gap (low spatial resolution), the experimental strain distribution profile first needs to be smoothened (discussed in the previous sub-chapter). In that regard, the program runs a polynomial fitting operation, where the user can define the degree of the polynomial curve. At this stage, the program divides the half block into  $n$  number of imaginary segments, each of length  $\Delta x$ , to enhance the spatial resolution and to precise the mathematical calculation. Here,  $i$  denotes a particular segment, which can range from 1,2,3 ... to  $n$ . It must be noted that underscores  $i - 1$  and  $i$  signify the starting and ending sections of a particular segment  $i$ .

Now, for a study case segment (for the  $i$ -th section), bond stress ( $\tau_i$ ) can be evaluated from Eq. 2.1. Eq. 2.3 can be written as Eq. 2.4 for generalising the transmitted load ( $P$ ) for the  $i^{\text{th}}$  section. As a next step, concrete strain in the study section ( $\varepsilon_{c,i}$ ) was determined from Eq. 2.5. Here,  $\varepsilon_{s,i}$  and  $\varepsilon_{s,i-1}$  denote the strain in the reinforcement bar at the current and the previous section.

$$E_s A_s \varepsilon_{s,i-1} = \varepsilon_{c,i} E_c A_c + \varepsilon_{s,i} E_s A_s; \quad (2.4)$$

$$\varepsilon_{c,i} = \frac{E_s A_s \varepsilon_{s,i-1} - E_s A_s \varepsilon_{s,i}}{E_c A_c}. \quad (2.5)$$

Now, the average of the strain deviations between reinforcement and concrete in the study section and the previous section can provide the change in the slip between these two consecutive sections ( $\Delta s_i$ ). It is the trapezoidal area between the reinforcement and concrete strain curve through the length  $\Delta x$ , hence can be expressed as Eq. 2.6. Next, from Eq. 2.7, the slip in the study section ( $s_i$ ) can be obtained by deducting the change in slip ( $\Delta s_i$ ) from the previous section slip ( $s_{i-1}$ ).

$$\Delta s_i = \left( \frac{\varepsilon_{s,i} + \varepsilon_{s,i-1}}{2} - \frac{\varepsilon_{c,i} + \varepsilon_{c,i-1}}{2} \right) \Delta x; \quad (2.6)$$

$$s_i = s_{i-1} - \Delta s_i. \quad (2.7)$$

Similarly, these calculations were performed at every segment until it reached the mid-section of the specimen. At the mid-section, the obtained slip value is supposed to be zero ( $s_n = 0$ ).

Based on these concepts and equations, an algorithm was developed in the MatLab program, which automatically calculates the local bond stress and local

slip from the reinforcement strains effectively. The algorithm in terms of a flowchart is shown in Fig. 2.9.

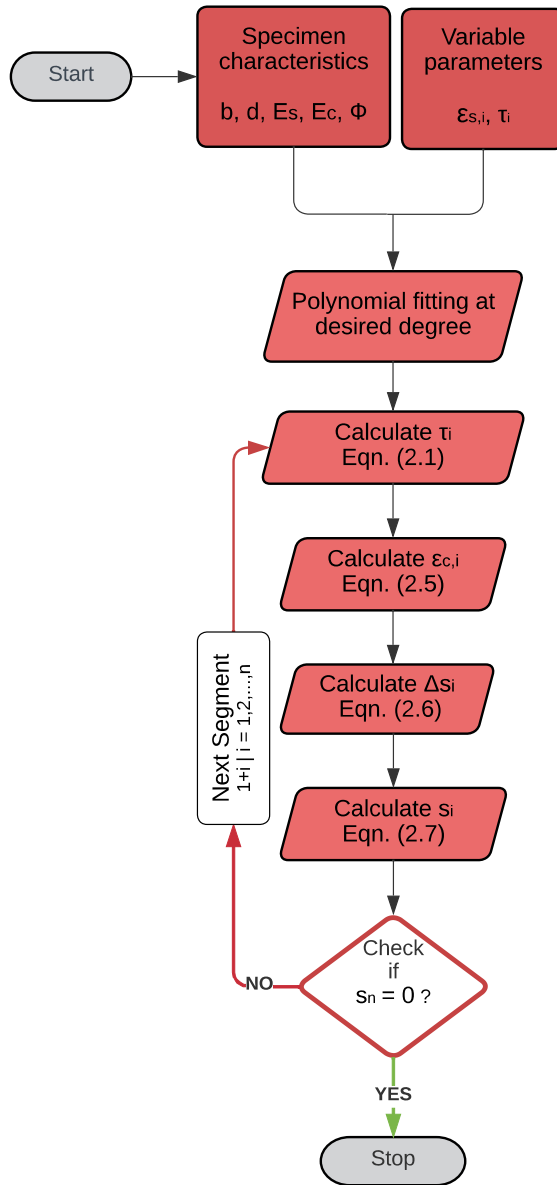


**Fig. 2.9.** Flowchart of the algorithm aimed at determining bond stress and slip on the ground of reinforcement strains

It is worth mentioning that in the algorithm flowchart, the segments are considered starting from the edge till the mid-section of the specimen. The concrete strain at the beginning of the first segment and the slip at the end of the last segment are considered to be zero. Also, note that the failure type of the RC ties was pull-out and a “good” bond condition between concrete and reinforcement was assumed.

The algorithm asks for the geometric characteristics of a specimen, such as its width, depth, modulus of elasticity of reinforcement steel and concrete and bar diameter. Also, the strain distribution data with corresponding monitoring points must be entered. After the polynomial fitting at a suitable degree, the algorithm moves to the first segment, where the beginning section is referred to as  $i = 0$ , and the ending section is referred to as  $i = 1$ . In the beginning section, concrete strain is assumed as zero ( $\varepsilon_{c,0} = 0$ ), and reinforcement strain ( $\varepsilon_{s,0}$ ) is taken from the input data. It must be noted that the entire first segment has constant bond stress ( $\tau_1$ ); hence it is calculated by Eq. 2.1 as the next step of the algorithm. Afterwards, the strain in concrete at the ending section of the first segment ( $\varepsilon_{c,1}$ ) is calculated through Eq. 2.5. For this calculation, reinforcement strain at the previous and current sections ( $\varepsilon_{s,0}$  and  $\varepsilon_{s,1}$ ) are needed, which are known from the experimental output.

Then, the algorithm calculates the change in slip ( $\Delta s_1$ ) for the current section and is followed by the calculation of the slip ( $s_1$ ) by Eqs. 2.6 and 2.7, respectively. Then, the program asks for a check if,  $s_n = 0$ ? For a negative response, the program records the current data and moves to the next segment by considering  $i = i + 1$ . But for a positive response, the program saves all the calculated data and stops the algorithm. The next section demonstrates the application of this tool to calculate bond–slip relationships from experimentally extracted strain distribution profiles.

### 2.3.2. Bond–Slip Relationship Results

To demonstrate the practical application of the above-mentioned tool, the author has chosen the study case RC tie specimen 200×200×390\_D20. The initial step was to input specimen characteristics, such as  $b = 200$  mm (specimen width),  $d = 200$  mm (specimen depth),  $\phi = 20$  mm (bar diameter),  $E_c = 41.5$  GPa (modulus of elasticity of concrete),  $E_s = 201.7$  GPa (modulus of elasticity of steel). Also, the experimentally extracted strain distribution data at multiple load levels (10 kN, 30 kN, 50 kN, 70 kN and 90 kN) were inserted. As discussed before, the program runs a polynomial approximation on the strain distribution profiles. Conforming to the next step of the algorithm, the bond stress ( $\tau_1$ ) was calculated for the first segment. Further, the program calculates the concrete strain ( $\varepsilon_{c,1}$ ) at that segment.

From the reinforcement and concrete strains, the change in slip ( $\Delta s_1$ ) was evaluated, followed by the slip ( $s_1$ ) at the first segment. Then, after checking (if  $s_n = 0$ ?), the program records the data and moves to the next segment. Similarly, the data of bond stress, concrete strain and slip were recorded and presented throughout the specimen length ( $L = 390$  mm) for multiple load levels, as seen in Fig. 2.10.

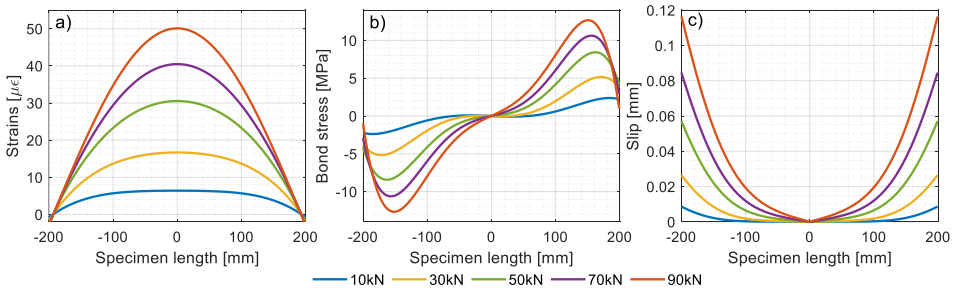


**Fig. 2.10.** Experimental results for the study case specimen 200×200×390\_D20:  
(a) concrete strains, (b) bond stress, and (c) slip at multiple load levels

Evidently, the bond stress at the mid-section of the RC tie is zero and gradually evolves with the distance from the centre (Fig. 2.10a). Maximum bond stresses were achieved at a section close to the specimen edge, followed by a gradual drop towards the specimen edge. This is because of the presence of a de-bonding zone at the proximity of the edge. It is also noticed that the de-bonding zone length increases with the load levels. The maximum bond stresses can be observed as 2.9 MPa, 5.2 MPa, 8.8 MPa, 11 MPa and 12.8 MPa for 10 kN, 30 kN, 50 kN, 70 kN and 90 kN load levels, respectively. This is probably due to the growing strain gradients with the increments in loads (Fig. 2.6). In the stress transfer approach, the bond stress between concrete and reinforcement controls the load-sharing mechanism between two materials. Hence, the variation in concrete strain can be noticed (Fig. 2.10b). The strain distribution pattern in concrete is opposite in nature than it was seen for reinforcement in Fig. 2.6.

At the mid-section, concrete holds the maximum strain, which gradually decreases along both the left and right wings and finally becomes zero at the specimen edges. Maximum concrete strain can be observed at 50 µε for 90 kN load level (Fig. 2.10b). Though minuscule in comparison to reinforcement strains, concrete strain is essential to calculate the relative displacement between two materials. Graphically, from the area between two curves (concrete and reinforcement strains), the slip was calculated and presented in Fig. 2.10c. Like bond stress, slip is usually zero at the mid-section of the specimen and increases towards the edge of the specimen. The gradient of the curves also increases with the increase in

loads. Maximum slip can be noticed as 0.12 mm for 90 kN load level at the edge of the specimen. The obtained bond stress and slip data were plotted together, and the bond–slip relationships at multiple load levels are presented in Fig. 2.11. Due to the symmetrical characteristics of the RC prisms, only half portion of the specimen was selected to effectively demonstrate the local bond–slip relationship.

Considering the symmetry in the specimen’s geometry with respect to its mid-section, half of the profile was taken to demonstrate the bond–slip relationship. In Fig. 2.11, the bond–slip curves display a parabolic pattern through all the load levels. Such local bond stress–slip format exhibits a more realistic and accurate manifestation of concrete–reinforcement interactive mechanics than the classical format (Dey, Valiukas et al. 2022). Each bond–slip curve is fundamentally divided into two parts: ascending and descending. The former branch represents the inherent features of the materials, whereas the latter part signifies the cracking effect on the bond degradation near the cracks.

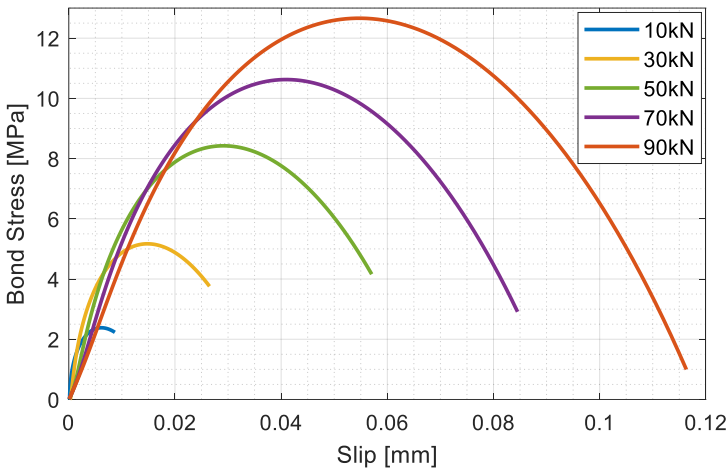


**Fig. 2.11.** Derived results of bond–slip relationships for the study case specimen 200×200×390\_D20 at multiple load levels

Fig. 2.11 shows that the ascending branches of bond–slip curves (at multiple loads) follow almost similar gradients. It indicates similar bond–slip law is being followed in the whole analysis. Although there is a marginal decline in the bond–slip curves’ ascending branches, it is apparent that higher load levels may cause damage to the concrete surrounding the reinforcement ribs. This damage can lead to a decrease in bond stress and an increase in slip, thus contributing to the observed degradation.

As anticipated earlier, the peak bond stresses are increasing gradually with the increase in load levels (2.9 MPa for 10 kN to 12.8 MPa for 90 kN) due to the gradual increase in reinforcement strain gradient with loads. Also, the slip corresponding to the peak bond stress increases with the increase in loads. For example, the slip at maximum bond stress at 30 kN load is 0.015 mm, whereas the same for 90 kN load is 0.055 (Fig. 2.11). It indicates more relative displacements between concrete and reinforcement at higher load levels. Similarly, the bond–slip relationships for all 13 RC tie specimens were evaluated through the mentioned algorithm (Fig. 2.9) and displayed in Fig. 2.12. Each subplot in Fig. 2.12 represents each specimen (RC ties) and its bond–slip curves at multiple load levels.

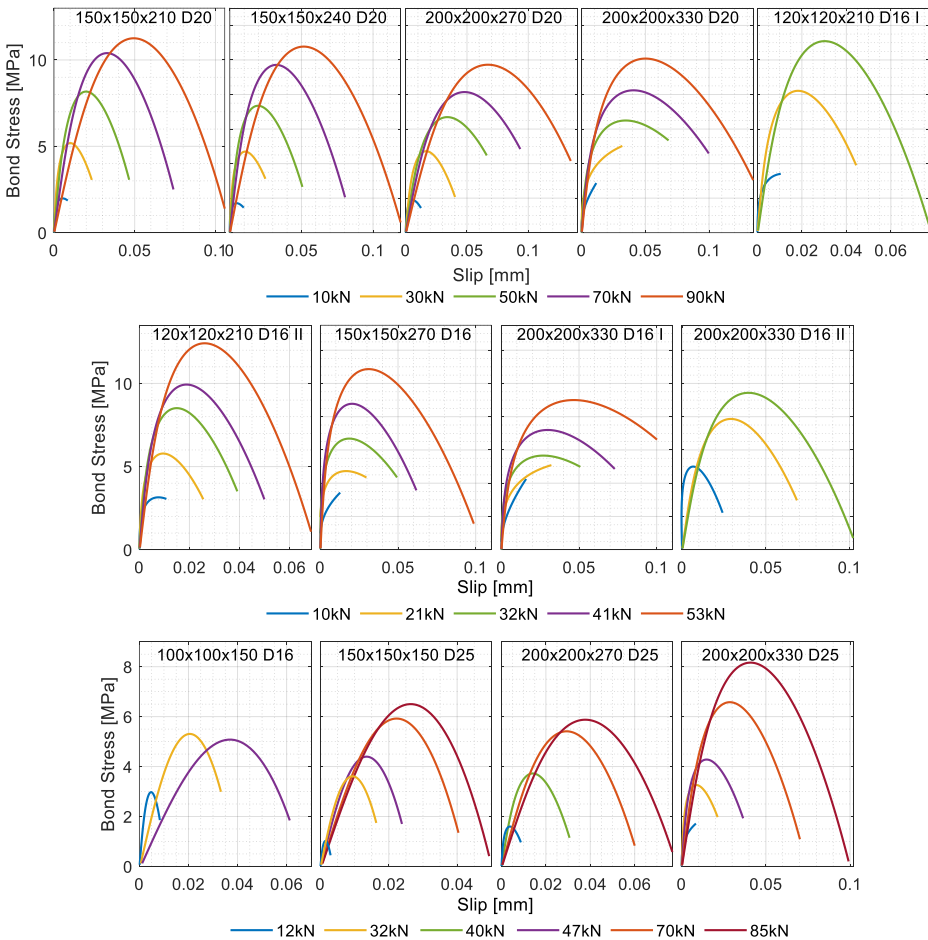


**Fig. 2.12.** Derived bond–slip relationships of 13 RC ties at multiple load levels

A nearly similar pattern of bond–slip can be noticed for all the RC tie specimens. On average, specimens with  $\varnothing 25$  bar have shown lower bond stresses than others (8 MPa at 85 kN load level for specimen  $200 \times 200 \times 330\_D25$ ) because of their comparatively lower strain distribution profiles (Fig. 2.7). On the other hand,  $\varnothing 20$  specimens produced more slip at similar load levels than  $\varnothing 25$  ones (the maximum slip of 0.11 mm at 90 kN load for the specimen  $150 \times 150 \times 210\_D20$ , but 0.03 mm at 85 kN for the specimen  $150 \times 150 \times 150\_D25$ ). Higher bar diameters have more peripheral surfaces, so the more bond is developed in the concrete–reinforcement interface, the lower the slip between the two materials. Alike the case study specimen, in most of the cases, a uniform gradient of the ascending branches (of bond–slip curves) at multiple load levels was noticed, except for specimens  $200 \times 200 \times 330\_D16\_II$  and  $100 \times 100 \times 150\_D16$  (Fig. 2.12). For the former, significant degradation can be noticed in the slope of bond–slip ascending branches (between 10 kN and 21 kN). Similar gradual degradation in the ascending branch slope can be observed between different load levels (12 kN, 32 kN and 47 kN) for the specimen  $100 \times 100 \times 150\_D16$ . In addition, unlike in other cases, a decrease in peak bond stress (5.4 to 5.1 MPa) and an increase in corresponding slip (0.02 to 0.036 mm) were noticed between the load levels 32 kN and 47 kN. The reason behind this can be the damage to the concrete around the reinforcement ribs, which results in deterioration in bond stress and enhance the slip.

Notably, the experimental results reveal that the occurrence of bond damage progresses from the application of tensile load. It is evident from the declining segment of bond–slip curves even at lower load levels (Fig. 2.11 and 2.12). The region in proximity to the edge, where the bond stress is impacted, is commonly referred to as the bond damage zone (Jakubovskis and Kaklauskas, 2021). This zone can be identified in the bond stress diagram, as shown in Fig. 2.13.

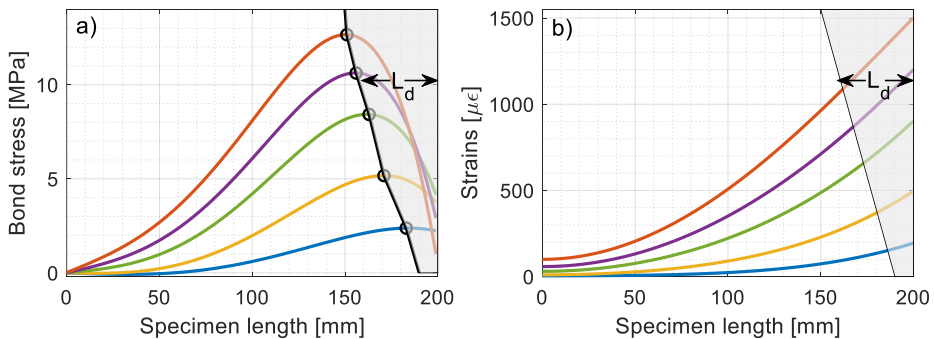


**Fig. 2.13.** Indication of bond damage zone and de-bonding length in the experimental results for the study case specimen  $200 \times 200 \times 390\_D20$ : (a) bond stress and (b) reinforcement strain profiles at multiple load levels

The area shaded in grey, located close to the edge of the specimen, denotes the bond damage zone in the case of the study specimen 200×200×390\_D20 (Fig. 2.13a). This phenomenon is also represented in the reinforcement strain diagram (Fig. 2.13b). The length of the bond damage zone, commonly referred to as the de-bonding length ( $L_d$ ), has been observed to increase with incremental loads.

Research findings indicate that the length of the de-bonding length shows an almost linear increase with higher levels of reinforcement strain. Moreover, the compressive strength of the concrete has a significant influence on the de-bonding length, with higher concrete compressive strength resulting in a shorter de-bonding length.

It is worth mentioning that the bond–slip curves displayed in Figs. 2.11 and 2.12 signify the behaviour of the RC structure at service load only. The upward-sloping sections of the bond–slip curves obtained from the current experiments are further used to develop a law for the bond–slip ascending branch (discussed in the next chapter). This may lead to the development of a constitutive bond–slip law, similar to some earlier research findings, such as Kanakubo et al. (Kanakubo et al., 2012) or Desir et al. (Desir et al., 1999).

## 2.4. Conclusions of the Second Chapter

This chapter focused on providing an overview of the experimental campaigns performed by the author during the course of this study, portraying the obtained results and the derivation of the bond–slip relationship. The main points can be expressed as:

1. The experimental results not only encompass normal-strength concrete but also shed light on the bond behaviour of high-strength concrete. The findings indicate that the strength of concrete has a relatively minor effect on the bond behaviour of RC members.
2. The experimental results indicate the presence of a bond damage zone, even in cases of lower load applications. The length of the bond damage zone increases with the increase in reinforcement strain and bar diameter and a decrease in concrete strength.
3. The results of the tests conducted in this chapter have demonstrated that ribbed bars with smaller diameters, at a given slip, exhibit a higher level of bond stress compared to those with larger diameters.
4. The assumed pattern bond–slip curve exhibits a more realistic and accurate manifestation of concrete–reinforcement interactive mechanics than

the classical format. The ascending branch of a bond–slip curve represents the inherent features of the materials, whereas the descending part signifies the cracking effect on the bond degradation in the close proximity of cracks.

# 3

---

## Novel Bond–Slip Model: Formation and Validation

The serviceability analysis of RC structures by classical approaches considers either a perfect bonding between concrete and reinforcement or a constant simplified bonding between two materials. As discussed before, due to the lack of skilful tools which can accurately and precisely assess the reinforcement strain from the core of the RC structure, the existing bond–slip models are not always accurate and conflict with one another (Mattia Francesco Bado, Casas, and Kaklauskas, 2021; Kaklauskas, Sokolov et al., 2019). On the other hand, researchers recommend the theory of stress transfer approach. It suggests the concrete–reinforcement interaction holds on the force transfer mechanism, in other words, bond stress. This can be well associated with the relative displacement between two materials or the slip, which is responsible for the RC damage in terms of cracking and deformation. A study of the bond–slip relationship offers a comprehensive and realistic perspective on the behavioural identity of RC, tension stiffening and cracking characteristics. It can be more powerful and accurate if sourced from double pull-out tests, as it provides the local bond stress and slip data extracted from the core of the RC structure. The test results of 14 RC tie specimens (reported in the previous chapter) create the ground on which a new bond–slip model will be developed. The current chapter aims at the process of establishing a novel three-dimensional bond–slip model defining the material characteristics as far as

the serviceability of RC structure is concerned. The research findings are published in the author’s publications, Dey et al. (2022).

### 3.1. Bond–Slip Model: Theory and Formation

The development of a new bond–slip model must be based on a consistent database and scientific approach. The current database consists of 14 RC tie specimens of diverse characteristics. As reported in the second chapter, multiple load levels were applied for each specimen to check the change in their structural behaviour. This creates a pool of data to develop a new bond–slip model. The subsequent sections represent the theory behind forming the new bond–slip model and showcase the model itself.

#### 3.1.1. Data Collection and Normalisation

The examination of bond stress reveals the significance of factors like concrete strength, depth of cover, diameter of bar, and length of embedment. Different researchers reported the influence of one or multiple parameters in the evolution of bond stress in RC structures. A detailed discussion of the parametric analysis was already presented in the first chapter of the dissertation. Keeping that analysis in mind, this study focused on the “design of experiments” (DOE) while choosing the characteristics of the specimens. DOE is a scientific way to design a task that can cover the variation of information under certain circumstances that are assumed to mirror the variation. It is indeed a powerful tool for data collection and analysis in a wide range of experimental atmospheres. In the current scenario, the variation was designed in terms of multiple parameters, such as embedded length ( $L$ ), bar diameter ( $\emptyset$ ), reinforcement ratio ( $pt\%$ ), concrete strength ( $f_c$ ) and concrete cover ( $c$ ). The variation of these parameters was (Fig. 3.1) designed to make the new bond–slip model effective and accurate through wide parametric ranges.

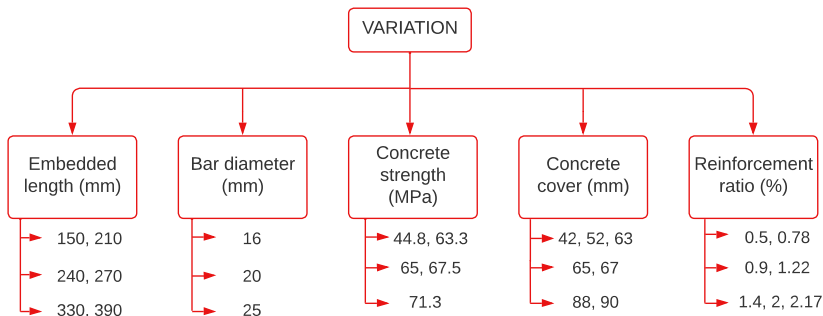


**Fig. 3.1.** Variation in parameters for the design of experiment (DOE)

Data collection was the next crucial step in the process of modelling. In the current study, the data of all dependent and independent parameters were gathered systematically. These were sourced from the experimental campaigns performed by the author and then derived through an algorithm (Fig. 2.9) based on mathematical programming.

It is important to mention that as the current test results (bond-slip) depict the behaviour of RC structures at service load only, the rising sections of the bond-slip relationships were taken to model a new bond-slip law. Fig. 3.2a displays only the ascending branches of bond-slip curves for the case study specimen  $200 \times 200 \times 390\_D20$  after trimming the descending branch of the curves. Similarly, the descending branches from the specimens' bond-slip results at multiple load levels were trimmed and plotted in one frame (Fig. 3.2b). Fig. 3.2b represents more than 6,300 data points used in formulating a new bond-slip model for the ascending branch.

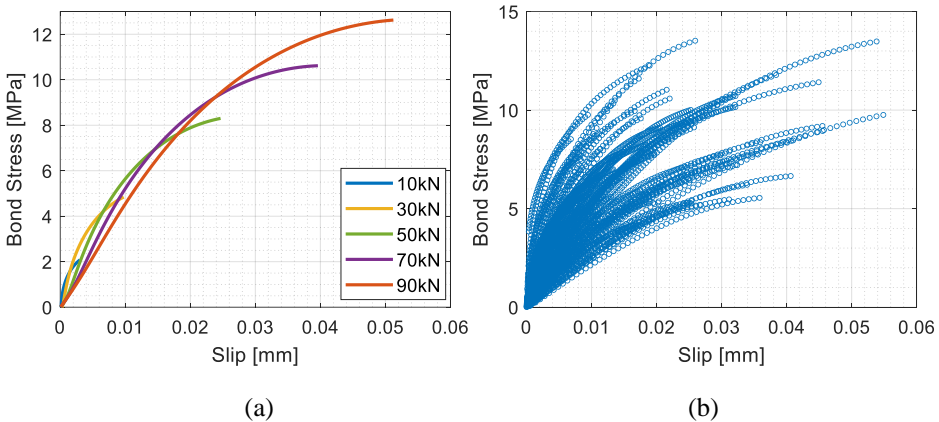


**Fig. 3.2.** Ascending branches of bond-slip relationships: (a) for the study case specimen  $200 \times 200 \times 390\_D20$  at multiple load levels and (b) dataset plot for all the specimens

As seen in Fig. 3.2b, the database was widely spread through a wide range of parameters. For further calculation, it was sensible to narrow down its range of spread. It was possible in the following step towards the modelling, “data normalisation”. This is a scientific process to re-organise the dataset in a more normalised form. The main objectives of this process are to reduce data modification errors, trim out non-essential data and simplify the query process. It was essential for easing and securing the establishment of a new bond-slip model. For this purpose, normalised bond stress was determined by dividing the bond stress ( $\tau$ ) by the maximum bond stress ( $\tau_{max}$ ). The latter can be obtained using Eq. 3.1, adopted from Model Code 2010 (fib Model Code, 2013).

$$\tau_{max} = 2.5\sqrt{f_c}, \quad (3.1)$$

where,  $f_c$  signifies the compressive strength of concrete. Differently, the independent parameter slip ( $s$ ) was normalised by dividing it by bar diameter ( $\emptyset$ ). The entire normalised dataset is presented in Fig. 3.3 below.

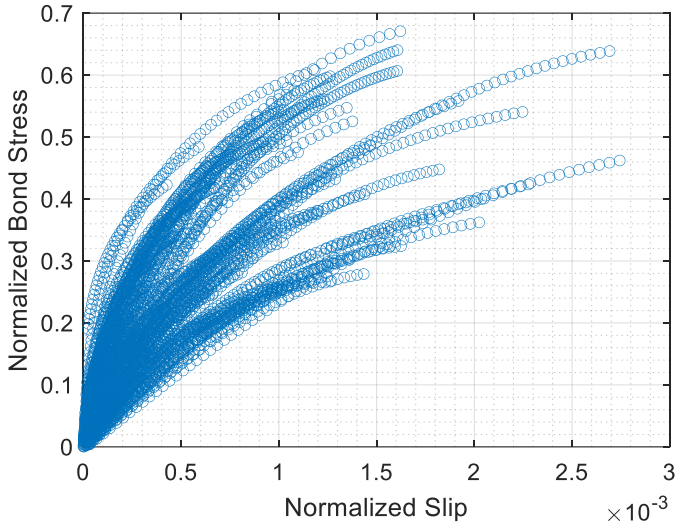


**Fig. 3.3.** Normalised dataset for modelling

Fig. 3.3 shows that the magnitude of both axes is minimised compared to Fig. 3.2 due to the data normalisation operation. This way, the influence of concrete strength ( $f_c$ ) and bar diameter ( $\emptyset$ ) was removed from the present dataset. Also, both axes (x and y) of Fig. 3.3 became dimensionless.

### 3.1.2. Multiple Linear Regression

Now, to deal with the parameters, a regression was the mathematical approach. In simple words, regression analysis is the linear approximation that fits with the data most closely to a specific mathematical basis. However, the current case involves multiple variables which could not be solved with linear regression analysis. So, the author relied on the fundamental approach of ‘multiple linear regression’ (MLR), which deals with one dependent parameter and multiple independent parameters. In the current study, the bond stress ( $\tau$ ) is considered the only dependent parameter and the others, such as embedded length ( $L$ ), bar diameter ( $\emptyset$ ), reinforcement ratio ( $pt\%$ ), concrete strength ( $f_c$ ), concrete cover ( $c$ ) and slip ( $s$ ), are the independent parameters. In addition, based on the literature review

and practical experience, the author decided to include some more independent parameters, such as local reinforcement strain ( $\varepsilon_s$ ), slip/diameter ( $s/\phi$ ), cover/diameter ( $c/\phi$ ) and diameter/embedded length ( $\phi/L$ ), which might influence the bond–slip relationship of an RC structure (Table 3.1). MLR is an effective statistical process often used for prediction and forecasting purposes. Mainly, it is dominant in estimating the relationship between dependent and independent parameters. So, when the MLR is applied to a reliable, consistent fixed dataset of dependent and independent variables, a powerful predicting relationship can be expected.

**Table 3.1.** Variables used for modelling purposes

Dependent Variable	$\tau$ or $\tau/\tau_{max}$
Independent Variables	$L, \phi, f_c, c, s, \varepsilon_s, \frac{s}{\phi}, \frac{c}{\phi}, \frac{\phi}{L}$

A comprehensive regression analysis was undertaken to assess the impact of various independent parameters on a dependent variable. Specifically, the analysis involved exploring the influence of these independent variables in a three-dimensional analysis framework by considering all possible combinations of the variables (mentioned in Table 3.1). Only a few of the various trials of three-dimensional correlations between the variables are presented in Fig. 3.4. Based on the outcome of the analysis, particular attention was directed towards examining the two most influential parameters concerning the bond stress ( $\tau$ ): concrete strength ( $f_c$ ) and slip/diameter ( $s/\phi$ ). These parameters were identified as the primary factors that significantly affect the bond stress between the relevant entities under investigation. The regression analysis provided valuable insights into the influence of the independent variables on the dependent variable, shedding light on the significance of concrete strength and slip/diameter in relation to bond stress. The findings of this analysis contribute to a better understanding of the factors affecting bond stress and can establish a quantitative relationship between them.

The current course of action was to model the entire dataset. It was done by a powerful surface fitting tool, which can discern an ideal mathematical expression to explain three-dimensional (3D) empirical data. Finally, from the  $p$ -value of the regression analysis, the most influential parameters were chosen (last subplot of Fig. 3.4). The  $p$ -value is a statistical measure that helps determine the strength of evidence against the null hypothesis in a hypothesis test. It quantifies the probability of obtaining results as extreme as the observed data, assuming the null hypothesis is true.

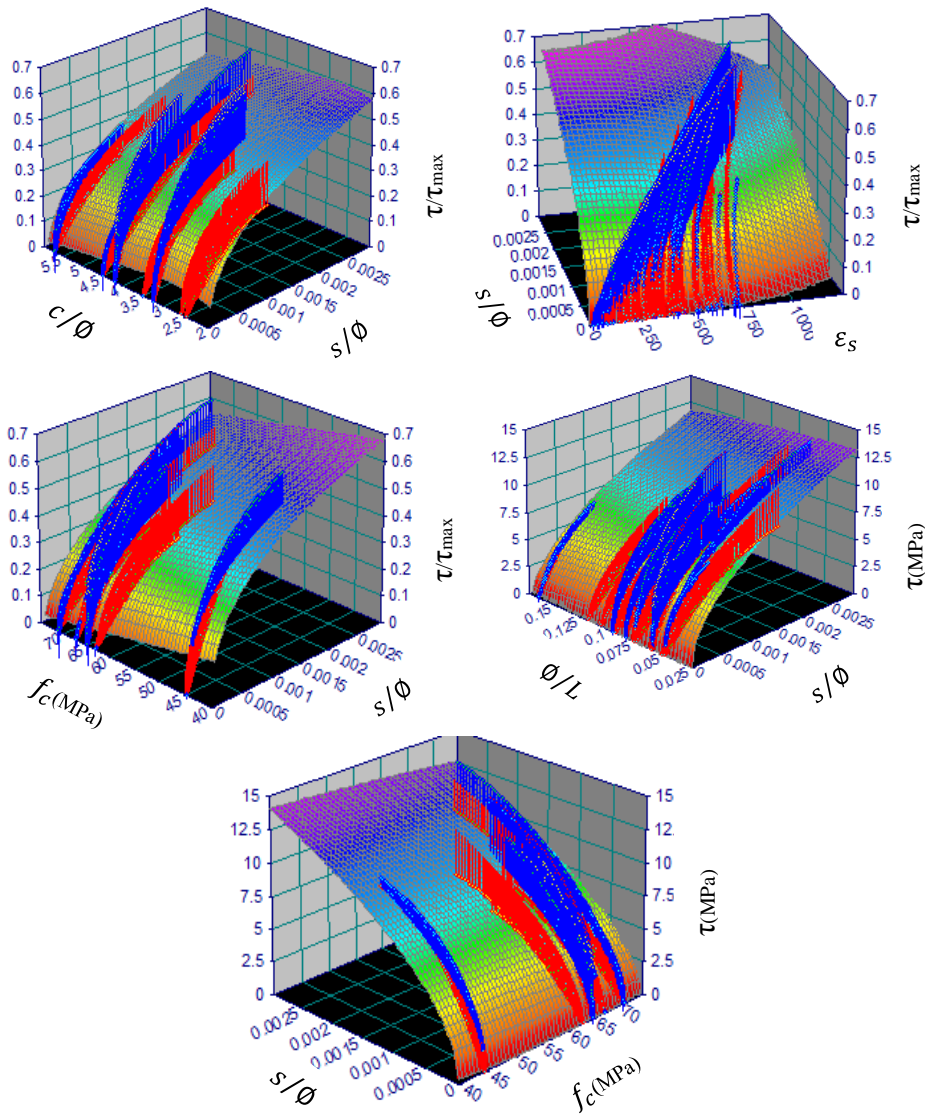


**Fig. 3.4.** 3D surface fitting with the experimental dataset for modelling

The succeeding step is to develop a mathematical expression using the most influential independent variables on the dependent variable.

### 3.1.3. Model Selection

The y-axis of the chosen correlation (last subplot of Fig. 3.4) indicates the dependent parameter bond stress ( $\tau$ ), whereas the x-axis and z-axis represent concrete strength ( $f_c$ ) and slip/diameter ( $s/\emptyset$ ), respectively. The surface signifies the best-fitting correlation among these three parameters based on the given dataset. This best-fitting 3-D correlation surface (Fig. 3.4) could be mathematically expressed in various ways.

The succeeding step was “model selection”, which refers to the task of selecting a model among a set of multiple model candidates. This selection could be based on performance and also the basis of simplicity in the expression. Among the models, the best performing (in terms of  $R^2$ ) one with a reasonably simple expression was chosen and presented in Eq. 3.2.  $R^2$  is a statistical measurement which explains how well a predicted line/surface fits the dataset.

$$\tau = 1.25 - 0.0035(f_c)^{1.5} + 250 \left(\frac{s}{\emptyset}\right)^\alpha ; \quad (3.2)$$

$$\alpha = 0.6 \text{ for } f_c < 50 \text{ MPa}; \alpha = 0.5 \text{ for } f_c \geq 50 \text{ MPa} .$$

The simple mathematical expression in Eq. 3.2 can effectively determine bond stress in terms of concrete strength, slip and bar diameter. During the analysis, the bond–slip pattern was dissimilar between normal-strength and high-strength concrete. To reflect this characteristic in the bond–slip model, one coefficient ( $\alpha$ ) was introduced. Hereby, as a novel bond–slip model for RC structures under service loads, the author proposed Eq. 3.2, where  $\alpha = 0.6$  for normal concrete strength (lower than 50 MPa), and  $\alpha = 0.5$  for high-strength concrete (equal to or greater than 50 MPa). This model can predict the structure’s bond–slip behaviour based on its inherent material properties, which will further help in serviceability predictions. The upcoming sub-chapter aims to substantiate the credibility of the proposed bond–slip model in terms of validation.

## 3.2. Model Validation

Model validation is a scientific process to evaluate the performance of a proposed model. It determines the capability and accuracy of the model in manifesting the system’s behaviour. So, model validation is utterly essential to establish a novel model and for its acceptance throughout the field of science.

Fundamentally, two techniques can be used for model validation. The first can be named “in-sample validation”, where the testing data is taken from the same dataset used to establish the model. The second technique is “out-of-sample validation”, which usually picks independent experimental data (collected from

the literature) to check the correctness of the proposed model. The author has performed both kinds of validation to establish the proposed model, described in the following sub-sections.

### 3.2.1. In-sample Validation

As discussed, the proposed model represents the ascending branch of bond–slip relationships between reinforcement and concrete in RC structures. For validation purposes, the experimental bond–slip data for all 14 RC ties were taken and compared with the proposed model. Fig. 3.6 represents the rising segment of bond–slip relationships at multiple load levels for the case study member, RC tie 200×200×390\_D20, further compared with the proposed model (Eq. 3.2).

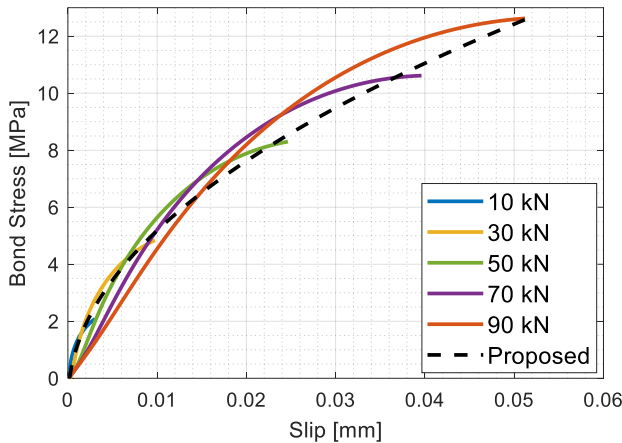


**Fig. 3.5.** Comparison between experimental and proposed model predicted bond–slip relationships for case study specimen RC tie 200×200×390\_D20 at multiple load levels

The solid curves of different colours in Fig. 3.5 represent different load levels, as indicated in the legend. Also, the ascending segments of bond–slip curves at multiple load levels are usually consistent and extremely close to each other. On the other hand, the black dotted curve presents the bond–slip relationship predicted by the proposed model. Fig. 3.5 portrays fair agreement between the experimental outputs and the proposed model predictions on the subject of bond–slip relationships. Similarly, the validation was performed by comparing the experimental bond–slip data of 13 RC ties with the proposed model’s predictions. Fig. 3.6 displays the model validation output, where each subplot represents a single RC tie tested in the current study.

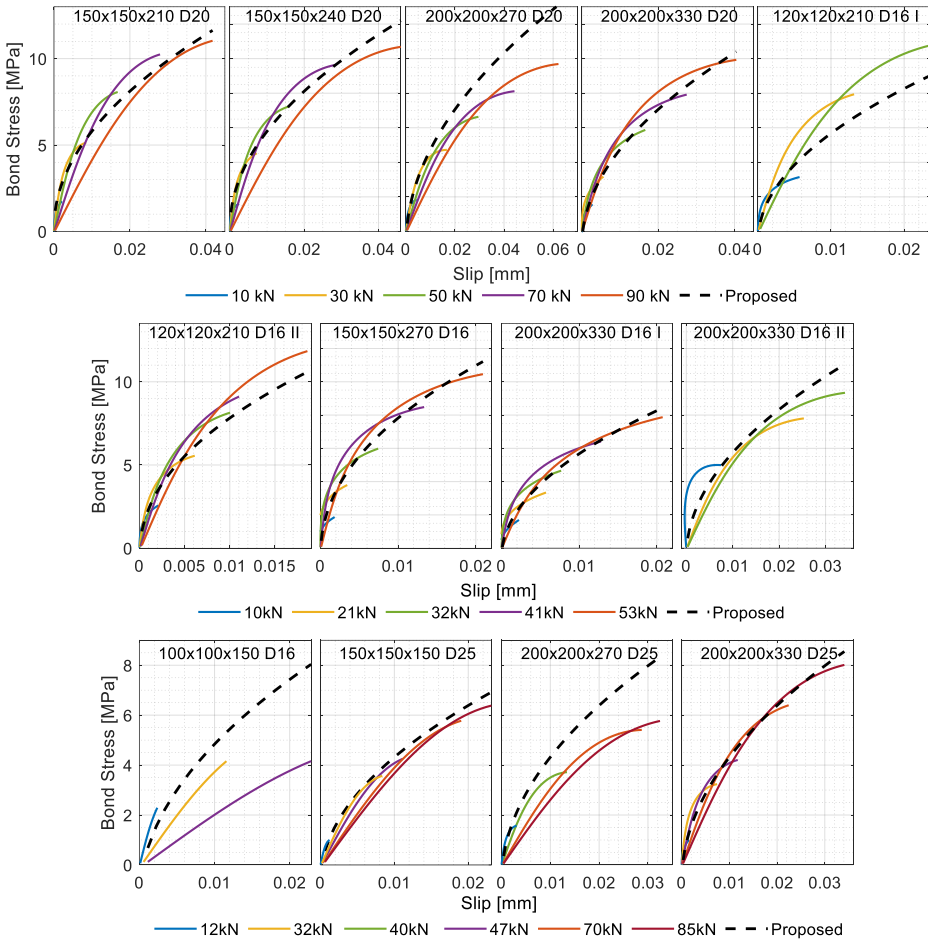


**Fig. 3.6.** Comparison between experimental and proposed model predicted bond-slip relationships for 13 RC ties at multiple load levels

Fig. 3.6 provides the overall idea about the compatibility of the proposed model among the dataset used to establish the same. Likewise, in the case study specimen (Fig. 3.5), the model-predicted bond-slip data agreed reasonably well with almost all RC ties. Slight exceptions can be noticed in the case of specimens 200×200×270\_D20, 120×120×210\_D16, 100×100×150\_D16 and 150×150×270\_D25. For the latter specimen, the proposed model exhibited satisfactory agreement with the bond-slip curve at a 40 kN load level.

However, as the load increased, the agreement between the model and the bond-slip curves deteriorated. This trend was observed consistently across the specimens mentioned above. The observed deterioration in agreement between

the proposed model and the bond–slip curve at higher load levels could be attributed to the degradation of bond–slip relationships. As the load increases, various factors, such as damage, de-bonding, internal cracking, and tension softening, may come into play, resulting in changes in the bond–slip behaviour. This could potentially affect the accuracy of the model’s predictions. Previous analyses have indicated that the formation of internal secondary cracks in concrete can lead to internal damage and bond deterioration near these cracks. Additionally, the radial pressure exerted by the reinforcing bar on the surrounding concrete can induce splitting cracks, further contributing to the deterioration mechanism. Although the damage near cracks is typically localised, it can significantly impact deformations, crack spacing, and the crack width of RC elements (Kaklauskas, 2017). The size of the damage zone is often related to the diameter of the bar and can vary from 2.5 to 5 $\phi$ . Factors such as load level and concrete grade also influence bond stress distribution near cracks. However, incorporating these parameters into analytical models poses significant challenges.

In other words, determining a specific RC specimen’s local bond–slip relationship is highly sensitive. Even slight changes in certain parameters or any disturbances due to the abovementioned factors can significantly impact the experimental bond–slip behaviour. In that case, the author suspects that one or multiple reasons could be responsible for the slight discrepancies observed between the model predictions and some specimens’ experimental bond–slip results.

After the in-sample validation, checking the model performance through some independent experimental data was important. The next section is devoted to that purpose.

### 3.2.2. Out-of-sample Validation

This validation part compares the model’s predicted bond–slip relationship with independent experimental data. For this purpose, the author has collected eight real-life experimental RC ties from different pieces of literature. Despite the limited availability of experimental bond–slip data (extracted from short RC ties), RC ties of diverse characteristics were chosen. Apart from the specimens’ characteristics, the RC ties were diversified in terms of strain monitoring techniques. As a common factor, they all underwent a double pull-out test. Their physical dimensions and strain monitoring techniques are mentioned in Table 3.2.

The first RC tie 150×150×405\_D25 from Houde (Houde, 1974) was similarly instrumented with strain gauge sensors as the current study. The milled groove was 9.5×3 mm, where the strain gauges were installed at uneven spacing (38–50 mm). The second specimen, 150×150×260\_D20, was taken from Kaklauskas et al. (Kaklauskas, Sokolov et al., 2019), equipped with an FBG optical fibre

(0.9 mm  $\emptyset$ ), fixed inside a shallow groove of dimension  $2 \times 1.5$  mm, milled on the surface of the reinforcement bar.

**Table 3.2.** Geometry of independent RC ties taken from the literature for validation

Reference	Specimen	Strain monitoring technique
Houde	150×150×405_D25	Strain gauge sensors
Kaklauskas et al.	150×150×260_D20	FBG optical fibre
Gudonis et al.	100×100×150_D16	Strain gauge sensors
Kankam	150×150×210_D25	Strain gauge sensors
Bado et al.	150×150×210_D20	DOFS
Jakubovskis and Kaklauskas	150×150×270_D20_I	Strain gauge sensors
	150×150×270_D20_II	Strain gauge sensors
	150×150×270_D20_III	Strain gauge sensors

Next two RC specimens, 100×100×150\_D16 and 150×150×210\_D25, were picked from Gudonis et al. (Gudonis et al., 2017) and Kankam (Kankam, 1997), respectively. In the former, the strain gauges were evenly spaced by 45 mm, whereas in the latter specimen, they were unevenly spaced by 12.5–37.5 mm. The specimen 150×150×210\_D20 from Bado et al. (Bado et al., 2020) was equipped with the modern-age monitoring tool DOFS, which was fixed on a  $1.5 \times 1$  mm groove on the reinforcement bar surface employing a cyanoacrylate glue and protected with a water-proof silicone layer. Lastly, the three identical specimens of dimensions 150×150×270 and  $\emptyset 20$  mm bar were taken from Jakubovskis and Kaklauskas (Jakubovskis and Kaklauskas, 2019), instrumented with strain gauges spaced 20 mm apart.

Fig. 3.7 compares independent experimental bond–slip data with the model-predicted ones for eight real-life RC ties mentioned above. As the experimental data were taken from respective literature, the available load levels were limited. That is why the legends of Fig. 3.7 at different rows are unlike and diversely ranged.

It is worth mentioning that due to the large diversification in specimens' dimensions and bar diameter, the x and y axes range couldn't be maintained uniformly. For example, the maximum achieved bond stress and slip are 19 MPa and 0.14 mm, respectively, at a 90 kN load level (Fig. 3.7c). On the other hand, under 100 kN load, bond stress is 6.7 MPa, and slip is 0.042 mm (Fig. 3.7e). This is mainly because of diverse specimen dimensions and bar diameter.

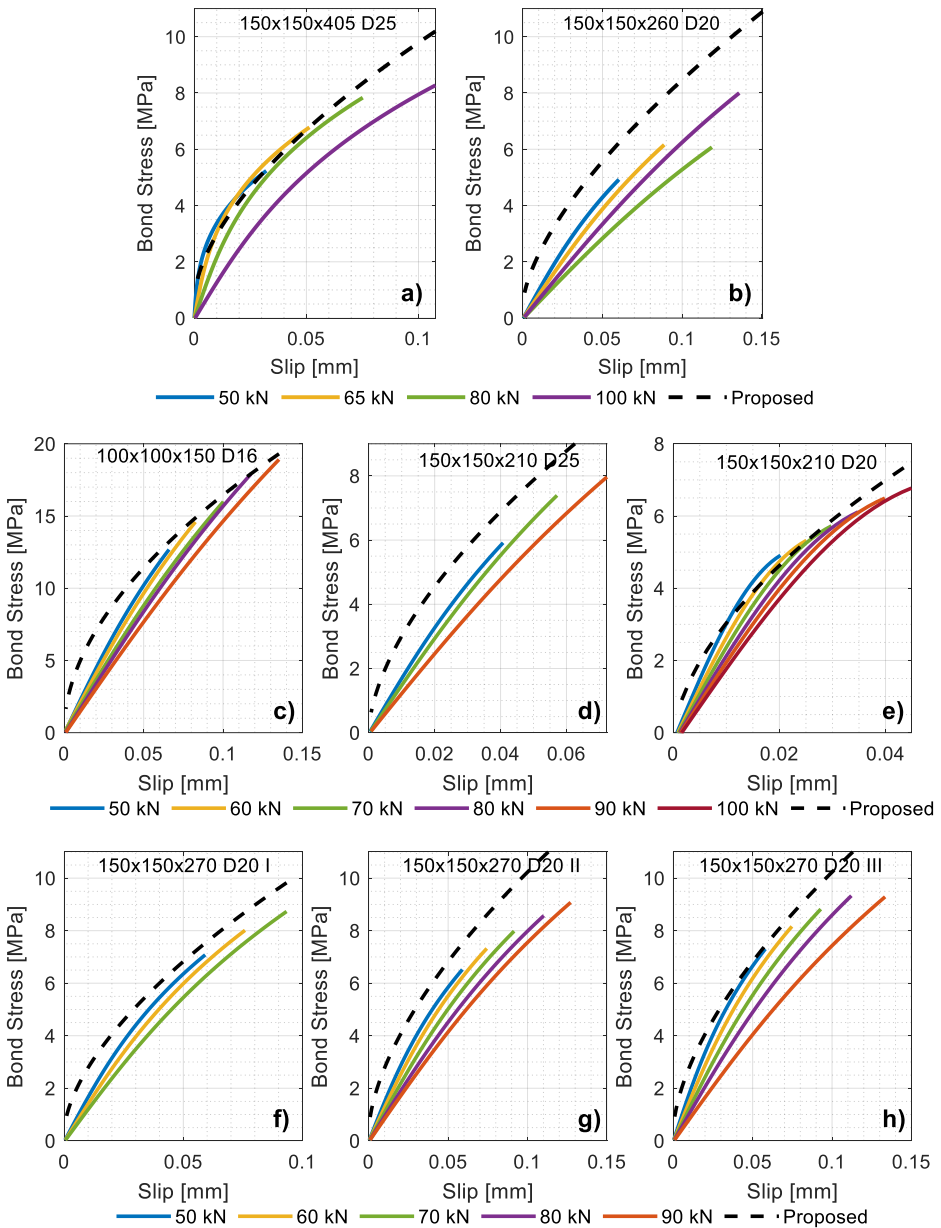


**Fig. 3.7.** Comparison between independent experimental and proposed model predicted bond-slip relationships for eight RC ties at multiple load levels

A smaller  $\emptyset$  bar has a lesser surface area in contact with concrete, lesser production of bond stress and higher slip between two materials. Another fact, a larger cover and longer embedded length can be the reasons for lesser bond stress between concrete and reinforcement. For most specimens (Fig. 3.7 a, c, e, f and h), the model predicted bond–slip relationships (indicated by black dotted lines) made an excellent agreement with nearly all the load levels. Except for a few cases (Fig. 3.7 b, d and g), the inconsistency between model predictions and experimental results is small at lower load levels but increases with the load increments. Nevertheless, reasonably close predictions (in most cases) of bond–slip relationships by the proposed model enhance the reliability and acceptability.

As discussed earlier, the present study is focused on developing a novel bond–slip model, which is suitable for predicting the serviceability performance of RC structures. Concerning the fact, the correct prediction of strain distribution throughout the specimen length is the uttermost credibility of a bond–slip model. The following sub-chapter performs the validation of the proposed model through strain distribution on the previously mentioned eight real-life independent specimens and also compares it with some existing popular bond–slip models.

### **3.3. Reinforcement Strains from Bond–Slip Models: Application and Validation**

A correct prediction of reinforcement strain distribution opens the door to multifaceted serviceability predictions of an RC structure. In other words, it creates the base for accurate predictions of deflections, crack spacing, crack widths, tension stiffening, creep, shrinkage, etc., which are essential for structural assessment by means of structural integrity, strength, security, soundness and utility. For this purpose, an efficient tool was necessary to predict strain distribution from a given bond–slip law. So far, no such tool has been available in the literature.

On the flip side, few bond–slip models are available in the literature, established on direct pull-out tests or beam tests (discussed in the First Chapter). But it is seen that the bond–slip models are not usually error-free and are conflicting among themselves. The primary reason for various incorrect and contradictory bond–slip models is the unavailability of an efficient tool that can smoothly corroborate and quickly calibrate the newly created models (Dey, Bado et al., 2022).

Concerning the fact, the author has developed and proposed a validation tool that can fast-track the strenuous and lengthy mathematical and experimental corroboration and comparison process with similar existing models. Besides, this tool opens a prospect for investigations on stress transfer analysis, bond–slip modeling and, eventually, the serviceability of RC structures. The upcoming section

elaborates on the theoretical background of the proposed validation tool and its application.

### 3.3.1. Validation Tool: Theoretical Background

The proposed validation tool can calculate the reinforcement strain profile from a case study bond–slip model at a load level. The geometrical and mechanical features of the RC specimen must be provided as the program input. The output reinforcement strain distribution is useful from multiple aspects, such as (1) the credibility of a bond–slip model can be checked by comparing the strain output with experimental strain distribution, (2) the reliability of a monitoring tool can be checked from the consistency in the strain output, and (3), most importantly, the serviceability prediction of an RC structure. The fundamentals and the mathematical background of the validation algorithm are discussed below.

The validation algorithm was programmed based on the stress transfer approach, as it offers a highly accurate manifestation of the behaviour of composite materials. Some assumptions are taken to develop the program, such as:

- Concrete strain is nil at the cracked section, eventually at the end of the specimen. The applied load is completely taken by the reinforcement.
- The RC specimen produces symmetric behaviour with respect to its mid-section.
- Slip becomes zero at the mid-section of the specimen.

The algorithm program analyses only half of the RC specimen block, considering its symmetric geometry. Here, the half block was divided into  $n$  number of small segments of length  $\Delta x$ . The user can alter segment quantities, which commands the fineness and complexity of the program. According to Fig. 3.8, beginning from the block's right edge section (segment 1), the program runs till the mid-section (segment  $n$ ), which can be referred to as the last segment of this calculation. A sequence of iterative calculations was carried out in each segment to define the precise and correct output.

Fundamentally, the program starts with the concept of equilibrium of forces (Eq. 2.2 and 2.3). Based on these, the reinforcement strain for the  $i^{\text{th}}$  segment can be evaluated by Eq. 3.3 or in a more simplified way by Eq. 3.4.

$$\varepsilon_{s,i} E_s A_s + \tau_i \pi \phi \Delta x = \varepsilon_{s,i-1} E_s A_s; \quad (3.3)$$

$$\varepsilon_{s,i} = \frac{\varepsilon_{s,i-1} E_s A_s - \tau_i \pi \phi \Delta x}{E_s A_s}. \quad (3.4)$$

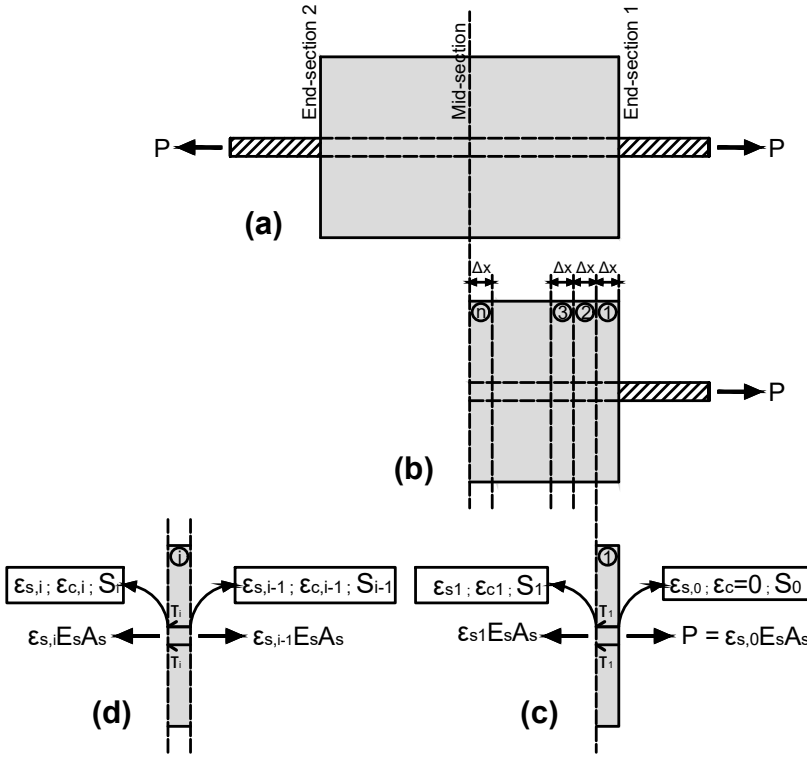


**Fig. 3.8.** Segmental divisions in half of the specimen and free body diagram of a segment: (a) full specimen, (b) symmetrical half of the specimen, (c) the first segment under consideration, and (d) the  $i^{th}$  segment

In Eq. 3.4, the acting bond stress ( $\tau_i$ ) in the section was directly calculated from the study case bond–slip model, where the initial slip  $s_0$  was assumed and input by the user, followed by Eq. 2.5 for calculating the concrete strain ( $\epsilon_{c,i}$ ), and Eqs. 2.6 and 2.7 for evaluating slip ( $s_i$ ) in that section. It must be noted that all the above-mentioned equations are effective at both ends of each small segment, but the bond stress ( $\tau_i$ ) remains the same throughout one segment.

Accounting for the fact, for the calculation of bar strain ( $\epsilon_{s,i}$ ) at the beginning of the segment, the considered bond stress value will be an average of the current ( $\tau_i$ ) and previous segment's ( $\tau_{i-1}$ ) bond stresses. Therefore, except for the first segment, for all other segments (when  $i > 1$ ) bar strain will be calculated by Eq. 3.5.

$$\epsilon_{s,i} = \epsilon_{s,i-1} - \left( \frac{\tau_i + \tau_{i-1}}{2} \frac{\pi \phi \Delta x}{E_s A_s} \right). \tag{3.5}$$

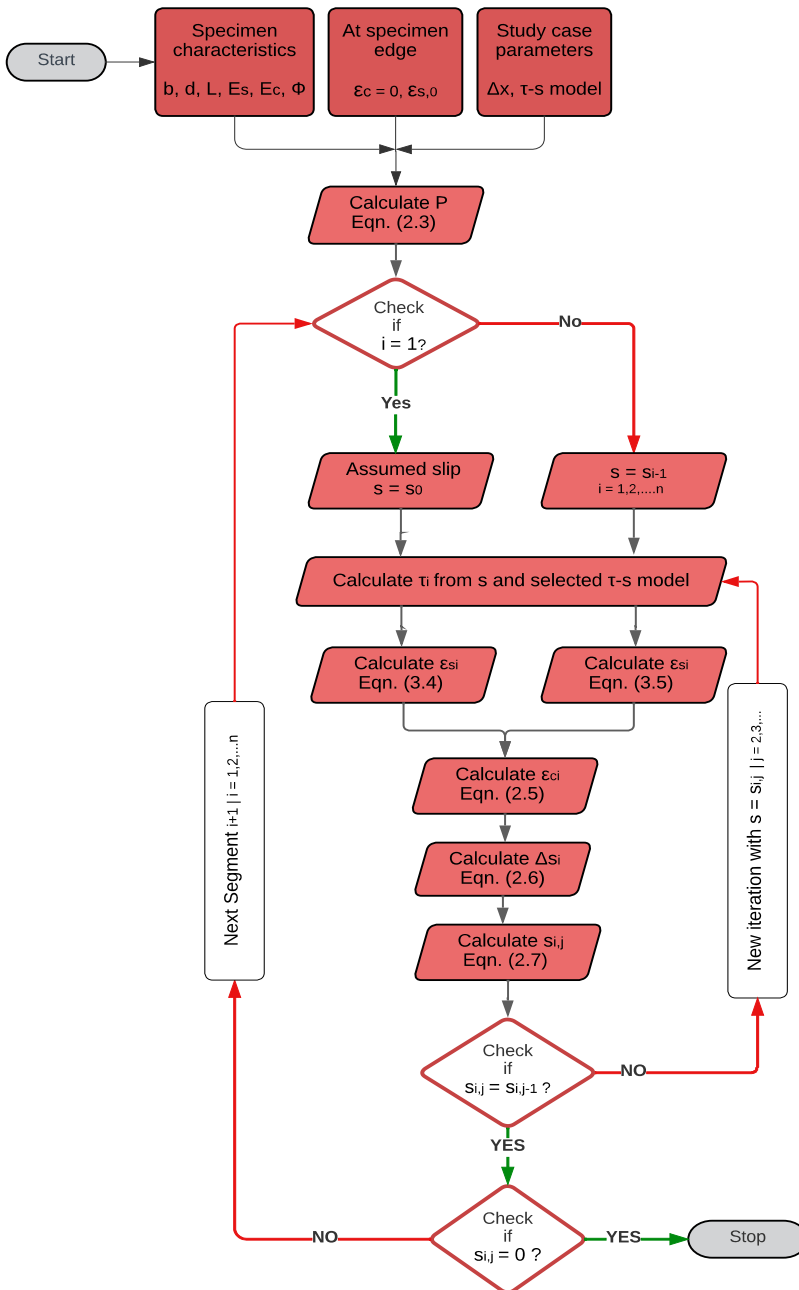


**Fig. 3.9.** Flowchart of the validation algorithm for determining reinforcement strains by an iterative process on the ground of a set bond-slip model

The rest of the calculations of  $\varepsilon_{c,i}$ ,  $\Delta s_i$  and  $s_i$  will be the same as in the first segment. The sequential logical steps of the entire program are represented in a flowchart in Fig. 3.9.

The algorithm (Fig. 3.9) asks the user to input some required data, such as (1) the geometrical characteristics of the RC specimen under investigation, (2) reinforcement strain ( $\varepsilon_{s0}$ ) at the loaded end of the RC specimen, and (3) the length of each small segment ( $\Delta x$ ). The latter opted by a user, will define the “spatial resolution” of the numerical analysis. As shown in the flowchart (Fig. 3.9), the program first calculates the acting tensile force ( $P$ ) by Eq. 2.3. The next step checks whether the current segment is the first or not (if  $i = 1$ ). For the first segment only, the program asks for the assumed slip value ( $s_0$ ) for further calculations. For all other segments, it automatically takes the slip value from the previous segment ( $s_{i-1}$ ). In both cases, the program next calculates the bond stress ( $\tau_i$ ) value from the given bond–slip law, followed by determining reinforcement strain through Eq. 3.4 for the first segment only and Eq. 3.5 for the rest of the segments. Then, the program calculates concrete strain, change in slip and slip at that section through Eqs 2.5, 2.6 and 2.7, respectively. Finally, the result of the slip ( $s_{i,j}$ ) is compared with the slip taken at the beginning of the analysis of that segment ( $s_{i,j-1}$ ). Here,  $i$  denotes the number of segments, whereas  $j$  indicates the number of iterations. If not a match, the program runs another iteration until the slip at the beginning and the end of one iteration matches ( $s_{i,j} = s_{i,j-1}$ ). Hereafter, the program moves to the next segment and follows the same algorithm loop. The indication of the last step comes from the final checking,  $s_{i,j} = 0$ . At this condition, the program stops the loop and provides the result; otherwise, it runs another loop for the next segment.

The output of this algorithm provides a series of reinforcement strain values depending upon the spatial resolution chosen by the user. It must be noted that the output from the validation tool is the reinforcement strain distribution for half of the specimen only. The full strain profile of an RC specimen can be obtained consequently on the ground of its symmetric geometry by duplicating on the other half. Further, the application of this validation tool will be demonstrated in the upcoming section.

### 3.3.2. Validation Tool: Application

This section demonstrates the application of the above-discussed validation tool. This tool fulfils two-fold objectives: (1) it portrays the capability of this tool in determining reinforcement strains from a given bond–slip model, and (2) the proposed bond–slip model (Eq. 3.2) is validated by comparing it with other existing models in terms of reinforcement strain distributions. A total of seven bond–slip models were compared and validated by calculating the strain distribution data for

specific case study loads using the algorithm. Among them, six models are existing, taken from the literature, and the last was the new model, expressed by Eq. 3.2. The chosen six existing models are the only available ones, including the slip in their models for determining bond stress between the concrete and reinforcement, shown in Table 3.3 with a brief background. This demonstration will showcase the accuracy and effectiveness of all bond–slip models (including the proposed one) in predicting the reinforcement strain distributions.

**Table 3.3.** Existing bond–slip models assessed using the validation tool

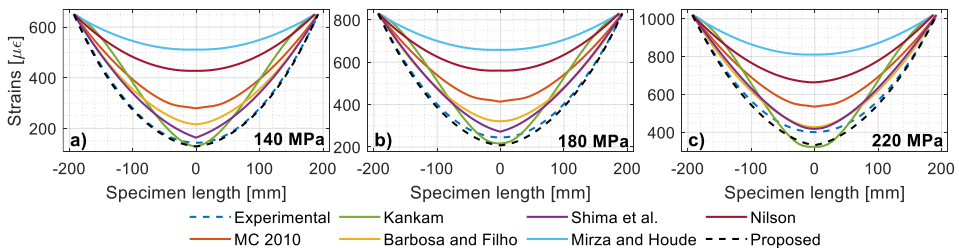
References	Bond–slip model	Notes/Description
Model Code 2010 (fib Model Code, 2013)	$\tau = \tau_b = \tau_{max} \left( \frac{s}{s_1} \right)^\alpha$ being $\tau_{max} = 2.5\sqrt{f_c}$	Determined with pull-out tests, $s_1 = 1$ and $\alpha = 0.4$ for confined concrete and good concrete–rebar bond
Kankam (Kankam, 1997)	$\tau = (35 - 0.3x)s^{0.5}$ hot-rolled ribbed bar; $\tau = (55 - 0.5x)s^{0.8}$ cold-worked ribbed bar	Determined with double pull-out test $x =$ distance between the measuring point and the middle of the concrete prism
Barbosa and Filho (Barbosa and Filho, 2016)	$\tau = 19.36s^{0.51}$ for $f_c < 50\text{ MPa}$ $\tau = 32.58s^{0.48}$ for $f_c > 50\text{ MPa}$	Determined with pull-out tests
Shima et al. (Shima et al., 1987)	$\tau = 0.9f_c^{2/3} \left( 1 - e^{-40s^{0.6}} \right)$	Determined with pull-out test, $S =$ slip/diameter
Mirza and Houde (Mirza and Houde, 1978)	$\tau = 1.95 \times 10^6 s - 2.35 \times 10^9 s^2 + 1.39 \times 10^{12} s^3 - 0.33 \times 10^{15} s^4$	Determined with double pull-out tests ( $\tau$ in psi and $s$ in inches)
Nilson (Nilson, 1971)	$\tau = 3.606 \times 10^6 s - 5.356 \times 10^9 s^2 + 1.986 \times 10^{12} s^3$	Determined with double pull-out tests ( $\tau$ in psi and $s$ in inches)

For the application of the validation tool with set bond–slip models, real-life, independent experimental specimens were needed. As this is the extended validation part of the proposed model, previously selected eight RC ties of diverse characteristics were used. Their geometry and reinforcement strain monitoring techniques were discussed in sub-chapter 3.2.2 and Table 3.2. For further details on their mechanical characteristics, the readers can refer to the cited articles. The author has decided to portray the reinforcement strain distribution based on multiple stress levels in steel reinforcement. Three different stress levels were chosen from the range of 30–70% of the steel yield strength. As the experimental data were collected from various literature, the chosen stress levels were not uniform for all eight RC ties. As an

example, for the first RC tie, 150×150×405\_D25 from Houde (1974), three chosen stress levels were 150 MPa, 180 MPa and 220 MPa, as provided by the source literature for the mentioned range (30–70% of steel yield strength). The following will demonstrate the data input procedure for the first RC tie (150×150×405\_D25 from Houde) required for strain derivation.

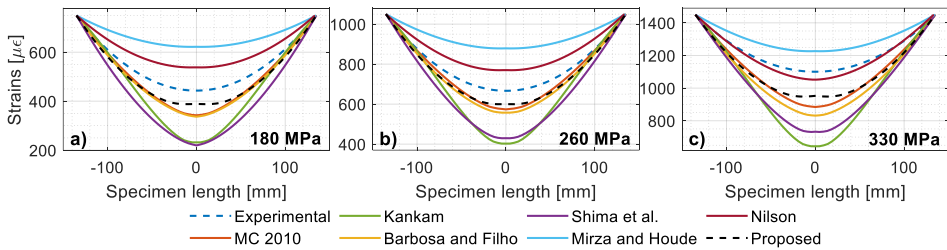
Following the algorithm (Fig. 3.9), some input data needs to be inserted to begin the program. The input data example for the first sample specimen (150×150×405\_D25) were  $b = 150$  mm (specimen width),  $d = 150$  mm (specimen depth),  $L = 405$  mm (specimen length),  $\varnothing = 25$  mm (bar diameter),  $E_c = 31\,000$  MPa (modulus of elasticity of concrete),  $E_s = 204$  GPa (modulus of elasticity of steel),  $\varepsilon_{s,0} = 650$   $\mu\varepsilon$  (reinforcement strain at the loaded end) for 140 MPa stress level,  $n = 60$  (the number of equal segments of the prism for running the mathematical calculation) and  $s_0 = 0.05$  mm (assumed slip at the endpoint of the prism). It is worth mentioning that the values  $\varepsilon_{s,0}$  and  $s_0$  were the same as experimentally obtained for a particular stress level. With the above data input, the algorithm was run through MatLab programming and the strain distribution profile at that specific stress level was obtained as an output. In this case, the mathematical iterations were performed for every 60 segments, and each segment's one strain value was evaluated and recorded accordingly. This procedure was executed for seven bond–slip models (six existing as in Table 3.2 and one proposed in the current study) to produce their strain predictions. Similar operations were done for 180 MPa and 220 MPa stress levels separately. The strain distribution outputs are presented in Fig. 3.10 at multiple stress levels.

In strain comparison diagrams (Fig. 3.10), the x-axis represents the specimen length, and the y-axis signifies reinforcement strains ( $\mu\varepsilon$ ). It must be noted that the y-axis range couldn't be kept the same because of large strain differences. For example, at a 150 MPa stress level, the maximum strain achieved by reinforcement is 650  $\mu\varepsilon$  (Fig. 3.10a), whereas, for 220 MPa, the maximum attained strain is 1010  $\mu\varepsilon$  (Fig. 3.10c).



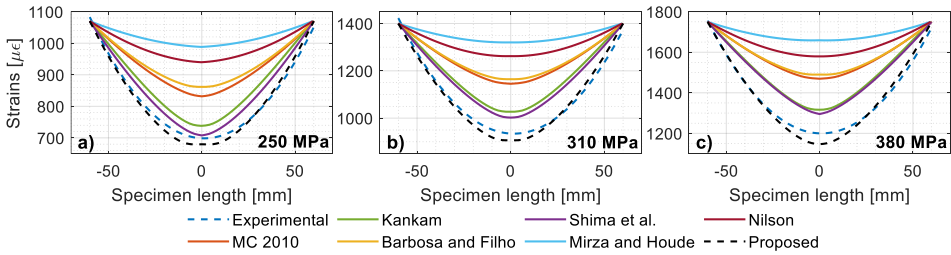
**Fig. 3.10.** Experimental and predicted strain distributions on the specimen 150×150×405\_D25 by Houde at stress levels (a) 140 MPa, (b) 180 MPa, and (c) 220 MPa

Although the strain predictions by all the models are quite consistent at all stress levels, most of the models overestimate the strains except the proposed model and Kankam’s model (at the central zone only). Mirza and Houde’s model shows the maximum overestimation though the magnitude becomes smaller for higher stress levels. The least overestimation was observed by Shima’s model, followed by Barbosa and Filho’s model, the MC 2010 model and Nilson’s model (Fig. 3.10). The proposed model made an excellent agreement with the experimental model at a stress level of 150 MPa, though the underestimation increased at higher stress levels, mainly near the mid-centre of the specimen. The strain prediction curves of Kankam’s model are steeper than others, and it underestimates the strains near the central zone of the specimen. Similar model predictions compared with the independent experimental data of Kaklauskas et al. (Kaklauskas, Sokolov et al., 2019) are presented in Fig. 3.11.



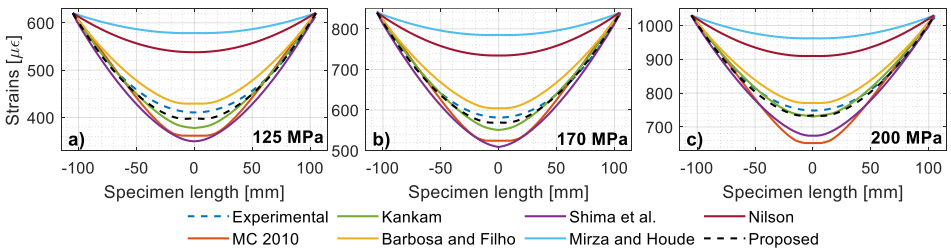
**Fig. 3.11.** Experimental and predicted strain distributions on the specimen  $150 \times 150 \times 260_{D20}$  by Kaklauskas et al. at stress levels (a) 180 MPa, (b) 260 MPa, and (c) 330 MPa

Fig. 3.11 displays a moderate match by the proposed model prediction with the experimental counterpart at 180 MPa and 260 MPa stress levels; it worsens at 330 MPa stress level. At the first two stress levels, Mirza and Houde’s model and Nilson’s model overestimate and the rest underestimate the strain predictions (Fig. 3.11a and b). However, only Mirza and Houde’s model overestimates the strain for the highest stress level (330 MPa). Interestingly, Nilson’s model had an excellent agreement with the experimental strain curve (Fig. 3.11c). The remaining models consistently underestimated the strain distributions, where Kankam’s model and Shima’s model show large discrepancies but the MC 2010 model and Barbosa and Filho’s model display comparatively lower discrepancies at all stress levels. Next, the model-wise strain comparison for Gudonis et al. (2017) specimen is portrayed at various stress levels in Fig. 3.12.



**Fig. 3.12.** Experimental and predicted strain distributions on the specimen 100×100×150\_D16 by Gudonis et al. at stress levels of (a) 250 MPa, (b) 310 MPa, and (c) 380 MPa

Fig. 3.12a displays a good agreement between the experimental strain profile with the proposed model as well as Shima’s model predictions; the rest of the model overestimates the strains throughout the specimen length. The proposed model has shown consistency in its agreement with the experimental model for all stress levels. But for other models, the discrepancy with the experimental model increases gradually at 310 MPa and 380 MPa stress levels (Fig. 3.12b and c). The next strain comparisons are displayed in Fig. 3.13 on the specimen taken from Kankam (Kankam, 1997).



**Fig. 3.13.** Experimental and predicted strain distributions on the specimen 150×150×210\_D25 by Kankam at stress levels of (a) 125 MPa, (b) 170 MPa, and (c) 200 MPa

This independent experimental data was extracted from an RC tie with a  $\phi$ -25 mm hot rolled steel reinforcement bar (Kankam, 1997). Kankam’s model prediction has shown an excellent match with the experimental models at all stress levels, particularly at 200 MPa (Fig. 3.13c). Also, Barbosa and Filho’s model and the proposed model made a reasonably fair agreement with the experimental counterpart (Fig. 3.13). Further, common in all stress levels, Mirza and Houde’s model and Nilson’s model overshoot strain values, whereas Shima’s model and MC 2010

model underestimate the predicted strains. The following Fig. 3.14 represents the experimental and model-predicted strains for the specimen taken from Bado et al. (Bado et al., 2020).

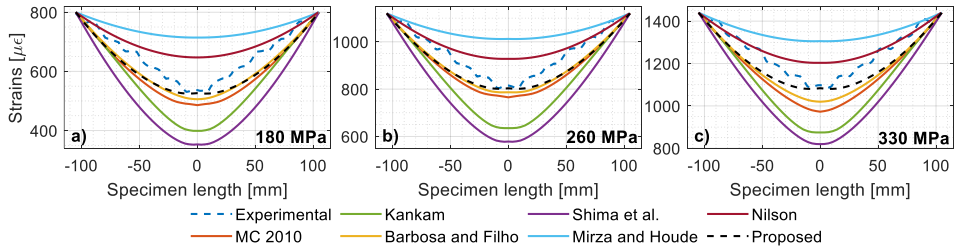


**Fig. 3.14.** Experimental and predicted strain distributions on the specimen  $150 \times 150 \times 210_{D20}$  by Bado et al. at stress levels of (a) 180 MPa, (b) 260 MPa, and (c) 330 MPa

The experimental curves (Fig. 3.14a, b and c) display a somewhat undulating strain profile, which is because of the use of DOFS sensing technology for strain sampling. Some common trends can be noticed for all the stress levels. Such as, the proposed model prediction matches the experimental results only at the central zone of the specimen, whereas Nilson's model made a reasonably good agreement with the experimental strain curves near the specimen edges only (Fig. 3.14). Moderate underestimation by the MC 2010 model and Barbosa and Filho's model, and excessive underestimation by Kankam's model and Shima's model can be noticed in Fig. 3.14. Mirza and Houde's model constantly overestimated the strain predictions at all the stress levels. The next specimen is one of the three identical double pull-out specimens from Jakubovskis and Kaklauskas (Jakubovskis and Kaklauskas, 2019), displayed in Fig. 3.15.

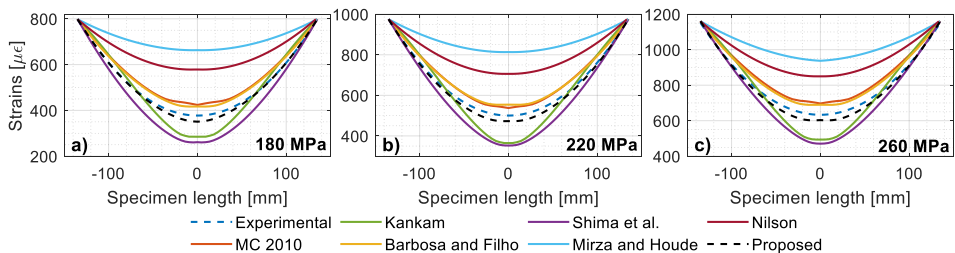


**Fig. 3.15.** Experimental and predicted strain distributions on the specimen  $150 \times 150 \times 270_{D20\_I}$  by Jakubovskis and Kaklauskas at stress levels of (a) 180 MPa, (b) 220 MPa, and (c) 260 MPa

All subplots of Fig. 3.15 indicate a good agreement between experimental strain profiles and the ones predicted by the proposed model. Although slight underestimation at the central zone can be noticed, otherwise, correct estimations are visible on both sides. On the other hand, moderate overestimations are observed for the MC 2010 model and Barbosa and Filho's model.

High discrepancies in strain predictions are seen in Mirza and Houde's model and Nilson's model in terms of overestimation, and Kankam's model and Shima's model in terms of underestimation (Fig. 3.15a, b and c). Overall, all models followed a similar trend through all the stress levels. A similar analysis of the second identical specimen from the same literature is presented in Fig. 3.16.

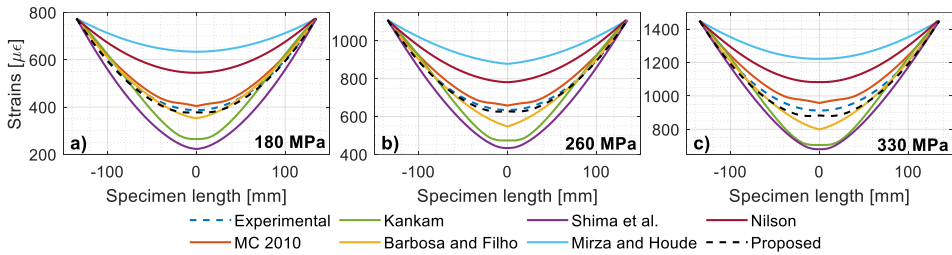


**Fig. 3.16.** Experimental and predicted strain distributions on the specimen 150×150×270\_D20\_II by Jakubovskis and Kaklauskas at stress levels of (a) 180 MPa, (b) 260 MPa, and (c) 330 MPa

Despite being identical to the previous specimen, a higher stress level (like 330 MPa) has been chosen because of the availability of independent experimental data. The proposed model predictions were somewhat fine at 180 MPa and 260 MPa stress levels (Fig. 3.16a and b) but slightly underestimated at 330 MPa (Fig. 3.16c). Reasonably good predictions (slight overestimation) can be seen using the MC 2010 model at all stress levels. Barbosa and Filho's model also produced a good match with the experimental counterpart except for the central zone. The strain discrepancy at this zone is increasing gradually with higher stress levels. Just as in the previous specimen, Mirza and Houde's model and Nilson's model constantly overestimate, and Kankam's model and Shima's model underestimate the strain profiles with high magnitude. The following Fig. 3.17 displays a similar analysis for the third identical specimen from the same authors (Jakubovskis and Kaklauskas, 2019).

Almost similar strain prediction pattern to the previous specimen, the best agreement is obtained by the proposed model, followed by the MC2010 model and Barbosa and Filho's model (Fig. 3.17). Among them, the proposed model marginally underestimates, and the MC2010 model marginally overestimates the strain profiles.

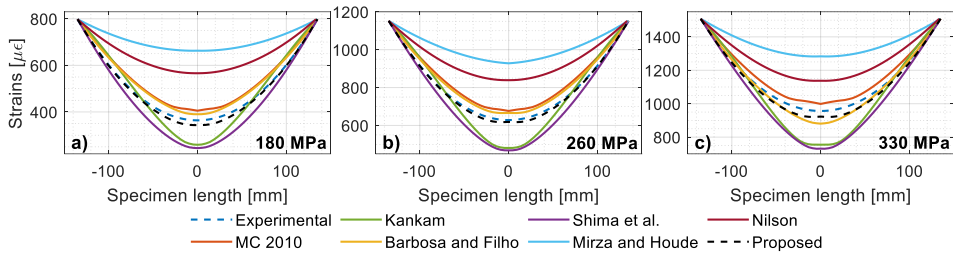


**Fig. 3.17.** Experimental and predicted strain distributions on the specimen 150×150×270\_D20\_III by Jakubovskis and Kaklauskas at stress levels of (a) 180 MPa, (b) 260 MPa, and (c) 330 MPa

Interestingly, Barbosa and Filho’s model overestimates the strains in 180 MPa and 260 MPa stress levels (Fig. 3.17a and b) but underestimates at 330 MPa stress levels (Fig. 3.17c). Persistent overestimation by Mirza and Houde’s model and Nilson’s model, and underestimation by Kankam’s model and Shima’s model can be noticed.

Overall, from the models’ strain prediction comparisons on different real-life RC ties at multiple stress levels (Fig. 3.10–3.17), the following excerpts can be summarised:

- Mirza and Houde’s model persistently overestimates the strain predictions for all the specimens at multiple stress levels. It produced the highest discrepancies in terms of overestimation with respect to experimental data.
- Nilson’s model mostly overestimated the strain profiles except for a few cases. The highest stress level of Kaklauskas’ specimen, it underestimates the strain profile slightly (Fig. 3.11c), and for Bado et al. specimen, shows a good match with the experimental strain curve along the specimen edges only (Fig. 3.14).
- In most of the cases, the MC2010 model and Barbosa and Filho’s model made a reasonable agreement (small discrepancies) with the experimental strain curves. Exceptionally, in the case of Kankam’s specimen, the MC2010 model showed a large disparity in all stress levels (Fig. 3.13).
- Shima’s model prediction mostly underestimates the strain profiles. The model overestimated the strain only for the Gudonis et al. specimen and the Houde specimen. However, in the latter case, the model predictions closely matched the experimental results (Fig. 3.10).
- The slopes of Kankam’s model predict comparatively steeper strain curves. Expectedly, this model made the best agreement with the experimental data of the Kankam specimen (Fig. 3.13). Apart from that, in most

cases, it overestimated near the specimen edges but underestimated at the central zone of the specimen (Fig. 3.17).

- The proposed model predictions are rather close to all the experimental strain outputs, except for the Kaklauskas specimen at 330 MPa (Fig. 3.11c). Importantly, irrespective of specimens, the model always underestimated the strain distributions.

Now, to quantify the models' performance in reinforcement strain prediction, a statistical analysis is needed. The following section demonstrates such an analysis based on the above results to mathematically justify the performance of the models.

### 3.3.3. Statistical Analysis

A statistical study was performed on the ground of the comparisons between experimental and calculated strains through the novel validation tool. To quantify the amount of mismatch in strain profiles, five equidistant locations were chosen along each specimen's length, as illustrated in Fig. 3.18.

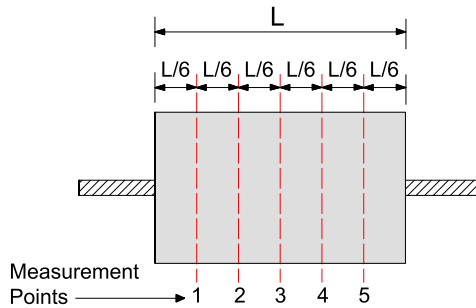


**Fig. 3.18.** Layout of selected points for statistical analysis

Further, the prediction accuracy was calculated through a ratio ( $\bar{\epsilon}$ ), expressed in Eq. 3.6. The ratio was determined at all five locations for each specimen and each model.

$$\bar{\epsilon}_i = \epsilon_{model,i} / \epsilon_{exp,i} \quad | \quad i = 1, 2, \dots, 5. \quad (3.6)$$

Here,  $\epsilon_{exp}$  refers to the strain value from the experimental curve and  $\epsilon_{model}$  indicates the strain value from the model-predicted curve at a particular location  $i$ . For each specimen and one particular model,  $i$  varies from 1 to 5, as there are five location points chosen for the calculation. This parameter ( $\bar{\epsilon}_i$ ) gives a clear idea about the prediction accuracy of the models. For example,  $\bar{\epsilon}_i = 1$  signifies the perfect assumption by the model, whereas  $\bar{\epsilon}_i < 1$  or  $\bar{\epsilon}_i > 1$  indicates

underestimation or overestimation, respectively. Fig. 3.19 reflects the performance of Kankam's model predictions over the experimental strain values of the Houde specimen at a 220 MPa stress level.

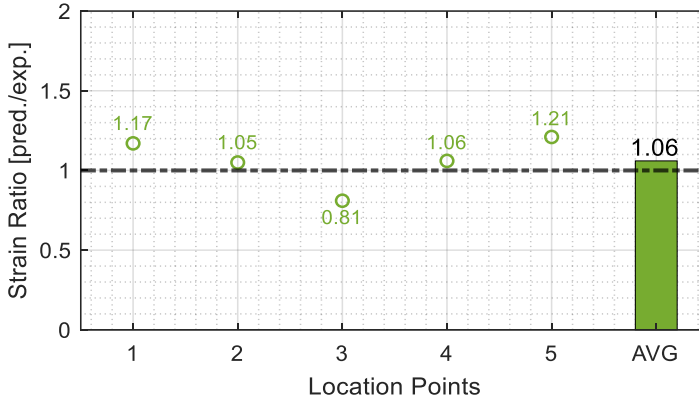


**Fig. 3.19.** Performance of Kankam's model on the Houde specimen 150×150×405\_D25 at a 220 MPa stress level in terms of the ratio  $\bar{\epsilon}$

The x-axis of Fig. 3.19 indicates five location points where the strains were measured for the statistical calculation, and the y-axis represents the strain ratio ( $\bar{\epsilon}$ ). The circular symbols signify the strain ratio values ( $\bar{\epsilon}_i$ ) at five location points. For the first location,  $\bar{\epsilon}_1 = 1.17$  means that Kankam's model strain prediction at that particular point is 17% higher than the experimental strain. As can be observed in Fig. 3.19, there is a maximum overestimation of 21% at location 5 and a 19% underestimation at location 3, which are also visible in Fig. 3.10c. Now, the average of all  $\bar{\epsilon}$  values at five locations are calculated to determine the mean strain ratio ( $\bar{\epsilon}_m$ ). In this case,  $\bar{\epsilon}_m = 1.06$  signifies that on average, Kankam's model overestimates the strain prediction by 6%, based on the experimental strain profiles of the Houde specimen at a 220 MPa stress level.

Similarly, the mean strain ratio ( $\bar{\epsilon}_m$ ) was calculated for each model based on each experimental strain profile. So, each model has three  $\bar{\epsilon}_m$  values for three different stress levels corresponding to one experimental RC tie. In total, 24  $\bar{\epsilon}_m$  values (samples) for eight independent specimens were calculated, which represents the performance of one model. Calculated  $\bar{\epsilon}_m$  values for all the models are given in Table 3.4.

Now, to put it in a nutshell, the average from the 24 mean strain ratio ( $\bar{\epsilon}_m$ ) samples (Table 3.4) were determined for each model, which can be referred to as the global mean. The latter reflects the overall performance of a case study model in terms of strain prediction accuracy.

**Table 3.4.** Calculated mean strain ratios for all assessed bond–slip models with respect to eight experimental RC tie specimens at multiple stress levels

Reference	Stress level (MPa)	MC2 010	Kankam	Barbosa and Filho	Shima	Mirza and Houde	Nilsson	Proposed
Houde	140	1.51	1.21	1.31	1.18	2.29	2.02	0.95
	180	1.40	1.14	1.21	1.16	1.95	1.72	0.93
	220	1.23	1.06	1.07	1.08	1.62	1.41	0.92
Kaklauskas et al.	180	0.88	0.77	0.87	0.70	1.24	1.14	0.90
	260	0.93	0.81	0.91	0.79	1.22	1.11	0.93
	330	0.88	0.77	0.84	0.79	1.08	0.98	0.89
Gudonis et al.	250	1.16	1.08	1.18	1.04	1.30	1.25	0.99
	310	1.18	1.10	1.18	1.08	1.30	1.25	0.99
	380	1.18	1.10	1.18	1.09	1.28	1.23	0.99
Kankam	125	0.95	0.97	1.04	0.92	1.29	1.23	0.98
	170	0.96	0.99	1.04	0.94	1.25	1.22	0.99
	200	0.94	1.00	1.03	0.95	1.21	1.19	0.99
Bado et al.	180	0.90	0.82	0.92	0.74	1.17	1.09	0.93
	220	0.92	0.84	0.94	0.78	1.12	1.05	0.94
	260	0.91	0.86	0.93	0.81	1.09	1.03	0.95
Jakubovskis and Kaklauskas I	180	1.09	0.93	1.08	0.83	1.50	1.35	0.97
	260	1.07	0.92	1.08	0.85	1.42	1.28	0.97
	330	1.08	0.94	1.07	0.88	1.34	1.24	0.97
Jakubovskis and Kaklauskas II	180	1.04	0.89	0.99	0.77	1.43	1.28	0.98
	260	1.04	0.90	0.96	0.83	1.28	1.17	0.99
	330	1.04	0.90	0.95	0.87	1.24	1.14	0.97
Jakubovskis and Kaklauskas III	180	1.09	0.93	1.08	0.83	1.54	1.37	0.97
	260	1.07	0.93	1.05	0.87	1.34	1.23	0.99
	330	1.04	0.91	0.97	0.88	1.24	1.14	0.99
Global Mean		1.07	0.94	1.05	0.90	1.37	1.25	0.97
Std. Dev.		0.16	0.12	0.12	0.14	0.27	0.22	0.03
CV		0.15	0.12	0.15	0.15	0.20	0.18	0.03

Table 3.3 reflects the closest prediction performance by the proposed model with a global mean of 0.97. It means that overall, the proposed model underestimates the strain distribution by almost 3%. On the other hand, the maximum overestimation was 37%, predicted by Mirza and Houde’s model (1.37). Apart from these, 25%, 7% and 5% overestimated predictions were performed by Nilson’s model (1.25), the MC2010 model (1.07) and Barbosa and Filho’s model (1.05), respectively. 6% and 10% lower predictions were performed by Kankam’s model (0.94) and Shima’s model (0.90), respectively.

Furthermore, to check the number of samples (mean strain errors), that differ from the global mean value, the standard deviation (Std. Dev.) for each model was calculated (Table 3.4). The minimum standard deviation was acquired by the proposed model (0.03), and the maximum was by Mirza and Houde’s model (0.27). The coefficient of variation (CV) represents a statistical measurement of the relative dispersion of samples among a set around its global mean (Table 3.4). The lower the CV value, the lesser the level of dispersion from the global mean value. It can be seen from Table 3.4 that the proposed model produced the least CV, which is 0.03. This implies that 3% of samples (mean strain errors) are distributed away from the mean (Fig. 3.20a). Kankam’s model has shown the second lowest CV (12%). The highest CV was observed for Mirza and Hode’s model (20%), followed by Nilson’s model (18%). For every single model, a single global mean, standard deviation and coefficient of variation provide an effective assessment of the ability of strain prediction. These are summarised through probability density curves or bell-shaped curves for individual models, shown in Fig. 3.20b.

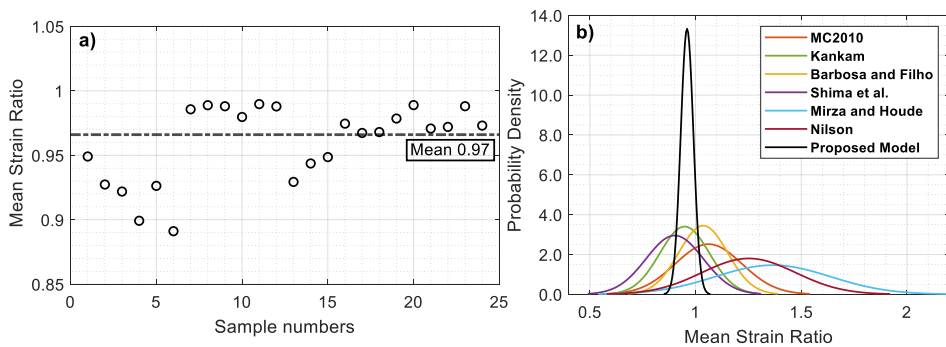


**Fig. 3.20.** Performance of bond–slip models through statistical analysis: (a) global mean strain ratios of the proposed model; (b) probability density curves for all the assessed bond–slip models

Fig. 3.20a represents the scatter plot of mean strain ratios for the proposed model, where the black line signifies the global mean of 0.97. The probability

density curves for all the models are displayed in Fig. 3.20b. As anticipated earlier, the proposed model displays the narrowest and tallest normal distribution curve due to its smallest standard deviation and coefficient of variation. It signifies a large data concentration around the mean value. On the other hand, the maximum spread in normal distribution can be seen for Mirza and Houde’s model, indicating a large data spread and hence, the most inconsistent one.

It is worth mentioning that the present investigation represents the preliminary stage of a comprehensive bond–slip study, where the author has primarily concentrated on the general aspects of the subject. Undoubtedly, exploring the other parameters, such as the influence of rib pattern, can be an intriguing avenue for future research, encompassing steel bars with different rib patterns as well as plain bars. This aspect holds promising potential for further investigations in the field.

### 3.4. Conclusions of the Third Chapter

The Third Chapter centred on developing and validating a novel bond–slip model. The essential takeaways can be summarised as follows:

1. The regression analysis determined that the slip/diameter ratio and concrete strength exhibit the most significant influence on the bond stress of RC structures.
2. The proposed model exhibits the ability to forecast the bond–slip behaviour of an RC member, particularly focusing on the ascending section of the bond–slip curve, encompassing its intrinsic material characteristics. In the future, the model holds the potential for utilisation in the advancement of constitutive bond–slip models aimed at predicting the serviceability of reinforced concrete structures.
3. The proposed validation tool’s ability to predict reinforcement strain can greatly streamline the strenuous and time-consuming process of mathematical and experimental verification and comparison with existing models. Besides, this tool opens a future scope of investigations on stress transfer analysis, bond–slip modelling and, eventually, the serviceability of RC structures.
4. As demonstrated by statistical analysis, the proposed model underestimated reinforcement strains by 3%. Similarly, Kankam’s model and Shima’s model underestimated the strains by 6% and 10%, respectively, whereas the predictions by the remaining model were on the safe side: 5% for Barbosa and Filho’s model, 7% for the MC2010 model, 25% for Nilson’s model, and 37% for Mirza and Houde’s model. The proposed

model has demonstrated the best prediction results in terms of scatter with the coefficient of variation (CV) being 3%, followed by 12% for Kankam's model, 15% for the MC2010 model, Shima's model, and Barbosa and Filho's model, 18% for Nilson's model, and 20% for Mirza and Houde's model.

---

## General Conclusions

The present study aimed to introduce a better and more modern approach to understanding the concrete–reinforcement interaction and its importance in the serviceability of RC structures. A new bond–slip model was developed as a result of investigating and analysing multiple RC ties subjected to tension. The author has developed and proposed a validation tool that can derive reinforcement strain distribution from a given bond–slip law. To summarise, the implementation of the stress transfer approach, the development of a novel model for the ascending part of the bond–slip relationship and a validation tool for reinforcement strain prediction have yielded the following observations and findings:

1. The standard pull-out test is unsuitable for predicting the local bond–slip behaviour of RC members under service load due to various constraints. Conversely, the double pull-out test, which overcomes these constraints and involves recording reinforcement strains along the bonded length, offers a more reliable approach for evaluating bond behaviour. However, a very limited number of double pull-out tests have been conducted in the past, and none of them has been aimed at forecasting the serviceability analysis of RC members.
2. The conducted regression analysis determined that the slip/diameter ratio and the concrete strength exert the most significant influence on the bond stress observed in RC structures.

3. The proposed bond model exhibits the capability of accurately predicting the correlation between bond stress and slip along the cracks of an RC tensile element.
4. The developed validation tool has demonstrated that the proposed bond–slip model is capable of accurately predicting the reinforcement strain distribution in RC tension members subjected to service load.
5. According to a statistical analysis that involved independent test data of RC ties, the proposed model displayed a 3% underestimation of reinforcement strains, along with a coefficient of variation (CV) indicating a scatter of 3%. These values represent the lowest levels when compared to existing bond–slip models. Consequently, the proposed model can be considered the most accurate and optimal in its ability to predict reinforcement strains in RC elements.
6. The proposed model exclusively encompasses the ascending branch of a constitutive bond–slip law, while the descending branch, which involves various phenomena such as damage, de-bonding, internal cracking, tension softening etc., can be a potential avenue for future research. This may enhance the model’s ability to predict the serviceability analysis of RC structures, thus offering potential utility in practical applications.

---

## References

Abrams, D. A. (1925). Studies on bond between concrete and steel. In *Proceedings. Am. Soc. Testing Mats.* (Vol. 25, Part II, p. 256).

ACI Committee 408. (2003). *408R-03: Bond and Development of Straight Reinforcing Bars in Tension*. American Concrete Institute.

Al-Jahdali, F. A., Wafa, F. F., and Shihata, S. A. (1994). Development length for straight deformed bars in high-strength concrete. *ACI Special Publication, SP-149*, 507–521. <https://doi.org/10.14359/4173>

Bado, M.F., Casas, J. R., Dey, A., and Berrocal, C. G. (2020). Distributed optical fiber sensing bonding techniques performance for embedment inside reinforced concrete structures. *Sensors*, 20(20). <https://doi.org/10.3390/s20205788>

Bado, Mattia Francesco, Casas, J. R., Dey, A., Berrocal, C. G., Kaklauskas, G., Fernandez, I., and Rempling, R. (2021). Characterization of concrete shrinkage induced strains in internally-restrained RC structures by distributed optical fiber sensing. *Cement and Concrete Composites*, 120(February), 104058. <https://doi.org/10.1016/j.cemconcomp.2021.104058>

Bado, M. F., Casas, J. R., and Kaklauskas, G. (2021). Distributed Sensing (DOFS) in Reinforced Concrete members for reinforcement strain monitoring, crack detection and bond-slip calculation. *Engineering Structures*, 226(February 2020), 111385. <https://doi.org/10.1016/j.engstruct.2020.111385>

- Barbosa, M. T. G., and Filho, E. S. (2016). The bond stress x slipping relationship. *Revista IBRACON de Estruturas e Materiais*, 9(5), 745–753. <https://doi.org/10.1590/s1983-41952016000500006>
- Bischoff, P. H. (2001). Effects of shrinkage on tension stiffening and cracking in reinforced concrete. *Canadian Journal of Civil Engineering*, 28(3), 363–374. <https://doi.org/10.1139/cjce-28-3-363>
- Borosnyoi, A., and Balazs, G. L. (2005). Models for flexural cracking in concrete: the state of the art. *Structural Concrete*, 6(2), 53–62. <https://doi.org/10.1680/stco.6.2.53.66711>
- Bureau of Indian Standards. (2000). *Plain and reinforced concrete - code of practice* (IS:456 - 2000, reaffirmed 2005).
- Cairns, J., and Jones, K. (1995). The splitting forces generated by bond. *Magazine of Concrete Research*, 47(171), 153–165.
- Cantarero, A. (2015). Raman scattering applied to materials science. *Procedia Materials Science*, 9, 113–122. <https://doi.org/10.1016/j.mspro.2015.04.014>
- Capoluongo, P., Ceroni, F., Ambrosino, C., Campopiano, S., Giordano, M., Cutolo, A., and Cusano, A. (2005). Fiber bragg grating sensors for breaking tests in reinforced concrete structures strengthened with embedded composite bars. *Biomedical Materials*, February 2014, 383–388.
- Chapman, R. A., and Shah, S. P. (1987). Early-age bond strength in reinforced concrete. *ACI Materials Journal*, 84(6), 501–510.
- Darwin, D., McCabe, S., Idun, E., and Schoenekase, S. (1992). Development Length Criteria: Bars without Transverse Reinforcement. *ACI Structural Journal*, 89, (6), 709–720).
- Davis, M., Hoult, N. A., and Scott, A. (2016). Distributed strain sensing to determine the impact of corrosion on bond performance in reinforced concrete. *Construction and Building Materials*, 114, 481–491. <https://doi.org/10.1016/j.conbuildmat.2016.03.205>
- Deif, A., Martín-Pérez, B., Cousin, B., Zhang, C., Bao, X., and Li, W. (2010). Detection of cracks in a reinforced concrete beam using distributed Brillouin fibre sensors. *Smart Materials and Structures*, 19(5). <https://doi.org/10.1088/0964-1726/19/5/055014>
- Desir, J. M., Romdhane, M. R. B., Ulm, F., and Fairbairn, E. M. R. (1999). Steel - concrete interface : revisiting constitutive and numerical modeling. *Computers and Structures*, 71, 489–503.
- Desnerck, P., Schutter, G. De, and Taerwe, L. (2010). A local bond stress-slip model for reinforcing bars in self-compacting concrete. In *Proceedings of Fracture Mechanics of Concrete and Concrete Structures* (Vol. 2, pp. 771–778). <https://biblio.ugent.be/publication/1579403>
- Di Sante, R. (2015). Fibre optic sensors for structural health monitoring of aircraft composite structures: Recent advances and applications. *Sensors*, 15(8), 18666–18713. <https://doi.org/10.3390/s150818666>

- Eligehausen, R., Popov, E. P., and Bertero, V. V. (1982). *Local bond stress- slip relationships of deformed bars under generalized excitations* (pp. 69–80). Earthquake Engineering Research Center, College of Engineering, University of California.
- Esfahani, M. R., and Rangan, B. V. (1998). Local bond strength of reinforcing bars in normal strength and high-strength concrete (HSC). *ACI Structural Journal*, 95(2), 96–106.
- Fib model code for concrete structures 2010*. (2013). International Federation for Structural Concrete(FIB), Switzerland, Federal Institute of Technology Lausanne-EPFL. <http://repositorio.unan.edu.ni/2986/1/5624.pdf>
- Friebele, E. J. (1998). Fiber Bragg grating strain sensors. *Optics and Photonics News*, 9(August), 566–580.
- García-taengua, E., Martí-vargas, J. R., and Serna, P. (2014). Splitting of concrete cover in steel fiber reinforced concrete: Semi-empirical modeling and minimum confinement requirements. *Construction and Building Materials*, 66, 743–751. <https://doi.org/10.1016/j.conbuildmat.2014.06.020>
- Gilbert, R. I. (2001). Shrinkage, cracking and deflection - The serviceability of concrete structures. *Electronic Journal of Structural Engineering*, 1, 15–37.
- Goto, Y. (1971). Cracks formed in concrete around deformed tension bars. *Journal Proceedings*, 68(4), 244–251.
- Gribniak, V. (2009). *Shrinkage influence on tension-stiffening of concrete structures* [Daktaro disertacija. Vilniaus gedimino technikos universitetas]. Technika.
- Gribniak, V., Jakubovskis, R., Rimkus, A., Ng, P. L., and Hui, D. (2018). Experimental and numerical analysis of strain gradient in tensile concrete prisms reinforced with multiple bars. *Construction and Building Materials*, 187, 572–583. <https://doi.org/10.1016/j.conbuildmat.2018.07.152>
- Gribniak, V., Rimkus, A., Torres, L., and Hui, D. (2018). An experimental study on cracking and deformations of tensile concrete elements reinforced with multiple GFRP bars. *Composite Structures*, 201(April), 477–485. <https://doi.org/10.1016/j.compstruct.2018.06.059>
- Gudonis, E., Ramanauskas, R., and Aleksandr, S. (2017). Experimental investigation on strain distribution in reinforcement of RC specimens. In *2nd International RILEM/COST Conference on Early Age Cracking and Serviceability in Cement-Based Materials and Structures (EAC2), Brussels, Belgium, 1(12-14 September)* (pp. 573–578).
- Hadi, M. N. S. (2008). Bond of high strength concrete with high strength reinforcing steel. *The Open Civil Engineering Journal*, 2(1), 143–147. <https://doi.org/10.2174/1874149500802010143>
- Harajli, M. H. (2004). Comparison of bond strength of steel bars in normal- and high-strength concrete. *Journal of Materials in Civil Engineering*, 16(4), 365–374. [https://doi.org/10.1061/\(ASCE\)0899-1561\(2004\)16:4\(365\)](https://doi.org/10.1061/(ASCE)0899-1561(2004)16:4(365))
- Henault, J. M., Quiertant, M., Delepine-Lesoille, S., Salin, J., Moreau, G., Taillade, F., and Benzarti, K. (2012). Quantitative strain measurement and crack detection in RC

structures using a truly distributed fiber optic sensing system. *Construction and Building Materials*, 37, 916–923. <https://doi.org/10.1016/j.conbuildmat.2012.05.029>

Hong, C. Y., Zhang, Y. F., Li, G. W., Zhang, M. X., and Liu, Z. X. (2017). Recent progress of using Brillouin distributed fiber optic sensors for geotechnical health monitoring. *Sensors and Actuators, A: Physical*, 258, 131–145. <https://doi.org/10.1016/j.sna.2017.03.017>

Hong, S., and Park, S. K. (2012). Uniaxial bond stress-slip relationship of reinforcing bars in concrete. *Advances in Materials Science and Engineering*, 2012, 328570. <https://doi.org/10.1155/2012/328570>

Houde, J. (1974). *Study of force-displacement relationships for the finite-element analysis of reinforced concrete*. McGill University.

International Organization for Standardization. (2004). *Eurocode 2: Design of concrete structures - Part 1-1 : General rules and rules for buildings* (EN 1992-1-1:2004).

Magnusson, J., and Engstrom, B. (2000). Anchorage of Ribbed bars in high strength concrete beams. In *PCI/FHWA/FIB International Symposium on High Performance Concrete Precast/ Prestressed Concrete Institute Federal Highway Administration Federation Internationale du Beton*.

Jakubovskis, R., and Kaklauskas, G. (2019). Bond-stress and bar-strain profiles in RC tension members modelled via finite elements. *Engineering Structures*, 194(January), 138–146. <https://doi.org/10.1016/j.engstruct.2019.05.069>

Jakubovskis, R., and Kaklauskas, G. (2021). Damage of bond in reinforced concrete: A detailed finite element analysis. *Structural Concrete*, April, 1–13. <https://doi.org/10.1002/suco.202100229>

Kaklauskas, G. (2017). Crack model for RC members based on compatibility of stress-transfer and mean-strain approaches. *Journal of Structural Engineering (United States)*, 143(9), 1–12. [https://doi.org/10.1061/\(ASCE\)ST.1943-541X.0001842](https://doi.org/10.1061/(ASCE)ST.1943-541X.0001842)

Kaklauskas, G., Gribniak, V., Jakubovskis, R., Gudonis, E., Salys, D., and Kupliauskas, R. (2012). Serviceability analysis of flexural reinforced concrete members. *Journal of Civil Engineering and Management*, 18(1), 24–29. <https://doi.org/10.3846/13923730.2011.643553>

Kaklauskas, G., Ramanauskas, R., and Jakubovskis, R. (2017). Mean crack spacing modelling for RC tension elements. *Engineering Structures*, 150, 843–851. <https://doi.org/10.1016/j.engstruct.2017.07.090>

Kaklauskas, G., Ramanauskas, R., and Ng, P. L. (2019). Predicting crack spacing of reinforced concrete tension members using strain compliance approach with debonding. *Journal of Civil Engineering and Management*, 25(5), 422–430. <https://doi.org/10.3846/jcem.2019.9871>

Kaklauskas, G., Sokolov, A., Ramanauskas, R., and Jakubovskis, R. (2019). Reinforcement strains in reinforced concrete tensile members recorded by strain gauges

and FBG sensors: Experimental and numerical analysis. *Sensors*, 1–13. <https://doi.org/10.3390/s19010200>

Kanakubo, T., Sato, Y., Uchida, Y., Watanabe, K., and Shima, H. (2012). Japan Concrete Institute TC Activities on bond behavior and constitutive laws in RC (Part 3: Application of Constitutive Laws for FEA ). *Bond in Concrete 2012*, 1(September), 105–112.

Kanazawa, T., Sato, Y., and Mikawa, T. (2017). Modeling of bond deterioration between steel bar and concrete subjected to freeze-thaw action. *Journal of Advanced Concrete Technology*, 15(8), 397–406. <https://doi.org/10.3151/jact.15.397>

Kankam, C. K. (1997). Relationship of bond stress, steel stress, and slip in reinforced concrete. *Journal of Structural Engineering*, 123(1), 79–85.

Kemp, E. L. (1986). Bond in reinforced concrete: Behavior and design criteria. *Journal of the American Concrete Institute*, 83(1), 50–57. <https://doi.org/10.14359/1760>

Kenel, A., Nellen, P., Frank, A., and Marti, P. (2005). Reinforcing steel strains measured by Bragg grating sensors. *Journal of Materials in Civil Engineering*, 17(4), 423–431. [https://doi.org/10.1061/\(ASCE\)0899-1561\(2005\)17:4\(423\)](https://doi.org/10.1061/(ASCE)0899-1561(2005)17:4(423))

Kerrouche, A., Boyle, W. J. O., Sun, T., Grattan, K. T. V., Schmidt, J. W., and Täljsten, B. (2009). Strain measurement using embedded fiber bragg grating sensors inside an anchored carbon fiber polymer reinforcement prestressing rod for structural monitoring. *IEEE Sensors Journal*, 9(11), 1456–1461. <https://doi.org/10.1109/JSEN.2009.2018355>

Lau, K. T., Chan, C. C., Zhou, L. M., and Jin, W. (2001). Strain monitoring in composite-strengthened concrete structures using optical fibre sensors. *Composites Part B: Engineering*, 32(1), 33–45. [https://doi.org/10.1016/S1359-8368\(00\)00044-5](https://doi.org/10.1016/S1359-8368(00)00044-5)

Lee, S. W., Kang, S. B., Tan, K. H., and Yang, E. H. (2016). Experimental and analytical investigation on bond-slip behaviour of deformed bars embedded in engineered cementitious composites. *Construction and Building Materials*, 127, 494–503. <https://doi.org/10.1016/j.conbuildmat.2016.10.036>

Leng, J. S., Winter, D., Barnes, R. A., Mays, G. C., and Fernando, G. F. (2006). Structural health monitoring of concrete cylinders using protected fibre optic sensors. *Smart Materials and Structures*, 15(2), 302–308. <https://doi.org/10.1088/0964-1726/15/2/009>

Leonhardt, F. (1988). Cracks and crack control in concrete structures. *PCI Journal*, 33(4), 124–145. <https://doi.org/10.15554/pcij.07011988.124.145>

Lundgren, K. (2005). Bond between ribbed bars and concrete. Part 1: Modified model. *Magazine of Concrete Research*, 57(7), 371–382. <https://doi.org/10.1680/mac.2005.57.7.371>

Marti, P., Alvarez, M., Kaufmann, W., and Sigrist, V. (1998). Tension chord model for structural concrete. *Structural Engineering International: Journal of the International Association for Bridge and Structural Engineering (IABSE)*, 8(4), 287–298. <https://doi.org/10.2749/101686698780488875>

Martin, H. (1973). Relationship between surface texture, and composite explosive effect of reinforcing steels for short term load. *German Committee for Reinforced Concrete*, 228.

Masukawa, J. (2012). *Degradation of Shear Performance of Beams due to Bond Deterioration and Longitudinal Bar Cutoffs* [Doctoral Thesis. University of Roronto].

Mirza, S. M., and Houde, J. (1978). Study of bond stress-slip relationships in reinforced concrete. *J Am Concr Inst*, 76(1). <https://doi.org/10.14359/6935>

Moallemi Pour, S., and Alam, M. S. (2016). Investigation of compressive bond behavior of steel rebar embedded in concrete with partial recycled aggregate replacement. *Structures*, 7, 153–164. <https://doi.org/10.1016/j.istruc.2016.06.010>

Nilson, A. H. (1972, July). Internal measurement of bond slip. *Journal Proceedings* (Vol. 69, No. 7, pp. 439-441).

Orangun, C. O., Jirsa, J. O., and Breen, J. E. (1977). Reevaluation of test data on development length and splices. *J Am Concr Inst*, 74(3), 114–122. <https://doi.org/10.14359/10993>

Rao, G. A., Pandurangan, K., Sultana, F., and Eligehausen, R. (2007). Studies on the pull-out strength of ribbed bars in high-strength concrete. In *Proceedings of the 6th international conference on fracture mechanics of concrete and concrete structures* (Vol. 2, pp. 775–780).

Rehm, G. (1961). The Fundamentals of Bond Between Reinforcement and Concrete. *Deutscher Ausschuss Für Stahlbeton*, 138(59).

Ruiz, M. F., Muttoni, A., and Gambarova, P. G. (2007). Analytical modeling of the pre- and postyield behavior of bond in reinforced concrete. *Journal of Structural Engineering*, 133(10), 1364–1372. [https://doi.org/10.1061/\(ASCE\)0733-9445\(2007\)133:10\(1364\)](https://doi.org/10.1061/(ASCE)0733-9445(2007)133:10(1364))

Scott, R. H., and Gill, P. A. T. (1987). Short-term distributions of strain and bond stress along tension reinforcement. *The Structural Engineer*, 65B, 65, 39–43,48.

Serviceability research, A. H. C. on. (1986). Structural serviceability: A critical appraisal and research needs. *Journal of Structural Engineering (United States)*, 112(12), 2646–2664. [https://doi.org/10.1061/\(ASCE\)0733-9445\(1986\)112:12\(2646\)](https://doi.org/10.1061/(ASCE)0733-9445(1986)112:12(2646))

Shima, H., Chou, L. L., and Okamura, H. (1987). Micro and Macro Models for Bond in Reinforced Concrete. In *Journal of the Faculty of Engineering, University of Tokyo, Series B* (Vol. 39, Issue 2, pp. 133–194).

Siempu, R., and Pancharathi, R. K. (2018). A study on the parameters influencing flexural bond stress in reinforced concrete. *Structures*, 16(September), 198–207. <https://doi.org/10.1016/j.istruc.2018.09.006>

Siempu, R., and Pancharthi, R. K. (2017a). Bond characteristics of concrete made of recycled aggregates from building demolition waste. *Magazine of Concrete Research*, 69(13), 665–682. <https://doi.org/10.1680/jmacr.16.00400>

Siempu, R., and Pancharthi, R. K. (2017b). Bond performance of ribbed steel reinforcing bars in vibrated and self-compacting concrete. In *Proceedings of the Institution of Civil Engineers: Structures and Buildings*, 170(6), 419–436. <https://doi.org/10.1680/jstbu.16.00083>

- Slowik, V., Schlattner, E., and Klink, T. (2004). Experimental investigation into early age shrinkage of cement paste by using fibre Bragg gratings. *Cement and Concrete Composites*, 26(5), 473–479. [https://doi.org/10.1016/S0958-9465\(03\)00077-5](https://doi.org/10.1016/S0958-9465(03)00077-5)
- Stewart, M. G. (1996). Serviceability reliability analysis of reinforced concrete structures. *Journal of Structural Engineering*, 122(7), 794–803. [http://ascelibrary.org/doi/abs/10.1061/\(ASCE\)0733-9445\(1996\)122:7\(794\)](http://ascelibrary.org/doi/abs/10.1061/(ASCE)0733-9445(1996)122:7(794))
- Sulaiman, M. F., Ma, C. K., Apandi, N. M., Chin, S., Awang, A. Z., Mansur, S. A., and Omar, W. (2017). A review on bond and anchorage of confined high-strength concrete. *Structures*, 11(January), 97–109. <https://doi.org/10.1016/j.istruc.2017.04.004>
- Tepfers, R. (1979). Cracking of concrete cover along anchored deformed reinforcing bars. *Magazine of Concrete Research*, 31(106), 3–12. <https://doi.org/10.1680/mac.1979.31.106.3>
- Villalba, S., and Casas, J. R. (2013). Application of optical fiber distributed sensing to health monitoring of concrete structures. *Mechanical Systems and Signal Processing*, 39(1–2), 441–451. <https://doi.org/10.1016/j.ymsp.2012.01.027>
- Wenkenbach, I. (2011). *Tension stiffening in reinforced concrete members with large diameter reinforcement* [Thesis Master of Science. Durham University]. <http://etheses.dur.ac.uk/3250/>
- Windisch, A. (1985). A modified pull-out test and new evaluation methods for a more real local bond-slip relationship. *Materials and Structures*, 18(3), 181–184. <https://doi.org/10.1007/BF02472967>
- Yazdizadeh, Z., Marzouk, H., and Hadianfard, M. A. (2017). Monitoring of concrete shrinkage and creep using Fiber Bragg Grating sensors. *Construction and Building Materials*, 137, 505–512. <https://doi.org/10.1016/j.conbuildmat.2017.01.084>
- Yoon, H. J., Song, K. Y., Kim, H. M., and Kim, J. S. (2011). Strain monitoring of composite steel girder bridge using distributed optical fibre sensor system. *Procedia Engineering*, 10, 2544–2547. <https://doi.org/10.1016/j.proeng.2011.04.419>
- Zeni, L., Picarelli, L., Avolio, B., Coscetta, A., Papa, R., Zeni, G., Di Maio, C., Vassallo, R., and Minardo, A. (2015). Brillouin optical time-domain analysis for geotechnical monitoring. *Journal of Rock Mechanics and Geotechnical Engineering*, 7(4), 458–462. <https://doi.org/10.1016/j.jrmge.2015.01.008>



---

# List of Scientific Publications by the Author on the Topic of the Dissertation

## Papers in the Reviewed Scientific Journals

Dey, A., Vastrad, A. V., Bado, M. F., Sokolov, A., and Kaklauskas, G. (2021). Long-term concrete shrinkage influence on the performance of reinforced concrete structures. *Materials*, 14(2), 254. <https://doi.org/10.3390/ma14020254>

Dey, A., Valiukas, D., Jakubovskis, R., Sokolov, A., and Kaklauskas, G. (2021). Experimental and numerical investigation of bond-slip behavior of high-strength reinforced concrete at service load. *Materials*, 15(1), 293. <https://doi.org/10.3390/ma15010293>

Dey, A., Bado, M. F., and Kaklauskas, G. (2022). Validation of reinforced concrete bond stress–slip models through an analytical strain distribution comparison. *Materials and Structures*, 55(10), 240. <https://doi.org/10.1617/s11527-022-02071-y>

## Papers in Other Editions

Dey, A., Bado, M. F., Sokolov, A., and Kaklauskas, G. (2020). Distributed sensing, fiber Bragg gratings and strain gauges for strain monitoring of RC tensile elements. In *Proceeding of the fib Symposium 2020, Concrete Structures for Resilient Society, 22nd to 24th November, Shanghai, China*. <https://doi.org/10.1002/suco.202070010>

Dey, A., Valiukas, D., Sokolov, A., Jakubovskis, R., and Kaklauskas, G. (2021). Experimental and Numerical investigation of bond performance of RC tension members. In *fib Symposium 2021, 14–16th June, Lisbon, Portugal*.  
<https://doi.org/10.1002/suco.202170060>

---

# Summary in Lithuanian

## Įvadas

### Problemos formulavimas

Viena svarbiausių gelžbetonio (toliau – GB) konstrukcijų savybių yra jų tinkamumas eksploatuoti atsižvelgiant į konstrukcijos praktiškumą, efektyvumą ir jos eksploatacinę būklę viso gyvavimo laikotarpiu. Nors tinkamumą eksploatuoti galima vertinti pagal daugelį kriterijų: deformacijas, pasireiškiančias vibracijas, išvaizda, galimą konstrukcijų šiluminį judėjimą, atsparumą ugniai ir kt., tačiau vienais svarbiausių, susijusių su būtinomis eksploatacinėmis savybėmis grįstu projektavimu, laikomi įlinkio ir pleišėjimo kriterijai. Šiais laikais, siekiant užtikrinti konstrukcijų tinkamumą eksploatuoti, dažnai taikomas vidutinių deformacijų metodas. Šis metodas neretai grindžiamas tam tikromis supaprastintomis prielaidomis, pavyzdžiui, tariama, kad sukibimo įtempiai tarp betono ir armatūros per visą nagrinėjamojo GB elemento ilgį yra pastovūs arba kad tarp betono ir armatūros egzistuoja ideali sąveika. Šios prielaidos smarkiai supaprastina armatūros ir betono sąveikos analizę, tačiau pakeičia realią sukibimo elgseną fiktyvia. Dėl šios priežasties, remiantis tokiomis klaidingomis prielaidomis, sukurti modeliai tarpusavyje dažnai prieštarauja ir nėra patikimi (netikslūs).

Siekiant efektyviai įveikti šiuos iššūkius, disertaciniame darbe norima sukurti naują modelį, nusakantį sukibimo įtempių ir slinkties tarpusavio ryšį GB konstrukcijose. Bus taikomas šiuolaikiškas ir tikroviškas įtempių perdavimo metodas, pagrįstas tiksliais betono ir armatūros sąveiką apibūdinančiais duomenimis, naudojant galimas eksperimentines

deformacijos stebėjimo priemonės. Kaip neatskiriama platesnio tyrimo sudedamoji dalis, dabartinis modelis apima tik kylančiąją sukibimo įtempių ir slinkties fizikinio modelio dalį. Krentančioji dalis, apimanti įvairius reiškinius, tokius kaip sukibimo pažeidimas dėl didėjančios apkrovos bei išilginių plyšių, vidinių plyšių, tempiamojo betono įtempių plyšyje ir kt., reikalauja išsamesnių eksperimentinių duomenų ir lieka būsimiems tyrimams. Ateityje eksperimentinius rezultatus papildžius naujais duomenimis, tikimasi sukurti tokį sukibimo įtempių ir slinkties modelį, kuriuo bus galima tiksliai prognozuoti GB konstrukcijų pleišėjimą ir deformacijas.

Iki šiol vis dar nėra pasiūlytos efektyvios priemonės, skirtos jau esamiems ir (arba) naujai sukurtiems modeliams patikrinti ir kalibruoti. Šiame tyrime taip pat siekiama išspręsti ir šią problemą, sukuriant programinį paketą, skirtą armatūros deformacijų pasiskirstymui GB elemente nustatyti, žinant konkretų sukibimo ir slinkties modelį.

### **Darbo aktualumas**

Įtempių perdavimo metodas – šiuolaikinė teorija, pagal kurią betono ir armatūros sąveika priklauso nuo sukibimo jėgos perdavimo elgsenos. Šių medžiagų sąveika, paprastai vadinama sukibimu, daro didelę įtaką konstrukcijos elgsenai. Ryšiui paprastai būdingi pagrindiniai šlyties įtempių (atsirandančių sąsajos srityje) ir slinkties (santykinio poslinkio tarp šių medžiagų) principai. Ryšio įtempis ir slinktis laikomi dviem tarpusavyje susijusiais pagrindiniais jėgos perdavimo elementais.

Yra nustatyta, jog įtempių perdavimo metodas visiškai nusako faktinę vidinę elgseną betono ir armatūros sąlyčio zonoje, todėl tai yra universali priemonė, skirta GB konstrukcijų pleišėjimui, plyšio pločiui ir deformacijoms tirti. Deja, egzistuojančiais sukibimo ir slinkties modeliais vis dar negalima tiksliai prognozuoti GB konstrukcijų sukibimo elgsenos. Tikėtina to priežastis – iki šiol nėra patikimų priemonių, kuriomis būtų galima veiksmingai ir tiksliai įvertinti armatūros deformacijų pasiskirstymą gelžbetoniniame elemente. Dėl šios priežasties būtina sukurti naują sukibimo ir slinkties modelį, kuris būtų paremtas įtempių perdavimo metodu bei sudarytų sąlygas tiksliai prognozuoti armatūros deformacijas ir tokiu būdu užtikrintų GB konstrukcijų tinkamumą eksploatuoti.

Be to, šiuo metu svarbu sukurti priemonę, leidžiančią patikrinti skirtingų sukibimo ir slinkties modelių patikimumą bei prognozuoti deformacijų pasiskirstymą armatūroje.

### **Tyrimo objektas**

Šio tyrimo objektas – sukibimo įtempių ir slinkties tarpusavio ryšys GB konstrukcijų betono ir armatūros sąlyčio zonoje, tarp dviejų gretimų plyšių veikiant eksploatacinėms apkrovoms.

### **Darbo tikslas**

Šio darbo tikslas – sukurti naują armatūros ir betono sukibimo modelį, skirtą tempiamiesiems GB elementams, veikiamiems eksploatacinių apkrovų.

## Darbo uždaviniai

Darbo tikslui pasiekti keliami šie uždaviniai:

1. Atlikti išsamią esamų sukibimo modelių literatūros apžvalgą ir nustatyti jų patikimumą.
2. Įvertinti įvairių veiksnių įtaką GB konstrukcijų sukibimo įtempių ir slinkties ryšiui.
3. Naudojant deformacijų stebėsenos įrangą, atlikti dvipusio armatūros ištraukimo bandymus, skirtus gelžbetoninių elementų armatūros deformacijų pasiskirstymui nustatyti.
4. Sukurti fizikinį armatūros ir betono sukibimo ir slinkties modelį.
5. Siekiant patikrinti naujus ir esamus sukibimo ir slinkties modelius, sukurti programą (skaičiavimo algoritmą), skirtą deformacijų pasiskirstymui nustatyti.
6. Atlikti įvairių modelių deformacijų lyginamąją statistinę analizę.

## Tyrimo metodika

Šioje disertacijoje taikoma nauja metodika, leidžianti nustatyti betono ir armatūros sukibimo ir slinkties ryšį, nagrinėjant jų sąveikos mechanizmą eksploatacinės apkrovos sąlygomis. Ši metodika grindžiama dvigubais armatūros strypo ištraukimo iš betono bandymais, išilgai armatūros strypo tenzometriniais jutikliais matuojant deformacijas. Atlikus matematinę ir parametrinę analizę, buvo pasiūlyta nauja GB konstrukcijų sukibimo įtempių ir slinkties modeliavimo formulė. Sukurta „MatLab“ kompiuterinė programa naudojama armatūros deformacijų pasiskirstymui konstrukcinio elemento ilgyje nustatyti, taikant siūlomą modelį, kurio adekvatumas buvo patvirtintas tiek autoriaus eksperimentiniais bandiniais, tiek nepriklausomais eksperimentais. Taip pat buvo atlikta statistinė analizė, įvertinant siūlomo modelio patikimumą ir pagrįstumą ir palyginant jį su kitais žinomais metodais.

## Darbo naujumas

Toliau išvardyti teorinių ir eksperimentinių tyrimų mokslinio naujumo aspektai.

1. Dvigubo ištraukimo bandymo metodas veiksmingai pašalina apribojimus, su kuriais susiduriama atliekant standartinius ištraukimo bandymus, įskaitant problemas, susijusias su vidutiniais sukibimo įtempiais, idealia medžiagų sąveika, betono gniuždymo įtempiais ir t. t. Naudojant tenzometrinius deformacijų jutiklius, eksperimentais patikimai gali būti nustatyta sukibimo įtempių ir slinkties elgsena.. Šiose eksperimentinėse programose gauti nauji bandymo duomenys leis papildyti turimus ribotus duomenis.
2. Šiame tyrime konceptualiai remiamasi įtempių perdavimo metodu, o eksperimentiškai – dvipusio armatūros ištraukimo bandymų rezultatais. Remiantis šiuolaikinėmis skaičiavimo metodikomis, buvo sukurtas naujas fizikinis modelis, leidžiantis prognozuoti kylančiąją sukibimo ir slinkties ryšį apibūdinančios kreivės dalį GB konstrukcijose. Pasisitelkus šį modelį taip pat galima prognozuoti tikslų

eksploatacinės apkrovos veikiamų GB elementų armatūros deformacijų pasiskirstymą.

3. Šiame tyrime pasiūlytas algoritmas, skirtas sudėtingam ir ilgai trunkančiam eksperimentiniam modelio patikros ir palyginimo su panašiais esamais modeliais procesui paspartinti. Be to, ši priemonė atveria naujas GB konstrukcijų įtempių perdavimo analizės, sukibimo ir slinkties modeliavimo galimybes.

### **Darbo rezultatų praktinė reikšmė**

1. Šiuo tyrimu patvirtinama, kad įtempių perdavimo metodas pritaikomas sprendžiant su konstrukcijos tinkamumu eksploatuoti susijusias problemas. Norint suprasti realią GB konstrukcijos elgseną ir ekonomiškiau bei patikimiau projektuoti būsimas GB konstrukcijas, pasiūlytą modelį galima integruoti į analitinius ir skaitinius metodus.
2. Naujas disertacijoje siūlomas algoritmas atveria plačių galimybių esamiems ir būsimiems sukibimo ir slinkties modeliams tikrinti, vertinti bei palyginti. Žinant atitinkamą sukibimo ir slinkties ryšį, šis algoritmas taip pat leidžia gauti GB elementų armatūros deformacijų pasiskirstymo tendencijas.

### **Ginamieji teiginiai**

Ginamieji teiginiai grindžiami atlikto tyrimo rezultatais ir darbo autoriaus sukaupta patirtimi:

1. Neviršijant eksploatacinės apkrovos siūlomas sukibimo ir slinkties modelis gali tiksliai prognozuoti sukibimo įtempių ir slinkties elgseną tarp dviejų gretimų tempiamojo GB elemento plyšių.
2. Modelis rodo, kad betono stipris bei slinkties ir armatūros strypo skersmens santykis turi didelę įtaką GB konstrukcijų sukibimo elgsenai.
3. Įvairių modelių armatūros deformacijų prognozavimo tikslumą galima įvertinti, patikrinti bei palyginti naudojant disertacijoje siūlomą programą.
4. Esant eksploatacinėms apkrovoms, palyginti su esamais modeliais, siūlomas modelis gana tiksliai prognozuoja GB konstrukcijų armatūros deformacijų pasiskirstymą.

### **Darbo rezultatų aprobavimas**

Doktorantūros studijų metu (2019–2023 m.) autorius disertacijos rezultatus paskelbė trijuose tarptautiniuose žurnaluose, įtrauktuose į Web of Science duomenų bazę (Dey et al., 2021a; Dey et al., 2021b; Dey et al. 2022), ir dviejuose tarptautinių mokslinių konferencijų straipsnių rinkiniuose:

1. Dey, A., Bado, M. F., Sokolov, A., and Kaklauskas, G. (2020). Distributed sensing, fiber Bragg gratings and strain gauges for strain monitoring of RC tensile

elements. In *Proceeding of the fib Symposium 2020, Concrete Structures for Resilient Society, 22nd to 24th November, Shanghai, China*.

2. Dey, A., Valiukas, D., Sokolov, A., Jakubovskis, R., and Kaklauskas, G. (2021). Experimental and numerical investigation of bond performance of RC tension members. In *fib Symposium, 2021, 14-16th June, Lisbon Portugal*.

## Disertacijos struktūra

Disertaciją sudaro įvadas, trys skyriai, bendrosios išvados, literatūros sąrašas (83 šaltiniai), autoriaus mokslinių publikacijų disertacijos tema sąrašas ir santrauka lietuvių kalba. Disertacijos apimtis – 112 puslapių, joje pateiktas 41 grafikas ir 12 lentelių.

## Padėka

Naudodamasis proga, autorius norėtų išreikšti didžiulę padėką visiems, kurie jį palaikė rengiant šią daktaro disertaciją. Visų pirma autorius dėkoja savo tėvams Asima Dey ir Swapan Kumar Dey, seseriai Subarna ir nuolatinei gyvenimo bendražygei Sarmistha už jų nepalaužiamą meilę, padrąšinimą ir suteiktą motyvaciją visais doktorantūros darbo metais.

Autorius taip pat išreiškia nuoširdžią padėką savo doktorantūros studijų vadovui, Gelžbetoninių konstrukcijų ir geotechnikos katedros profesoriui habil. dr. Gintariui Kaklauskui už visokeriopą pagalbą, patirtį, kantrybę ir pasitikėjimą autoriumi. Vadovo perduotos žinios ir motyvacija labai prisidėjo prie autoriaus akademinio ir profesinio augimo. Autorius nuoširdžiai dėkoja savo vyresniesiems kolegoms dr. Mattia Francesco Bado ir dr. Aleksandrui Sokolovui už visokeriopą paramą atliekant šį tyrimą. Jų draugiškas padrąšinimas, atsiliepinimai ir idėjos buvo labai naudingi tobulinant šį darbą ir pavertė jį pačiu tikriausiu bendradarbiavimu. Autorius taip pat dėkingas visai prof. G. Kaklauskos tyrimo komandai, ypač Domui Valiukui, už draugišką palaikymą ir pagalbą atliekant šį tiriamąjį darbą.

Autorius reiškia padėką ir prof. dr. Dariui Bačinskui, dr. Aidiui Jokūbaičiui, dr. Vladimirui Popovui ir dr. Raimondui Bliūdžiui už patarimus ir pastabas tobulinant disertaciją. Jis taip pat nori išreikšti nuoširdžią padėką prof. dr. Juozui Valivoniui ir doc. dr. Ronaldui Jakubovskiui už paramą ir patarimus. Autorius yra dėkingas ir dr. Skirmantei Mozūriūnaitei, Vaivai Miškinytei, Daivai Jurėnienei ir Dovilei Jodenytei už draugišką ir palaikančią motyvaciją. Taip pat dėkoja Amarjeet, Simran ir Karoliui už jų nuolatinį palaikymą.

Galiausiai autorius yra dėkingas Gelžbetoninių konstrukcijų ir geotechnikos katedrai, Doktorantūros mokyklai, Tarptautinių studijų centrai ir Lietuvos mokslų tarybai už finansinę paramą doktorantūros studijų metu. Jis taip pat dėkoja Vilniaus Gedimino technikos universiteto Tarptautinio mobilumo biurui ir Trento universitetui (UniTN) už suteiktą galimybę stažuotės metu įgyti vertingos ir naudingos patirties.

## 1. Betono ir armatūros sąveikos ir sukibimo stiprio tyrimo metodų apžvalga

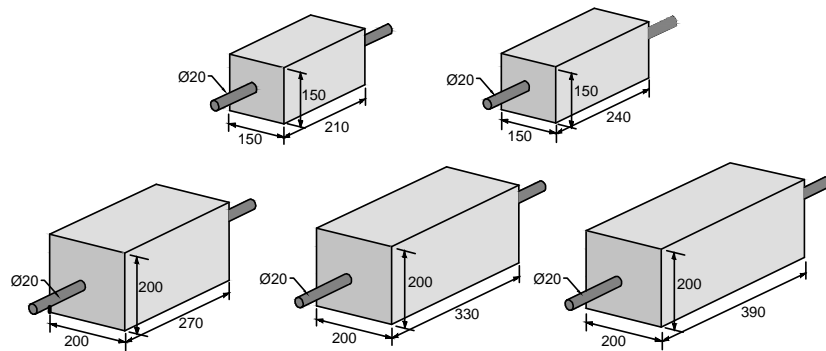
Šiame skyriuje autorius išsamiai apžvelgia sukibimo ir slinkties tyrimų tematiką, kuri yra šios disertacijos pagrindas. Pirmoje šio skyriaus dalyje išsamiai pristatomas GB konstrukcijų tinkamumo eksploatuoti aktualumas ir aptariama jo priklausomybė nuo betono ir armatūros sąveikos. Antroje dalyje pateikiama esamų sukibimo ir slinkties modelių apžvalga. Šioje dalyje taip pat aptariami galimi atitinkamų tyrimų metodai ir būdai. Be sukibimo ir slinkties modelių, taip pat apžvelgiami kai kurie sukibimo stiprio modeliai ir svarbiausi jų parametrai. Galiausiai aptariami prietaisai, naudojami armatūros deformacijų stebėsenai – nuo klasikinių, tokių kaip tenzometriniai jutikliai, iki itin modernių DOFS – su pagrindiniais jų veikimo principais ir iliustracijomis.

Atlikus išsamią literatūros apžvalgą, paaiškėjo keli prieštaringi faktai, į kuriuos būtina atkreipti dėmesį. Įvairiuose tyrimuose nustatyta daugybė skirtingų parametru, lemiančių armatūros ir betono sukibimą, tačiau įvairiuose literatūros šaltiniuose šie parametrai ne visada sutampa. Tarp jų dažniausi yra šie: betono stipris, apsauginis sluoksniu, armatūros strypų skersmuo, inkaravimo ilgis ir armavimo koeficientas. Be to, pateikta daugybė metodų, skirtų betono ir armatūros sukibimo ir slinkties mechanizmui tirti: tiesioginio armatūros ištraukimo bandymas, vieno sijos galo bandymas, visos sijos bandymas, dvipusio armatūros ištraukimo bandymas ir kt. Iš jų tik keli buvo pripažinti neatitinkančiais realybės ir turinčiais daug trūkumų. Be to, šiame tyrime svarbus vaidmuo tenka deformacijų stebėsenos įrangai. Matyti tendencijos, jog tenzometriniais jutikliais gaunami rezultatai yra patikimiausi ir tiksliausi, o FBG ir DOFS atveju pastebėta tam tikra rezultatų neatitiktis ir pernelyg didelis jautrumas. Dėl šių priežasčių ir dėl to, kad nėra universalios naujų modelių patikros ir kalibravimo priemonės, esami modeliai nėra tikslūs ir vienas kitam neretai prieštarauja. Šie trūkumai taip pat neleidžia nusakyti tikslaus sukibimo įtempių priklausomybės nuo slinkties matematinio modelio. Atsižvelgiant į minėtus veiksnius, būtina sukurti patikimą armatūros deformacijų nustatymo algoritmą, skirtą esamų ir būsimų modelių patikrai, bei sukurti tikslų betono ir armatūros sukibimo ir slinkties modelį, skirtą GB konstrukcijų tinkamumui eksploatuoti užtikrinti.

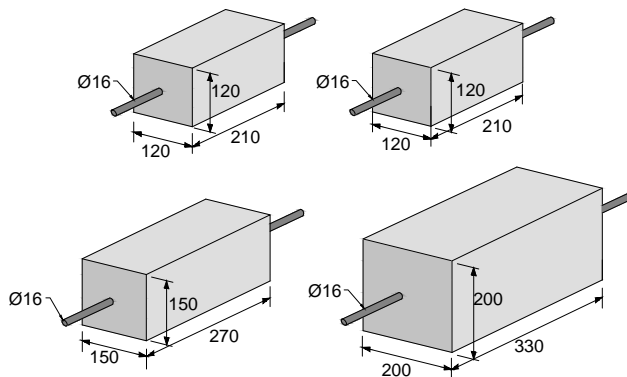
## 2. Plieno deformacijų stebėsenos gelžbetoniniuose elementuose tyrimai

Šiame skyriuje aprašyti autoriaus atlikti eksperimentiniai tyrimai, skirti GB konstrukcijų elementų betono ir armatūros sukibimo ir slinkties ryšiui nustatyti. Pirmoje skyriaus dalyje aprašoma visa bandymų eiga, pradedant nuo elektrinių tenzometrinių jutiklių (naudojamų armatūros deformacijoms matuoti) tvirtinimo proceso ir baigiant dvipusio armatūros ištraukimo bandymais laboratorijoje. Skyriuje taip pat pateikiamos trijose bandymų serijose naudotų bandinių geometrinės ir medžiagų charakteristikos. Antroje dalyje pristatomi eksperimentinių bandymų rezultatai – armatūros deformacijų pasiskirstymas. Galiausiai pateikiama, kaip iš eksperimentiniu būdu gauto deformacijų pasiskirstymo gaunamas sukibimo ir slinkties ryšys.

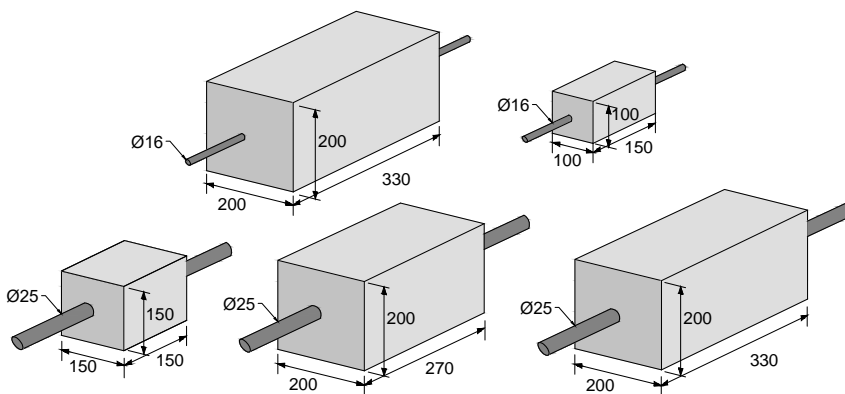
Pirmoje šio skyriaus dalyje išsamiai pristatomos trys bandymų serijos (S2.1 pav.).



(a)



(b)

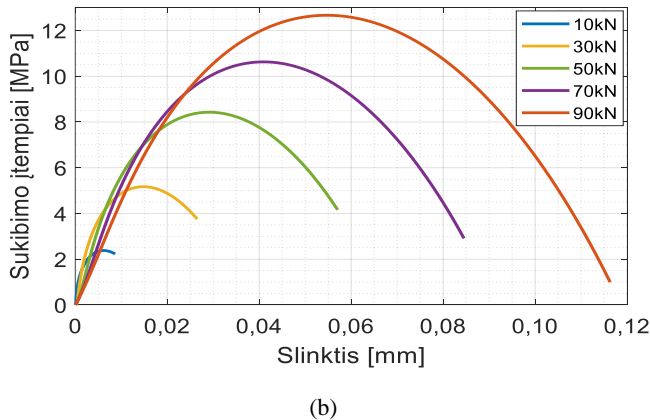
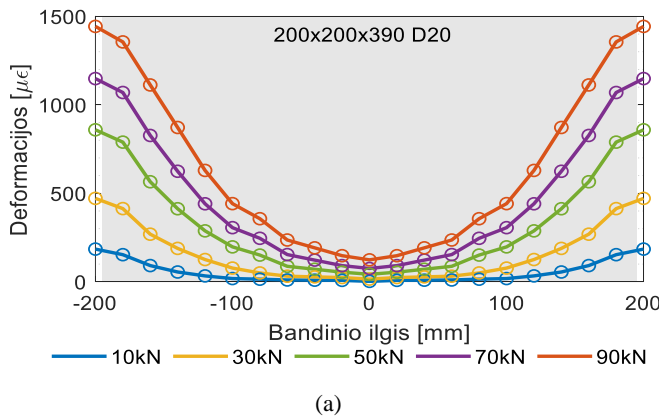


(c)

**S2.1 pav.** Modeliui kalibruoti pasitelktų GB tempiamų elementų geometrinės iliustracijos:  
a) 1 serija; b) 2 serija; c) 3 serija

Siekiant nustatyti betone esančios armatūros deformacijas, prie išilgai perpjautų modifikuotų plieninių strypų buvo pritvirtinti elektriniai tenzometriniai jutikliai. Pasiruošimas šios eksperimentinės programos bandymams buvo itin subtilus ir pareikalavo daug laiko. Iš viso buvo paruošta 16 GB tempiamų elementų, centriškai armuotų vienu armatūros strypu. Šioje programoje panaudoti trijų skirtingų skersmenų rumbuotieji strypai ( $\varnothing 16$ , 20 ir 25 mm). Siekiant išvengti nepageidaujamų plyšių, buvo specialiai pasirinkti trumpi GB tempiami elementai (trumpesni už vidutinį atstumą tarp plyšių).

Atlikus GB tempiamų elementų dvipusio armatūros ištraukimo bandymus, buvo gauti deformacijų pasiskirstymo išilgai bandinio ilgio duomenys. Pastebėta, kad, didėjant apkrovai, deformacijų profilių kreivės staigiai kyla aukštyn (S2.2a pav.).



**S2.2 pav.** Nagrinėjamo bandinio 200x200x390\_D20 analizė esant keliems įtempimų lygiams: a) armatūros deformacijų pasiskirstymas; b) sukibimo įtempimų priklausomybės nuo slinkties

Tai rodo deformacijų gradiento funkcijos – sukibimo įtempimų didėjimą. Sukibimo ir slinkties ryšys nustatomas naudojant programą, parašytą programiniame pakete MATLAB. Programos algoritmas pagrįstas įtempimų perdavimo metodu, kuris remiasi tiesiogine

sukibimo įtempių ir armatūros deformacijų priklausomybę. Numatomo sukibimo ir slinkties modelio kreivė tikroviškiau ir tiksliau atskleidžia betono ir armatūros sąveikos mechaniką nei klasikiniai iki šiol taikomi metodai (S2.2b pav.). Kylančioji sukibimo ir slinkties ryšį nusakančios kreivės dalis atspindi medžiagoms būdingas savybes, o krentančioji kreivės dalis rodo žymų lokalių antrinių plyšių poveikį armatūros ir betono sukibimui. Atsižvelgiant į bandinio geometrijos simetriškumą jo vidurio pjūvio atžvilgiu, sukibimo ir slinkties ryšiui nustatyti buvo naudojama tik pusė deformacijų pasiskirstymo profilio. Visais atvejais buvo pastebėta, kad, didėjant apkrovai, didėja didžiausias sukibimo įtempis ir jį atitinkanti slinkties.

Taikant minėtąjį algoritmą, buvo nustatytos visų 14 GB tempiamų bandinių sukibimo priklausomybės nuo slinkties funkcijos. Rezultatai parodė, kad tempiamuosiuose elementuose, armuotuose mažesnio skersmens rumbuotosios armatūros strypais, esant tam tikrai slinkties reikšmei, atsiranda didesni sukibimo įtempiai, lyginant su elementais, armuotais didesnio skersmens strypais.

Eksperimentų metu gautos kylančiosios sukibimo ir slinkties priklausomybę išreiškiančių kreivių dalys naudojamos kuriant sukibimo ir slinkties modelį. Jis išsamiau aprašytas kitame skyriuje.

### 3. Naujasis sukibimo ir slinkties modelis: kūrimas ir patvirtinimas

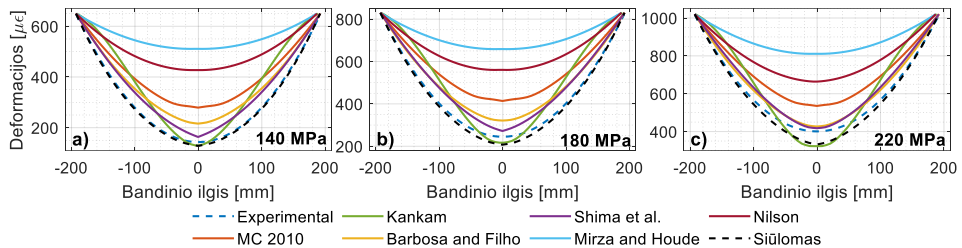
Pirmoje šio skyriaus dalyje autorius aptaria teorinius tyrimus ir pagrindines aplinkybes, kuriomis remiantis buvo sukurtas naujasis sukibimo ir slinkties modelis. Pirmiausia buvo gauti ir išanalizuoti 14 GB tempiamų bandinių dvipusio armatūros ištraukimo rezultatai (aprašyti 2 skyriuje). Tuomet sudarytas duomenų rinkinys, kuriame įtrauktos eksperimentiniai metodais gautos GB tempiamųjų elementų sukibimo ir slinkčių kylančiosios kreivių dalys, veikiant skirtingų lygių apkrovai. Kuriant modelį buvo pasitelkta daugialypė tiesinė regresija (toliau – DTR), nes duomenų rinkinys buvo surinktas naudojant platų įvairių parametru diapazoną. Galiausiai, atlikus tam tikras surinktų duomenų matematinės operacijas, kaip antai reikšmių normalizavimą, tinkamo matematinio modelio pasirinkimą ir kt., buvo sukurtas ir pasiūlytas sukibimo įtempių priklausomybės nuo slinkties modelis (S3.1 lygtis). Remiantis šia analize nustatyta, kad, lyginant su kitais ištirtais parametrais, betono stiprio ( $f_c$ ) bei slinkties ir skersmens ( $s/\emptyset$ ) santykis turi didžiausią įtaką GB konstrukcijų sukibimo įtempiams.

$$\tau = 1,25 - 0,0035(f_c)^{1,5} + 250 \left( \frac{s}{\emptyset} \right)^\alpha ; \quad (S3.1)$$

$$f_c < 50 \text{ MPa} \Rightarrow \alpha = 0,6; f_c \geq 50 \text{ MPa} \Rightarrow \alpha = 0,5.$$

Antroje šio skyriaus dalyje aprašomas patikros procesas, atliktas lyginant pasiūlytus sukibimo ir slinkties modelių rezultatus su eksperimentiniais. Visų pirma, atlikta patikra pasitelkiant 14 eksperimentinių GB tempiamų elementų, naudotų sukibimo ir slinkties modeliui sukurti. Antra, atlikta patikra įtraukiant imčiai nepriskiriamus duomenis, pasitelkiant 8 nepriklausomus eksperimentinius įvairių parametru GB tempiamus elementus, kurių rezultatai buvo surinkti iš įvairių šalių literatūros šaltinių. Abiem atvejais gautas labai geras siūlomo modelio ir eksperimentinių rezultatų sutapimas.

Paskutinėje šio skyriaus dalyje atliekama naujo modelio patikra pasitelkiant eksperimentinį deformacijų pasiskirstymą aštuoniuose realiuose nepriklausomuose bandiniuose. Gauti rezultatai taip pat palyginami su kelių labiausiai žinomų sukibimo ir slinkties modelių rezultatais. Šiam tikslui pasiekti autorius sukūrė ir pasiūlė algoritmą, skirtą sudėtingam ir ilgai trunkančiam matematiniam modelio patikros ir palyginimo procesui paspartinti. Aptarus teorinį kontekstą ir matematinę priemonės pagrindą, jos pritaikymas parodytas įvertinus septynis sukibimo ir slinkties modelius (įskaitant siūlomą modelį), tiriant aštuonis nepriklausomus eksperimentinius GB elementus, esant skirtingiems įtempių lygiams. Lyginant eksperimentines ir modeliais apskaičiuotas deformacijų reikšmes, galima susidaryti aiškų vaizdą apie modelių tikslumą. Esamų modelių prognozuojamos armatūros deformacijų kreivės, esant skirtingiems armatūros įtempių lygiams, atsižvelgiant į Houde bandinio eksperimentinius duomenis, pavaizduotos S3.1 pav. Čia aiškiai matyti, kad siūlomas modelis armatūros deformacijas prognozuoja tiksliausiai.

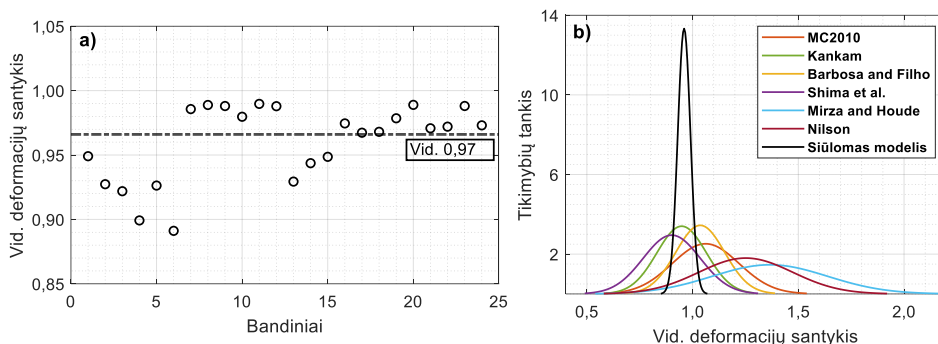


**S3.1 pav.** Eksperimentais nustatytas ir prognozuojamas deformacijų pasiskirstymas bandinyje 150×150×405\_D25, remiantis Houde, esant įtempių lygiams: a) 140 MPa; b) 180 MPa; c) 220 MPa

Remiantis aštuonių nepriklausomų bandinių rezultatais (kiekvieną bandinį veikiant trims skirtingų lygių įtempimams), atlikta statistinė vidutinių armatūros deformacijų analizė (S3.1 lentelė). S3.1 lentelėje matyti, kad, lyginant su kitais modeliais, siūlomo modelio rezultatai yra geriausi – teorinių ir eksperimentinių reikšmių santykių (teorija / eksperimentas) vidurkis artimiausias vienetui (0,97). Kankam, Shima, Barbosa ir Filho teorinių bei eksperimentinių reikšmių santykių vidurkiausiai atitinkamai lygūs 0,94, 0,90, 1,05, 1,07, 1,25 ir 1,37.

**S3.1 lentelė.** Įvairių sukibimo ir slinkties modelių vidutinių teorinių deformacijų reikšmių palyginimas su eksperimentinėmis, naudojant 8 GB tempiamuosius elementus iš įvairių autorių eksperimentinių programų

Statistiniai duomenys, pagrįsti deformacijų santykiu	Įvertinti modeliai						
	MC2010	Kankam	Barbosa ir Filho	Shima	Mirza ir Houde	Nilson	Siūlomas
Vidurkis	1,07	0,94	1,05	0,90	1,37	1,25	0,97
Standartinis nuokrypis	0,16	0,12	0,12	0,14	0,27	0,22	0,03
VK	0,15	0,12	0,15	0,15	0,20	0,18	0,03



**S3.2 pav.** Sukibimo ir slinkties modelių palyginimas atliekant statistinę analizę: a) siūlomo modelio vidutinių deformacijų santykiai; b) visų įvertintų sukibimo ir slinkties modelių tikimybių tankio kreivės

Atsižvelgiant į vidutinių armatūros deformacijų teorinių ir eksperimentinių reikšmių santykių (teorija / eksperimentas) sklaidą, siūlomas modelis taip pat yra tiksliausias – variacijos koeficientas neviršija 3 %. Kitų modelių: Kankam, MC2010, Shima, Barbosa ir Filho, Nilson, Mirza ir Houde – teorinių ir eksperimentinių reikšmių santykių variacijos koeficientai atitinkamai lygūs 12 %, 15 %, 15 %, 15 %, 18 % ir 20 %. Siūlomo modelio sklaidos rezultatas parodytas S3.2a pav. Visų modelių tikimybių tankio kreivės pavaizduotos S3.2b pav. Čia matyti, jog siūlomam modeliui būdinga siauriausia ir aukščiausia normaliojo skirstinio kreivė, nes jo standartinis nuokrypis ir variacijos koeficientas yra mažiausi. Kita vertus, didžiausią normaliojo skirstinio sklaidą galima pastebėti Mirza ir Houde modelyje, kurio duomenys yra labai pasklidę, taigi ir mažiausiai patikimi.

## Bendrosios išvados

Šiame tyrime pasiūlyta geresnė ir modernesnė betono ir armatūros sąveikos modeliavimo koncepcija. Išanalizavus iš įvairios literatūros surinktą ir turimą tempiamųjų GB elementų imtį, buvo sukurtas naujas sukibimo įtempių priklausomybės nuo slinkties modelis. disertacijoje taip pat pristatytas algoritmas, skirtas esamiems ir būsimiems sukibimo modeliams vertinti, patikrinti ir palyginti. Žinant sukibimo ir slinkties modelį, algoritmas taip pat leidžia nustatyti armatūros deformacijų pasiskirstymą. Pritaikius įtempių perdavimo metodą, sukūrus naują sukibimo ir slinkties modelį bei programą, skirtą armatūros deformacijoms prognozuoti, toliau pateikiami pastebėjimai ir išvados:

1. Standartiniai tiesioginio armatūros ištraukimo bandymai dėl daugelio apribojimų netinka GB elementų, veikiamų eksploatacinės apkrovos, lokaliai sukibimo ir slinkties elgsenai modeliuoti. Šiuo atveju sukibimo elgsenai vertinti racionaliau taikyti patikimesnius dvipusio armatūros ištraukimo bandymus, kurie eliminuoja šiuos apribojimus, kai išilgai tempiamojo elemento matuojamos armatūros deformacijos. Deja, praeityje atlikta labai nedaug dvipusio armatūros ištraukimo bandymų ir nė vienas iš jų nebuvo skirtas GB elementų tinkamumo eksploatauoti analizei.

2. Atlikus regresinę analizę nustatyta, jog slinkties ir skersmens santykis bei betono gniuždomasis stipris turi reikšmingą įtaką GB konstrukcijų sukibimo įtempiams.
3. Siūlomas sukibimo modelis GB elemento ruože tarp plyšių geba tiksliai numatyti ryšį tarp sukibimo įtempių ir slinkties.
4. Remiantis disertacijoje pristatytu algoritmu, nustatyta, kad siūlomas sukibimo ir slinkties modelis tiksliai prognozuoja armatūros deformacijų pasiskirstymą veikiamuose eksploatacinės apkrovos tempiamuosiuose GB elementuose.
5. Statistinė analizė, atlikta naudojant aštuonių nepriklausomų GB tempiamų elementų bandymų duomenis, parodė, jog siūlomo modelio prognozuotos armatūros deformacijos vidutiniškai 3 % buvo mažesnės už eksperimentines. Modeliui nustatytas variacijos koeficientas neviršija 3 %. Šios reikšmės buvo mažiausios, pasiūlytąjį modelį palyginus su kitais metodais.
6. Siūlomas modelis apima tik kylančiąją sukibimo įtempių nuo slinkties priklausomybės kreivės dalį, o krentančioji kreivės dalis, apimanti kitus reiškinius, tokius kaip sukibimo pažaidos zona, vidinis pleišėjimas, betono elgsena plyšyje ir kt., gali būti potenciali ateities tyrimų kryptis. Įvertinus šiuos veiksnius būtų galima dar tiksliau modeliuoti GB konstrukcijų sukibimo elgseną.



Alinda DEY

CONSTITUTIVE BOND-SLIP MODELLING  
OF REINFORCED CONCRETE MEMBERS  
AT SERVICE LOAD

Doctoral Dissertation

Technological Sciences,  
Civil Engineering (T 002)

FIZIKINIS GELŽBETONINIŲ ELEMENTŲ  
SUKIBIMO ĮTEMPIŲ IR SLINKTIES RYŠIO  
MODELIAVIMAS ESANT EKSPLOATACINEI APKROVAI

Daktaro disertacija

Technologijos mokslai,  
statybos inžinerija (T 002)

Lietuvių kalbos redaktorė Rita Malikėnienė  
Anglų kalbos redaktorė Jūratė Griškėnaitė

2023 09 01. 10,0 sp. l. Tiražas 20 egz.  
Leidinio el. versija <https://doi.org/10.20334/2023-038-M>  
Vilniaus Gedimino technikos universitetas  
Saulėtekio al. 11, 10223 Vilnius  
Spausdino UAB „Ciklonas“  
Žirmūnų g. 68, 09124 Vilnius